Preliminary modelling of ship manoeuvring in ice using a PMM

Lau, M.

Publisher's version / Version de l'éditeur:
https://doi.org/10.4224/8895076
Technical Report (National Research Council of Canada. Institute for Ocean Technology); no. TR-2006-02, 2006

DOCUMENTATION PAGE

REPORT NUMBER	NRC REPORT NUMBER	DATE		
	TR-2006-02	February 2006		
REPORT SECURITY CLASSIFICATION Unclassified		**DISTRIBUTION** Unlimited		
TITLE **Preliminary Modeling of Ship Manoeuvring in Ice Using a PMM**				
AUTHOR(S) Michael Lau				
CORPORATE AUTHOR(S)/PERFORMING AGENCY(S) Institute for Ocean Technology				
PUBLICATION Institute for Ocean Technology				
SPONSORING AGENCY(S) Institute for Ocean Technology, Marine Institute				
IMD PROJECT NUMBER 42_953_10		**NRC FILE NUMBER**		
KEY WORDS PMM, ice, Terry-Fox, ship, manoeuvring, model test, analytical model		**PAGES** 40	**FIGS.** 24	**TABLES** 4

SUMMARY

The Institute for Ocean Technology (IOT) of the National Research Council of Canada (http://www.iot-ito.nrc-cnrc.gc.ca/) has conducted physical, numerical and mathematical modeling of ship manoeuvring characteristics in ice, as part of a larger effort to develop reliable modeling techniques to assist in the design of new ice-worthy vessels and in the simulation of their navigating characteristics. This report presents results from a preliminary series of physical and mathematical modeling of the problem. The report focuses on the interaction processes and the influence of ship motions on the yaw moment exerted on the ship hull. The dominant ice-ship interaction processes are identified. The results show a large influence of ship motions and interaction geometry on the measured yaw moments. The geometrical aspect of the interaction processes is described and its influences on ice loads are discussed. Conclusions are made and recommendations for future works are provided.

ADDRESS

National Research Council
Institute for Ocean Technology
P. O. Box 12093, Station 'A'
St. John's, Newfoundland, Canada
A1B 3T5

Tel.: (709) 772-5185, Fax: (709) 772-2462

National Research Council Canada | Conseil national de recherches Canada

Institute for Ocean Technology | Institut des technologies océaniques

PRELIMINARY MODELING OF SHIP MANOEUVRING IN ICE USING A PMM

Michael Lau

February 2006

ABSTRACT

The Institute for Ocean Technology (IOT) of the National Research Council of Canada (http://www.iot-ito.nrc-cnrc.gc.ca/) has conducted physical, numerical and mathematical modeling of ship manoeuvring characteristics in ice, as part of a larger effort to develop reliable modeling techniques to assist in the design of new ice-worthy vessels and in the simulation of their navigating characteristics. This report presents results from a preliminary series of physical and mathematical modeling of the problem. The report focuses on the interaction processes and the influence of ship motions on the yaw moment exerted on the ship hull. The dominant ice-ship interaction processes are identified. The results show a large influence of ship motions and interaction geometry on the measured yaw moments. The geometrical aspect of the interaction processes is described and its influences on ice loads are discussed. Conclusions are made and recommendations for future works are provided.

ACKNOWLEDGMENTS

The investigations presented in this report were partially funded by the Atlantic Innovation Fund through the Marine Institute, Newfoundland. J.C. Liu provided assistance during model testing, and in the development of the mathematical model. Dr. A. Derradji-Aouat and Dr. F.M. Williams provided valuable discussions through out the project. Work term student A. van Thiel provided assistance during model testing and its documentation. Their and the ice tank personnel's support is gratefully acknowledged.

TABLE OF CONTENTS

APPENDICES

LIST OF TABLES

LIST OF FIGURES

LIST OF SYMBOLS

(In order of appearance)

β Drift angle [deg]
σ_f Flexural strength [Pa]
h_i Ice thickness [m]
V Tow velocity [m/s]
R_t Total resistance in ice [N]
R_{br} Resistance due to breaking of ice [N]
R_c Resistance due to clearing of ice [N]
R_b Resistance due to buoyancy of ice [N]
C_{br} Coefficient of R_{br}
ρ_i Density of ice [kg/m^3]
B Maximum beam of model at waterline [N]
V_m Model velocity [m/s]
C_c Coefficient of clearing resistance, R_c
C_b Coefficient of buoyancy resistance, R_b
$\Delta\rho_i$ Difference in density between ice and tank water [kg/m^3]
F_n Froude number
R_{ps} Pre-sawn ice resistance [N]
S_n Strength number
N_{ow} Yaw moment in baseline open water [N·m]
r Yaw rate [deg/s]
W_i Initial channel width [m]
W_f Final channel width [m]
ℓ_c Ice characteristic length [m]
R Turning radius [m]
v Sway velocity [m/s]
N_v Ice derivative of sway velocity [kg·m/s]
N_r Ice derivative of yaw moment [kg·m/s^2]
N Total yam moment [N·m]
N_o A yaw moment component [N·m]
N_{tot} Total yam moment [N·m]
N_{br} Ice breaking component of total yam moment [N·m]
N_b Ice submergence component of total yaw moment [N·m]
N_c Ice clearing component of total yaw moment [N·m]
P_{Vm} Maximum load per unit width [N/m]
y_m End deflection [m]
γ_w Specific weight of water [N/m^3]
a Maximum displacement in forward direction [m]
α Stem angle [deg]
ℓ_a Average breaking length [m]
P_{Va} Average vertical force per unit width [N/m]
ϕ Angle between normal of bow and vertical line [deg]
η Angle between hull side surfaces and vertical line [deg]
$F_{h\#}$ Horizontal loads (# 1-3) [N]
$\ell_{\#}$ Geometric lengths in Figure 4.2 (# 1-6) [m]
$\Delta\ell_{\#}$ Ice breaking width adjustments (# 1,2) [m]
W_b Total width of ice broken by bow [m]
$F_{v\_\#}$ Vertical component of buoyant forces on side of bow (# 1,2) [N]
$F_{h\_\#}$ Horizontal component of buoyant forces on side of bow (# 1,2) [N]
γ_i Specific weight of ice [N/m^3]
S Horizontal projection of bow surface [m^2]

PRELIMINARY MODELING OF SHIP MANOEUVRING IN ICE USING A PMM

1.0 INTRODUCTION

Recent development of offshore oil and gas reserves in several countries, together with economic studies to increase transportation through the Arctic, has led to a renewed interest in the manoeuvrability of vessels in ice. Past experiences with icebreakers have shown that the manoeuvrability of a ship can be improved by modifying specific features of the hull and the propulsion system and by using manoeuvring aids, such as a thruster or a bubbler.

Despite a sizeable volume of work, there is not yet a universally accepted analytical method of predicting ship performance in ice. In 2003, the Institute for Ocean Technology (IOT) of the National Research Council of Canada (http://www.iot-ito.nrc-cnrc.gc.ca/) initiated a comprehensive physical, numerical and mathematical modeling of ship manoeuvring characteristics in ice, as part of a larger effort to develop reliable modeling techniques to assist in the design of new ice-worthy vessels and in the simulation of their navigating characteristics. The objective is to develop a physical representation of the complex interaction processes of a ship manoeuvring in ice and to build a mathematical model to satisfactorily predict its performance. In turn, the mathematical model will provide a tool for ship designers to use as part of the assessment of ship navigation in ice infested routes. It can also be incorporated into marine simulators to train mariners, or into automatic ship control systems for better ship manoeuvring.

Ship manoeuvres and the manoeuvrability of a ship in various ice conditions are complex subjects. Our present understanding of the nature of ice-ship interactions is still limited. Considering the complexity of the loads imposed by ice during ship manoeuvres, a preliminary series of ship manoeuvring experiments in ice were conducted in December 2003 and January 2004 under Project 42_953_10. The objectives of this initial phase of the program are to assess the application of the PMM modeling techniques in modeling the ship manoeuvring in ice conditions, probe data for a concurrent analytical and numerical model development, and to gain insight to assist in further experimentation. In this report, the results of the model tests and a brief mathematical model are presented.

The parameters analyzed are the velocity, sway force, yaw, drift angle, surge load, sway load, and yaw moment. As the yaw moment and turning radius are the important indicators of the manoeuvring performance, this report will focus on the interaction processes and the influence of ship motions on the yaw moment exerted on the ship hull. The dominant ice-ship interaction processes are identified. The test results show a large influence of ship motions and interaction geometry on the measured yaw moments. The geometrical aspect of the interaction processes is described and its influences on ice loads are discussed. Conclusions are made and recommendations for future works are provided.

Experimental Uncertainty Analysis (EUA) was conducted on the results of the manoeuvring tests as a step towards developing a procedure for EUA for ship manoeuvring in ice. The EUA procedure (Derradji, 2004) developed in IOT for resistance testing was followed and the results are documented in an accompanying report (Lau and Derradji, 2006).

2.0 **TEST PROGRAMS**

In the ice tank, the *Terry Fox* model (scale = 1:21.8) was towed in five ice sheets using the PMM with the model restrained in roll. The model was outfitted with a rudder. Tests with different rudder angles were tested in open water only. Both straight movement and turning circle manoeuvres were tested. The target flexural strength and ice thickness of the ice sheets was the same for all experiments (35 kPa and 40 mm). During the turning circle manoeuvring tests, the drift angle β was set to zero degrees. Bubble ice was required for all ice sheets.

Three different types of experiments were conducted. They were:

1. Experiments in Level Ice
2. Experiments in Pre-sawn Ice (Resistance runs only)
3. Experiments in Open Water

2.1 Test Set-up

In these tests, the main components of the test set up are the ice tank, the *Terry Fox* ship model, the Planar Motion Mechanism (PMM), the Data Acquisition System (DAS) and video cameras.

2.1.1 Ice tank

The ice tank is 96 m long, 12 m wide and 3 m deep, with useable ice sheets of 76 m in length, making this tank the longest in the world. Thus, it allows for tests at higher speeds and longer test runs. The 12 m width of the tank enables ship experiments of various manoeuvres, and for straight test runs in continuous ice, three tracks may be used (center channel, north quarter point, and south quarter point) in each ice sheet. The ability to perform three continuous ice tests per sheet significantly improves the cost effectiveness. The effect of the tank walls on the center channel is also reduced because there is less confinement due to the tank walls with the wider ice tank.

2.1.2 *Terry Fox* ship model

The experiments were carried out with a 1:21.8 scaled model of the Canadian Coast Guard's icebreaker *Terry Fox* (IOT model # 417) (Figure 2.1). The model hydrostatics are provided in Appendix A and summarized in Table 2.1. The model was mounted to the towing carriage through the PMM at the model's center of gravity. The model was towed with a controlled planar motion through a level ice sheet. The model surface was finished to a friction coefficient of 0.01 with Dupont's Imron paint.

2.1.3 Planar Motion Mechanism (PMM)

Marineering Limited (1997) provided details on the development and commissioning of the PMM. The PMM was designed to study manoeuvring of ships in both ice and open water.

The PMM apparatus (Figure 2.2) consists of two primary components: a sway sub-carriage that is mounted beneath the main towing carriage, and a yaw assembly that is connected to the sway sub-carriage. The apparatus allows the model to yaw and sway in a controlled manner, while measuring the sway and surge forces as well as the yaw moment. The combination of sway and yaw allows a variety of maneuvers to be performed.

The PMM dynamometer has 3 cantilever type load cells for measuring surge force, sway force, and yaw moment. A load cell aligned along the model's surge axis measures surge force. The other two load cells aligned along the model's sway axis measure sway force. Yaw moment is measured by resolving the outputs from the two sway load cells. The specifications for the PMM are given in Table 2.2.

2.1.4 Data Acquisition System (DAS) and video

In each experiment, tow force, turning moment and ship motions were measured. The transducer for outputs were sampled digitally at 50 Hz and filtered at 200 Hz.

Two video recordings were made of each test, one on the starboard side that is manually controlled to follow the model's manoeuvres, and the other looking down ahead of the model at the port side.

All details regarding the instrumentation used in this test program and their calibration sheets are provided in Appendix B.

2.2 Ice Conditions

The experiments were carried out in CD-EG/AD/S ice (Spencer and Timco, 1990). With inclusions of air bubbles into the growing ice sheet, the model ice significantly improves the scaling of ice density, elastic, and fracture properties. For each ice sheet, flexural, compressive, and shear strengths were measured frequently throughout the test period. A strength versus time curve was created for each ice sheet and the strength values reported at each test time were interpolated from this curve. Flexural strength, σ_f, was measured using *in-situ* cantilever beams. A number of shear strength measurements were performed immediately after the flexural strength test to provided index values for comparison with the measured flexural strengths. The ratio of shear strength to downward breaking flexural strength varied from 1.03 to 3.16. The reported ice thickness, h_i, is the average thickness of approximately 65 measurements of the ice sheet thickness along the test path. The IOT standards and work procedures were followed for producing and characterizing level ice sheets.

All work procedures are given in the IOT documentations for system quality. The procedures followed to prepare the ice tank, seed, and grow the ice sheet are given in the IOT work procedures TNK 22, TNK 23, and TNK 37, respectively. The mechanical properties of the ice are determined according to the following work procedures: TNK 26 (for measuring the flexural strength), TNK 27 (for measuring the elastic modulus), TNK 28 (for measuring compressive strength), and TNK 30 (for measuring ice density). Ice thickness measurements were performed as per the work procedure TNK 25.

It should be noted that all of the above work procedures are valid for both bubbly ice and non-bubbly ice. Simply, in the case of non-bubbly ice, the bubbler system is turned off.

The test program required five (5) different ice sheets with a nominal thickness of 40 mm and a nominal flexural strength of 35 kPa at beginning of test day. The flexural strengths were tempered throughout the test day. A summary of the five ice sheets and their properties are presented in Appendix C.

2.3 Test Matrix

The complete test matrix is given in Appendix D and summarized in Table 2.3. For the tests described in this program, the ice sheets had a target ice thickness of 40 mm and a target flexural strength of 35 kPa. The following manoeuvres were utilized: (1) resistance runs in which the model was towed along a straight line at a zero drift angle, and (2) pure yaw through a constant radius manoeuvre so that the heading of the model was always tangential to the path of its center of gravity, resulting in zero sway force and a yaw moment. All tests in ice were performed with a zero degree rudder angle and a model velocity ranging from 0.02 m/s to 0.6 m/s. The constant radius manoeuvre was conducted with two turning radii (50 m and 10 m). Additional resistance tests were also conducted at a model velocity of 0.9 m/s. Concurrent to the testing in ice, manoeuvres in open water were also conducted. The open water runs were performed with a rudder angle of 0, 20, and 30 degrees.

2.3.1 Description of the experiments in ice

The experiments conducted in ice included level ice resistance runs, pre-sawn ice resistance runs, and arc manoeuvring runs in level ice. Figure 3 shows a picture of a typical test run in ice. Ship model speeds of 0.02 m/s, 0.05 m/s, 0.1 m/s, 0.2 m/s, 0.3 m/s, 0.4 m/s, 0.5 m/s, and 0.6 m/s were tested in ice (see Appendix D).

Appendix E summarizes the channel width measurements obtained in the ice tests and shows the run schematics for the resistance and manoeuvring tests. Figures E.2 to E.6 show schematics for the ice test runs in each sheet. The resistance tests were conducted in the first two ice sheets, NMS1 and NMS2 (Figures E.2 and E.3). The manoeuvring tests were conducted in the next three ice sheets NMS3, NMS4, and NMS5 (Figures E.4, E.5 and E.6).

For the straight runs, the following test run scenario was performed. Initially, a level ice test run was conducted along the centerline of the tank. In NMS1, the model was towed at a constant speed of 0.1, 0.6, and 0.9 m/s with an approximately 20 m run distance each, and a creep test performed at the end (0.02 m/s). Afterwards, the model was tested at the quarter-point (on either side of the center-line). Again, the model was towed at the set constant speeds of 0.1, 0.6 and 0.9 and 0.02 m/s (creep speed). For the south quarter point test, a pre-sawn ice test was performed. In NMS2, the same schematic was uses and speeds tested were 0.1, 0.3, and 0.6 m/s, followed by a creep test.

For turning circle tests, the model was towed at a constant yaw rate with the prescribed arc radius (10 m and 50 m) and model speed. For 50 m arc radius, the model was towed at a model speed of 0.02, 0.1, 0.3, and 0.6 m/s with a yaw rate of 0.02, 0.11, 0.34, and 0.69 deg/s, respectively. For 10 m arc radius, the model was towed at a model speed of 0.02, 0.05, 0.1, 0.2, 0.3, 0.4, 0.5, and 0.6 m/s with a yaw rate of 0.11, 0.29, 0.57, 1.15, 1.72, 2.29, 2.86, and 3.44 deg/s, respectively.

2.3.2 Description of the experiments in open water

The open water tests for the corresponding ice test runs were baseline open water tests. The experiments conducted in open water included resistance runs and arc manoeuvring. Ship model speeds of 0.02 m/s, 0.05 m/s, 0.1 m/s, 0.2 m/s, 0.3 m/s, 0.4 m/s, 0.5 m/s, 0.6 m/s, and 0.9 m/s were tested with three rudder angles (0, 20, and 30 degrees) (See Appendix D). Note that all open water tests were conducted in the ice tank with calm water conditions (no waves).

3.0 TEST RESULTS

Result of the test is summarized in Table 3.1. Plots for typical test results are given in Appendix F.

3.1 Resistance Tests

3.1.1 Test Results

<u>Open water</u>
Baseline open water resistance tests were completed in the ice tank for test speeds corresponding to the ice tests conducted. Figure 3.1 shows the measured tow force versus model velocity for the open water resistance runs. The numerical values for the mean tow force at each speed are:

Model Velocity (m/s)	**Mean Tow Force (N)**
0.1	0.18
0.3	1.41
0.6	4.81
0.9	10.48

The resistance (given in N) in baseline open water, $R_{ow,}$ can be obtained from the regression line in Figure 3.1:

$$R_{ow} = 11.717 \cdot V^2 + 1.0809 \cdot V - 0.0182 \tag{3.1}$$

where V is the tow velocity (in m/s).

<u>Ice tests</u>
Figure 3.2 shows the measured tow force versus model velocity for the resistance tests in both pre-sawn and continuous ice. The numerical values for the mean tow force at each speed are:

Model Velocity (m/s)	**Pre-sawn Ice**	**Level Ice**
	Mean Tow Force (N)	**Mean Tow Force (N)**
0.02	4.50	9.02
0.1	5.95	10.38
0.3	9.01	15.74
0.6	16.36	23.85

3.1.2 Components for ship model resistance in ice

The resistance data were analyzed according to IOT Standards for ship resistance in ice (IOT/42-8595-S/TM7). This procedure provides a way to correlate data obtained from a previous test series by Spencer et al (1988) conducted with the same ship, but with different model hull friction and ice conditions. The total ice resistance is calculated as the sum of four components: open water, ice buoyancy, ice breaking, and ice clearing, as shown in Equation 3.2. The fundamental reason for this approach is that the individual components may not all scale in the same manner to full-scale (Spencer, 1992).

$$R_t = R_{br} + R_c + R_b + R_{ow} \tag{3.2}$$

where R_t is the total resistance in ice
R_{br} is the resistance due to breaking of ice
R_c is the resistance due to clearing of ice
R_b is the resistance due to buoyancy of ice
R_{ow} is the resistance due to open water

<u>Dimensionless numbers</u>
Dimensionless numbers associated with each individual component can be derived through dimensional analysis. These coefficients are useful because they allow scaling in conditions varying from the test conditions in which they were obtained and they help identify any outliers (outliers are discarded data points). The coefficients of ice resistance are defined as:

$$C_{br} = \frac{R_{br}}{\rho_i B h_i V_M{}^2} \tag{3.3}$$

where C_{br} is the coefficient of the breaking resistance, R_{br}
ρ_i is the density of ice
B is the maximum beam of model at waterline
h_i is the ice thickness
V_m is the model velocity

$$C_c = \frac{R_c}{\rho_i B h_i V_M^2} \tag{3.4}$$

where C_c is the coefficient of the clearing resistance, R_c

$$C_b = \frac{R_b}{\Delta\rho_i g B h_i T} \tag{3.5}$$

where C_b is the coefficient of the buoyancy resistance, R_b
$\Delta\rho_i$ is the difference in density between ice and tank water
g is the acceleration of gravity (9.808 m·s^{-2})
T is the maximum draft of model

A non-dimensional strength number is defined as:

$$S_n = \left[\frac{\rho_i B V_M^2}{\sigma_f h_i}\right]^{1/2} \tag{3.6}$$

where σ_f is the flexural strength of ice

And a Froude number, F_n, defined as:

$$F_n = \frac{V_M}{\sqrt{g h_i}} \tag{3.7}$$

<u>Open water component, R_{ow}</u>
Baseline open water resistance tests were given in Section 3.1.1. The open water component is a directly measured value. The trend line, i.e., Equation 3.1, obtained from the measured resistance allows us to calculate R_{ow} for other velocities.

<u>Ice buoyancy component, R_b</u>
The open water component is subtracted from the measured pre-sawn ice resistance, R_{ps}, to determine the total clearing component:

$$R_{ps} - R_{ow} = R_c + R_b \tag{3.8}$$

$R_c + R_b$ is plotted against model speed, as shown in Figure 3.3. The clearing component, R_c, is a velocity dependent component; therefore, at zero velocity only the ice buoyancy component remains. R_b is estimated from the y-intercept of the $R_c + R_b$ versus model speed graph (Figure 3.3). The ice buoyancy component can also be estimated by subtracting the open water component from pre-sawn ice resistance at low speeds, such as creep tests (0.02 m/s).

Ice buoyancy is calculated using the following equation:

$$Buoyancy = \Delta\rho_i g B h_i T \tag{3.9}$$

Buoyancy is plotted against the estimated ice buoyancy component found in the previous step, as shown in Figure 3.4. Using the slope of the regression equation in Figure 3.4, R_b is re-calculated using Equation 3.5. For this test series, C_b = 0.261.

Ice clearing component, R_c

Using the pre-sawn data, the ice-clearing component can also be determined by re-arranging Equation 3.8 to solve for R_c. Subtracting the ice buoyancy component R_b calculated using Equation 3.5 from the total clearing component leaves only the ice-clearing component. This clearing component is a speed dependent or dynamic clearing component.

The ice-clearing coefficient is calculated for each pre-sawn test greater than creep speed using Equation 3.4. A thickness Froude number, F_n, is calculated for all pre-sawn ice tests using Equation 3.7.

The calculated C_c*'s* are then plotted against F_n on a ln-ln graph, as shown in Figure 3.5. The linear regression of the data yields:

$$C_c = e^{-0.3029} \cdot F_n^{-1.1069} \tag{3.10}$$

From the resulting linear regression line, the slope and intercept can be used later in calculating C_c for any value of F_n.

Ice breaking component, R_{br}

The clearing resistance is re-computed for the conditions that existed during the level ice resistance tests by using the plot of C_c against F_n in Figure 3.6 and its regression line. The buoyancy resistance is re-computed for the test conditions from Equation 3.3 above, given that C_b was determined in Figure 3.4. The breaking resistance R_{br} is then computed by subtracting both these from the total ice resistance, R_t. C_{br} is then calculated from Equation 3.3, and plotted against the strength number, S_n, given by Equation 3.6, on a ln-ln basis, as shown in Figure 3.6. The linear regression of the data yields:

$$C_b = e^{5.2961} \cdot S_n^{-1.8672} \tag{3.11}$$

From the resulting linear regression line, the slope and intercept can be used later in calculating C_{br} for any value of S_n.

The detailed computations are given in Appendix G.

Comparison to Spencer et al (1988) data

Spencer et al (1988) performed resistance test using the same model in three thickness: 82, 54 and 45 mm. Only the data from 45 mm thick ice (comparable to the present ice condition) is used in this comparison. Their data was re-analyzed following the standard procedure as shown in the previous section. Furthermore, Spencer et al tested the model with a friction coefficient of 0.1 while we tested the model with 0.01 hull friction, therefore Spencer et al's data was adjusted to the 0.01 friction before comparison according to the friction adjustment curves they developed for the model hull. (Their curves are re-produced in Figure 3.7.) The ice breaking components from Spencer et al's data were comparable to those from the present test series shown in Figure 3.8, showing good agreement between both data sets. The detailed computations are given in Appendix G.

3.2 Manoeuvring

3.2.1 Test results

Open water

Baseline open water manoeuvring tests were completed in the ice tank for test speeds corresponding to the ice tests conducted. Figure 3.9 shows the measured yaw moment N_{ow} versus model yaw rate r curves for the open water manoeuvring runs grouped according to rudder angle. The numerical values for the mean yaw moment at each model speed[1] are:

Model Velocity (m/s)	Rudder Angle 0 degrees		Rudder Angle 20 degrees		Rudder Angle 30 degrees	
	Mean Yaw Moment (N·m)		Mean Yaw Moment (N·m)		Mean Yaw Moment (N·m)	
	R = 10 m	R = 50 m	R = 10 m	R = 50 m	R = 10 m	R = 50 m
0.1	0.93	0.07	3.04	-0.04	3.39	0.09
0.3	-0.63	-0.90	n/a	n/a	n/a	n/a
0.6	-7.96	-4.47	-5.06	-4.96	-5.99	-5.27
0.9	-21.02	-10.41	-23.30	-10.54	-24.45	-11.78

The yaw moment (given in N) in baseline open water manoeuvring, $N_{ow,}$ for the two turning radii with zero rudder angle can be obtained from the regression lines in Figure 3.9:

$$N_{ow} = 0.4516r^2 - 0.7781r \tag{3.12}$$

where r is the yaw rate (given in deg/s). The regression lines corresponding to the other rudder angles are also given in Figure 3.9.

Ice tests

Figure 3.10 shows the measured yaw moment versus model yaw rate curves for the ice manoeuvring runs. The results for Runs 132, 133, 148, and 153 are not shown, as those measurements were suspicious due to problems with the model's initial alignment. These results were not corrected for ice strength, which may contribute to the scattering of data. The numerical values for the mean yaw moment at each speed are:

[1] Yaw Rate = Model Speed / Turning Radius

Model Velocity (m/s)	Level Ice Mean Yaw Moment (N·m)	
	R = 10 m	R = 50 m
0.02	n/a	15.86
0.05	67.91	n/a
0.1	77.58	38.24
0.2	84.26	n/a
0.3	113.52	25.96
0.4	93.42	n/a
0.5	114.19	n/a
0.6	123.00	84.81

3.2.2 Icebreaking pattern and channel width

As the ship advances into an unbroken ice field, individual cusps or wedges begin to break off from the level ice at the point of contact at the bow of the advancing side of the hull. These broken cusps and wedges are then rotated downward, pushed farther down the hull, and eventually cleared away from the hull at the sides. Once the rest of the level ice sheet contacts the hull, the same breaking process continues. This sequential icebreaking creates a channel wide enough for the passage of the hull. Figure 3.11 shows an idealization of the channel created by the hull. The breaking initiated at the bow creates an initial channel width, W_i, slightly wider than the ship's beam For a tighter turn, further ice breaking at the leeward side of the hull may be necessary to create a final channel width, W_f, wide enough for its passage.

The broken channel width was surveyed every two meters along the tank length. The actual measured data for channel edge positions in the model tests are discontinuous and unavoidable with human errors. Detailed measurements of channel width and the estimate for each run are given in Appendix E, and is summarized in the following table:

Run #	Yaw Rate *r* (deg/s)	Channel Width *w* (m)	Run #	Yaw Rate *r* (deg/s)	Channel Width *w* (m)
152	1.72	1.3	132	1.72	1.2
153	0.11	1.1	133	0.57	1.15
164	2.86	1.25	148	3.44	1.35
165	3.44	1.2	128	0.11	1
168	2.29	1.15	130	0.34	1.05
169	1.72	1.25	144	0.69	1.1
170	1.15	1.1	146	0.02	1
171	0.57	1.05	Straight	0	0.99

The result shows a slight increase in broken channel width with yaw rate as shown in Figure 3.12. Lau et al (1999) predicted a channel width of about 0.4 times the ice characteristic length, l_c, wider than the maximum ship beam, i.e., 1.02 m for the straight run which agrees well with the present measurement of 0.99 m.

The location of ice-ship contacts, and hence the local icebreaking load, can be estimated by considering the geometry of the interaction during turning. The zones for possible contact at different parts of the ship can be defined by a number of concentric circles. These circles can be enlarged or contracted by 0.2 l_c, to take account of the ice breaking at both sides as shown in Figure 3.11. For a typical ship, the zone of possible ice contact for the outer side is always larger than the inner side, and W_f is greatly dependent on the turning radius, as shown in Figure 3.13. In Figure 3.13, the measured W_f is also plotted with the theoretical W_f, showing agreement between theory and test data.

3.2.3 The effect of yaw rate on heading control of the PMM

Desired heading control with a zero drift angle β was not achieved in the present model tests. Figure 3.14 is a plot of measured drift angle versus yaw rate of the model. For a yaw rate smaller than 1 degree/s, the drift angle can be controlled to less than 0.5 degrees; however, when the required yaw rate exceeded 0.5 deg/s, the heading control became a problem since the average drift angle increased to as much as 4 degrees for a yaw rate of 3.5 deg/s.[2] This problem introduces considerable complication to the data analysis as it imposes varied amount of sway velocity to the model's motions from test to test. Nevertheless, its influence on the yaw moment will be examined using the mathematical model presented in the next section.

3.2.4 The effect of ship turning on yawing moment

The results for the turning circle runs are given in Figure 3.15. Two turning circle radii of 50 m and 10 m were tested, each with the velocity ranging from 0.02 m/s to 0.6 m/s. These velocities corresponded with a yaw rate ranging from –0.02 deg/s to –3.4 deg/s. The runs with 10 m turning manoeuvres were performed in ice with an average flexural strength of 20.1 kPa, and the runs with 50 m turning manoeuvres were performed in ice with an average flexural strength of 31.5 kPa. The data has been corrected to correspond with 20 kPa ice flexural strength before comparison. Despite large data scattering, the data shows a bi-linear relationship between yaw moment and yaw rate, with a moment offset at 12.7 Nm and 43 Nm for the 50 m and 10 m turning manoeuvres, respectively. The change in slope occurs at a yaw rate of approximately –0.5 deg/s.

[2] The version of software used was under development and had known issues related to computation of initial heading angle. This may contribute to the source of error in heading control.

The fitting of data for the 10 m turning manoeuvres at the yaw rate less than or equal to –0.5 deg/s was only approximate, as only two data points within this range were available for analysis. It was assumed to have the same slope as its 50 m counterpart.

Preliminary analysis was performed to understand the observed trend. It is believed that the moment offsets were mainly contributed by velocity independent ice breaking and submergence components, and the initial slope was determined by velocity dependent ice clearing and the open water components. The bilinear trend as exhibited by the test data and, in particular, the relatively constant yaw moment for the 10 m turning manoeuvres beyond a yaw rate of 1 deg/s, was unexpected. It is believed to be an artifact of the increase of drift angle starting at approximately –0.5 deg/s yaw rate, due to the poor heading control of the PMM system as shown in the preceding section and explained in Section 4.

4.0 MATHEMATICAL MODELING

In the following section, a conceptual model of turning moment imposed on the ship hull during a steady turn is presented with its preliminary implementation. The discussion will be focused on the initial moment offsets, and the effect of the interaction geometry on their values. This model forms the framework for future mathematical model development. This report only details the velocity independent load components of the model.

4.1 Effect of Ice/Ship Interaction Geometry on Yaw Moment

Ice breaking during turns is complex, and it depends not only on the interaction geometry but also on its load history (or load memory). The stochastic nature of ice breaking further complicates the analysis. For simplicity, we will consider a simple ice breaking geometry at the bow with a zero sway velocity, i.e., a perfect heading. We will also consider only the ice breaking component and a situation where the ship model turns at a very low speed, i.e., V_m=0.02 m/s. While the ship turns, it affects the ice breaking patterns at both side of the bow, and initiates an imbalance of sway force acting on the bow, even with a negligible speed. During a steady turn at this speed, it is anticipated that the ice breaking patterns (and hence the unbalance sway forces) are highly sensitive to the turning radius *R*, but not the sway velocity *v* nor yaw rate *r*. For this geometric consideration alone, we will expect another term N_o to be included at the left hand side of Equation 4.1 to account for this influence:

$$-N_o - N_v v - N_r r = N \tag{4.1}$$

where N_v is the ice derivative for sway velocity, *v*
N_r is the ice derivative for yaw moment, *r*
N is the total yaw moment

N_o is believed to be a function of ship/ice interaction geometry and ice properties in relation to ice breaking, i.e., *R*, *L* (ship length), *B* (ship beam), ice strength, ice thickness, etc. This component may be derived by considering static ice load distribution around the hull using appropriate ice models and interaction geometry (See Section 4.2.). This will contribute to the moment offset.[3] The term N_o may be measured by performing creeping speed model test with zero drift angle for different turning radius *R*. Since the velocity for this test is negligible, the yaw moment will contribute to this term only. Section 4.3 shows the effect of drift angle on the value of N_o as predicted by the analytical model presented in this report.

[3] There may also be a velocity dependent ice breaking component which can be incorporated into N_r and N_v

N_v is the sway velocity dependent component when $v \neq 0$. In most operation conditions, the ship's yaw velocity is substantial and this term cannot be ignored. N_v may be estimated by performing a straight run with a range of constant drift angle.

The contribution from water and broken ice resistance to N_r can be estimated by a number of existing methods. One method (Menon et al, 1986) used in this work is by assuming an unbalance sway force (hence, the moment) as a function of the difference in ice and water volumes that is created by the two sides of the ship during a steady turn. N_r may be estimated by performing a constant yaw run with zero drift angle.

4.2 Components for Ship Model Manoeuvring in Ice

Analogous to ice resistance (Spencer, 1992), the expression for total yaw moment, N_{tot}, is divided into the hydrodynamic, N_{ow}, icebreaking, N_{br}, ice submergence (buoyancy component), N_b, and ice clearing, N_c, components:

$$N_{tot} = N_{br} + N_c + N_b + N_{ow} \tag{4.2}$$

The fundamental reason for this approach is that different components may not all scale to full-scale in the same manner. The icebreaking term has ice strength and ice thickness as parameters, and takes into account the effect of channel width and interaction geometry on the zone of application of the ice forces. The ice submergence term calculates the buoyancy forces. These two components are insensitive to model speed, and hence contribute to the moment offset at zero ship speed. The ice clearing and the open water terms include ice added mass and inertial contribution, and hence are velocity dependent.

This section presents a simple analysis of the ice breaking and buoyancy components to illustrate the importance of ship-ice interaction geometry during ship manoeuvring.

4.2.1 Breaking component, N_{br}

For the case of a semi-infinite beam on an elastic foundation end loaded by a concentrated transverse force, the maximum vertical load per unit width, P_{Vm}, and the associated end deflection, y_m, are given as follows:

$$P_{Vm} = 0.68\sigma_f(\gamma_w \cdot h_i^5 / E)^{1/4} \tag{4.3}$$

$$y_m = \frac{2P_{Vm}}{l_c \cdot \gamma_w} \tag{4.4}$$

where σ_f is the flexural strength of ice

γ_w is the specific weight of water
h is the thickness of ice
E is the Young's modulus of ice
l_c is the characteristic length of the ice beam

Assuming an idealization of the ice breaking force-displacement history, as shown in Figure 4.1, the maximum displacement of the ship in the forward direction, a, before ice failure, is related to y_m:

$$a = y_m / \tan \alpha \tag{4.5}$$

where α is the stem angle

If the average breaking length, l_a, is taken as $0.2l_c$ (Lau et al., 1999), then the average vertical force per unit width, P_{Va}, acting on the ship surface where ice breaking occurs is equal to:

$$P_{Va} = P_{Vm} \frac{a}{2 * 0.2 l_c} = 5.7 \frac{\sigma_f^2 \cdot h_i}{E \cdot \tan\alpha} \tag{4.6}$$

Assume that the ship manoeuvres at a constant yaw rate with a radius, R, as shown in Figure 4.2. We will neglect the frictional component and assume the energy required for ice-breaking is proportional to the volume of broken ice created. If the effects of the broken ice pieces' sizes are neglected, then the ice will contact the bow and the half side of the hull with the three horizontal loads, F_{h1}, F_{h2}, F_{h3}, which can be computed as follows:

$$F_{h1} = P_{Va}(l_1 - l_2) \tan \phi \tag{4.7}$$

$$F_{h2} = P_{Va}(l_2 - l_3) \tan \phi \tag{4.8}$$

$$F_{h3} = P_{Va}(l_3 - l_4) \tan \eta \tag{4.9}$$

where l_1, l_2, l_3 and l_4 are the geometric lengths as shown in Figure 4.2
ϕ is the angle between the normal of the bow and the vertical line
η is the angle between the hull side surfaces and the vertical line

Hence, the yaw moment due to ice breaking from the forward part is given as follows:

$$N_{br} = \left(-F_{h1} + F_{h2}\right) \cdot l_5 + F_{h3} \cdot l_6 \tag{4.10}$$

where l_5 and l_6 are the lengths between the respective force centers to the ship's mass center

We used a two dimensional beam-bending model, in which the structure was regarded as having an infinite width. The edge effects should be considered when calculating ice forces. Modification to the above formulation was implemented by considering the ice breaking width adjustments, ∇l_1 and ∇l_2, as shown in Figure 4.3. By assuming the following proportionality from a geometric consideration:

$$\frac{\nabla l_1}{\nabla l_2} = \frac{l_1 - l_2}{l_2 - l_3} \tag{4.11}$$

The total width, W_b, of ice broken by the bow is equal to:

$$W_b = \nabla l_1 + \nabla l_2 + l_1 - l_3 \tag{4.12}$$

4.2.2 Submergence component, N_b

The buoyancy force on the hull was calculated by considering the amount of ice covering the different parts of the hull. For the bow part, as shown in Figure 4.4, the vertical components, F_{v_1} and F_{v_2}, of the buoyant forces acting at the respective side of the bow can be calculated using the following equations:

$$F_{v\_1} = \frac{l_1 - l_2}{l_1 - l_3}(\gamma_w - \gamma_i)hS \tag{4.13}$$

$$F_{v\_2} = \frac{l_2 - l_3}{l_1 - l_3}(\gamma_w - \gamma_i)hS \tag{4.14}$$

where γ_i is the specific weight of ice
S is the horizontal projection of the bow surface

Ignoring the ice/hull friction, the corresponding horizontal forces, F_{h_1} and F_{h_2}, on the respective side of the bow due to buoyancy are given as follows:

$$F_{h\_1} = \frac{l_1 - l_2}{l_1 - l_3}(\gamma_w - \gamma_i)hS \tan(\phi) \tag{4.15}$$

$$F_{h\_2} = \frac{l_2 - l_3}{l_1 - l_3}(\gamma_w - \gamma_i)hS \tan(\phi) \tag{4.16}$$

And the yaw moment, N_b, due to buoyancy forces from the bow is equal to:

$$N_b = \left(-F_{h\_1} + F_{h\_2}\right) \cdot l_5 \quad (4.17)$$

The lengths l_1, l_2, l_3 and l_5 are given in Figure 4.2. Similarly, the buoyant forces on other parts of the wetted surface of the hull can also be calculated.

4.3 Effect of Turning Radius on the Static Yaw Moments

According to the present model, the components N_{br} and N_b are independent of yaw rate, but greatly influenced by the turning radius, *R*, as shown in Figure 4.5. As the ship manoeuvres in tighter turns, it needs to break more ice at the inner side, resulting in an increasing yaw moment.

The total measured yaw moment due to the components N_{br} and N_b, corresponding to the two turning radii extrapolated to zero yaw rate, were compared to the present model in Figure 4.5. As shown in the figure, the model predicts a yaw moment of 30.7 Nm and 6.5 Nm for the 10 m and 50 m radii, respectively. In comparison with the measured values for 43 Nm and 12.7 Nm, the model under-predicted the moment offset by 29% and 49% for the 10 m and 50 m tests, respectively.

In the present analysis, the friction force and the in-planed ice compression were neglected in order to make the problem simpler. This tends to underestimate the ice load where a steep slope is present, i.e. at the side hull. When calculating the buoyancy force, some assumptions were made for the broken ice motions. All these simplifications may introduce uncertainties and errors to the predictions.

4.4 Effect of Drift Angle on the Static Yaw Moments

During turn manoeuvres, the drift angle may vary depending on the prevailing ice and ship conditions. Drift angle affects the location of ice ship contacts, and hence the resulting yaw moment component N_o. According to the proposed model, N_o can either be increased or decreased depending on the direction of the drift angle, as shown in Figure 4.6.

4.5 Possible Cause of the Bi-Linear Trend for Yaw Moment as Observed in this Model Test Series

The bi-linear trend with a moment offset as observed in the yaw moment versus yaw rate curve (see Figure 3.15) was different from that observed with previous open water tests of the same manoeuvres. Sections 4.1 and 4.2 give mathematical basis for the moment offset, observed with a satisfactory prediction.

This bi-linear behaviour is believed to be a result of the increase of draft angle with yaw rate associated with this test series (see Figure 4.6). However, further experimenting is needed to confirm this.

5.0 SUMMARY

In this report, the results from a multi-faceted study of ship manoeuvring test series were presented. A total of 43 ice test runs (using five different ice sheets) were used to generate data to analyse the manoeuvring characteristics (28 resistance test and 15 manoeuvring tests). A simple analysis illustrated the importance of interaction geometry on the interaction processes and the resulting yaw moment. Despite the simplicity of the problem treatment, the analysis gave a favourable prediction. Future work will include a refinement of the problem treatment, as well as an extensive series of numerical and physical experiments with the aim of developing a mathematical model to successfully predict a ship's manoeuvring performance in various ice conditions.

6.0 REFERENCES

Derradji-Aouat, A. (2004). “A Method for Calculations of Uncertainty in Ice Tank Ship Resistance Testing.” Proceedings of the 19th International Symposium on Sea Ice, Mombetsu, Japan.

Lau, M. and Derradji-Aouat, A. (2006). “Phase IV Experimental Uncertainty Analysis for Ice Tank Ship Resistance and Manoeuvring Experiments using PMM.” IOT/NRC report # TR-2006-02, Institute for Ocean Technology, St. John’s, Newfoundland.

Lau M., Mogaard J., Williams, F.M., and A. Swamidas (1999). “An Analysis of Ice Breaking Pattern and Ice Piece Size around Sloping Structures”. Proceedings of 18th International Conference on Offshore Mechanics and Arctic Engineering, St. John’s, Newfoundland, pp1-9.

Marineering Limited (1997). “The Development and Commissioning of a Large Amplitude Planar Motion Mechanism. Volume 1: Main Report.” IMD/NRC report # CR-1997-05, Institute for Ocean Technology, St. John’s, Newfoundland.

Menon B.C., Glen I.F., Steel M., and K. Hardiman (1991). “Investigation of Ship Manoeuvrability in Ice –Phase I.” Transport Canada, TP 10922E.

Spencer, D. (1992). “A Standard Method for the Conduct and Analysis of Ice Resistance Model Tests.” Proceedings of the 23rd ATTC, New Orleans, pp. 301-307.

Spencer, D.S. and Harris, C. (1997). “The Development and Commissioning of a Large Amplitude Planar Motion Mechanism for Manoeuvring of Ships in Ice and Open Water.” Contract Report CR-1997-5, NRC/IOT, St. John’s, Newfoundland.

Spencer, D., Molyneux, D., and A. Keinonen (1988). “Model Tests of M/V.’s *Terry Fox / Kalvik* and Their Correlation to Full-Scale.” IOT/NRC report # TR-AVR-12, Institute for Ocean Technology, St. John’s, Newfoundland.

Spencer, D.S. and Timco, G.W. (1993). “CD Model Ice – A Process to Produce Correct Density (CD) Model Ice.” Proceedings of the 10th International IAHR Symposium on Ice, Vol. 2, Espoo, Finland, pp. 745-755.

Table 2.1: Model Hydrostatics

IOT Model #417, scale 1/21.8, without appendages	
Displacement (kg)	665.6
Waterline Length (m)	3.739
Waterline Beam at Mid-Ship (m)	0.789
Draught at Mid-Ship (m)	0.368
Center of Buoyancy Forward of Mid-Ship (m)	-0.07
Center of Aft Body Buoyancy Forward of Mid-Ship (m)	0.594
Stem Angle (º)	23.27
Waterline Entrance Angel (º)	32.15

Table 2.2: Specifications of the PMM

Max Sway Amplitude (m)	± 4.0
Max Yaw Amplitude (º)	± 175
Max Sway Velocity (m/s)	± 0.70
Max Yaw Rate (º/s)	± 60.0
Max Sway Force (N)	± 2200
Max Yaw Moment (N-m)	± 3000

Table 2.3: Matrix of the test program

Turning Radius, *R*	∞	50	10
Rudder Angle (º)	0, 20, 30	0	
Model Speed,	0.02~0.9	0.02~0.6	
Yaw Rate, *r* (deg/s)	0	0.02~ 0.34	
Drift Angle, β (º)	0		
Ice Thickness (mm)	40		
Ice Strength (kPa)	35		

Table 3.1a: Summary of test results (open water tests)

Open Water Test	Model Speed (m/s)	Yaw Rate (deg/s)	Arc Radius (m)	Rudder Angle (deg)	Surge Resistance (N)	Yaw Resistance (Nm)
OW1_OP1_RA0_AR999_053	0.10	n/a	Straight	0	-0.2	n/a
OW1_OP6_RA0_AR999_054	0.60	n/a	Straight	0	4.3	n/a
OW2_0P9_RA0_AR999_057	0.90	n/a	Straight	0	10.1	n/a
OW4_0P1_RA0_AR50_058	0.10	0.12	50	0	-0.1	-0.1
OW5_0P6_RA0_AR50_059	0.60	0.69	50	0	4.4	-1.5
OW6_0P9_RA0_AR50_060	0.90	1.03	50	0	10.4	1.2
OW7_0P1_RA0_AR10_061	0.10	0.57	10	0	-1.1	-0.8
OW8_0P6_RA0_AR10_062	0.61	3.43	10	0	7.6	-9.0
OW9_0P9_RA0_AR10_063	0.91	5.15	10	0	19.4	-15.6
OW9A_0P9_RA0_CR10_064	0.90	5.14	10	0	22.6	-10.3
OW9A_0P9_RA0_CR10_064	0.89	5.15	10	0	24.1	-9.4
OW9A_0P9_RA0_CR10_064	0.90	5.14	10	0	21.4	-11.1
OW10_0P1_RA20_CR999_065	0.10	n/a	Straight	20	-0.3	n/a
OW10_0P6_RA20_CR999_066	0.60	n/a	Straight	20	4.7	n/a
OW12_0P9_RA20_CR999_067	0.90	n/a	Straight	20	11.0	n/a
OW13_0P1_RA20_AR50_068	0.10	0.12	50	20	0.0	0.2
OW14_0P6_RA20_AR50_069	0.60	0.69	50	20	5.0	6.7
OW15_0P9_RA20_AR50_070	0.90	1.03	50	20	10.5	20.9
OW16_0P1_RA20_CR10_071	0.10	0.57	10	20	-3.0	-0.4
OW16_0P1_RA20_CR10_071	0.10	0.57	10	20	-2.2	-0.3
OW16_0P1_RA20_CR10_071	0.10	0.57	10	20	-3.8	-0.4
OW17_0P6_RA20_CR10_072	0.60	3.42	10	20	5.1	3.0
OW17_0P6_RA20_CR10_072	0.59	3.42	10	20	5.6	2.6
OW17_0P6_RA20_CR10_072	0.61	3.43	10	20	4.5	3.4
OW18_0P9_RA20_CR10_073	0.90	5.14	10	20	23.3	22.1
OW18_0P9_RA20_CR10_073	0.89	5.14	10	20	25.6	19.9
OW18_0P9_RA20_CR10_073	0.90	5.14	10	20	21.1	24.3
OW19_0P1_RA30_CR999_074	0.10	n/a	Straight	30	-0.4	n/a
OW20_0P6_RA30_CR999_075	0.60	n/a	Straight	30	5.4	n/a
OW21_0P9_RA30_CR999_076	0.90	n/a	Straight	30	12.6	n/a
OW22_0P1_RA30_AR50_077	0.10	0.11	50	30	-0.1	0.4
OW23_0P6_RA30_AR50_078	0.60	0.69	50	30	5.3	10.0
OW24_0P9_RA30_AR50_079	0.90	1.03	50	30	11.8	26.7
OW25_0P1_RA30_CR10_080	0.11	0.57	10	30	-3.3	-0.5
OW25_0P1_RA30_CR10_080	0.10	0.57	10	30	-2.7	-0.8
OW25_0P1_RA30_CR10_080	0.11	0.57	10	30	-4.0	-0.2
OW26_0P6_RA30_CR10_081	0.60	3.42	10	30	6.0	6.2
OW26_0P6_RA30_CR10_081	0.59	3.42	10	30	6.9	4.7
OW26_0P6_RA30_CR10_081	0.61	3.42	10	30	5.1	7.7

Table 3.1a Summary of test results (open water tests) (con't)

Open Water Test	Model Speed (m/s)	Yaw Rate (deg/s)	Arc Radius (m)	Rudder Angle (deg)	Surge Resistance (N)	Yaw Resistance (Nm)
OW27_0P9_RA30_CR10_082	0.90	5.14	10	30	24.5	31.8
OW27_0P9_RA30_CR10_082	0.89	5.15	10	30	27.3	30.9
OW27_0P9_RA30_CR10_082	0.90	5.13	10	30	22.1	32.5
OW25A_0P1_RA30_CR10_083	0.10	0.57	10	30	-3.5	-0.4
OW25A_0P1_RA30_CR10_083	0.10	0.57	10	30	-2.7	-0.4
OW25A_0P1_RA30_CR10_083	0.10	0.57	10	30	-4.2	-0.4
OW28_0P1_OP6_0P9_RA00_CR999_084	0.10	n/a	Straight	0	0.4	n/a
OW28_0P1_OP6_0P9_RA00_CR999_084	0.60	n/a	Straight	0	4.9	n/a
OW28_0P1_OP6_0P9_RA00_CR999_084	0.90	n/a	Straight	0	10.4	n/a
OW29_0P6_RA0_AR999_096	0.60	n/a	Straight	0	4.8	n/a
OW30_0P3_RA0_AR999_097	0.30	n/a	Straight	0	1.3	n/a
OW33_0P3_RA0_AR50_098	0.30	0.34	50	0	0.9	-0.3
OW36_0P3_RA0_AR10_099	0.30	1.71	10	0	0.6	-3.1
OW28_0P1_RA0_AR999_100	0.10	n/a	Straight	0	0.1	n/a
OW31_0P1_RA0_AR50_101	0.10	0.11	50	0	-0.1	-0.3
OW32_0P6_RA0_AR50_102	0.60	0.69	50	0	4.5	-0.6
OW34_0P1_RA0_AR10_103	0.10	0.57	10	0	-0.7	-0.6
OW35A_0P6_RA0_AR10_105	0.61	3.42	10	0	8.3	-7.8

Table 3.1b: Summary of test results (pre-sawn ice tests)

Pre-sawn Ice Test	Surge Resistance (N)	Yaw Resistance (Nm)
ps_sqp_023	0.10	13.8
ps_sqp_023	0.60	31.2
ps_sqp_023	0.90	46.1
ps_sqp_023	0.02	11.2
PRESAWN_SQP_HB_112	0.10	6.0
PRESAWN_SQP_HB_112	0.30	9.0
PRESAWN_SQP_HB_112	0.60	16.4
PRESAWN_SQP_HB_112	0.02	4.5
PRESAWN_SQP_SC_113	0.10	2.0
PRESAWN_SQP_SC_113	0.30	4.9
PRESAWN_SQP_SC_113	0.60	12.7

Table 3.1c: Summary of test results (level ice tests)

Level Ice Test	Model Speed (m/s)	Yaw Rate (deg/s)	Arc Radius (m)	Surge Resistance (N)	Yaw Resistance (Nm)
lir_022	0.10	n/a	Straight	56.0	n/a
lir_022	0.60	n/a	Straight	79.3	n/a
lir_022	0.90	n/a	Straight	87.5	n/a
lir_022	0.02	n/a	Straight	38.0	n/a
LIR_CC_111	0.10	n/a	Straight	43.2	n/a
LIR_CC_111	0.30	n/a	Straight	40.5	n/a
LIR_CC_111	0.60	n/a	Straight	50.7	n/a
LIR_CC_111	0.02	n/a	Straight	34.3	n/a
LIR_NQP_114	0.10	n/a	Straight	19.8	n/a
LIR_NQP_114	0.60	n/a	Straight	26.8	n/a
LIR_NQP_114	0.90	n/a	Straight	45.9	n/a
LIR_NQP_114	0.02	n/a	Straight	18.0	n/a
LIR11_0P1_AR50_128	0.10	0.11	50	33.8	38.2
LIR11A_0P1_129	0.10	n/a	Straight	17.6	n/a
LIR12_0P3_AR50_130	0.30	-0.34	50	40.4	26.0
LIR12A_0P3_131	0.30	n/a	Straight	13.7	n/a
LIR13_0P3_AR10_132	0.30	-1.70	10	31.5	134.7
LIR14_0P1_AR10_133	0.10	-0.57	10	23.3	115.2
LIR_SQP_134	0.10	n/a	Straight	8.1	n/a
LIR_SQP_134	0.30	n/a	Straight	13.6	n/a
LIR_SQP_134	0.60	n/a	Straight	21.8	n/a
LIR21_OP6_AR50_144	0.60	-0.69	50	54.9	84.8
LIR21A_OP6_145	0.60	n/a	Straight	42.4	n/a
LIR22_OP02_AR50_146	0.02	0.00	50	28.9	15.9
LIR23A_OP6_AR10_148	0.61	-3.41	10	52.4	108.4
LIR24A_SQP_149	0.10	n/a	Straight	12.1	n/a
LIR24A_SQP_149	0.30	n/a	Straight	17.9	n/a
LIR24A_SQP_149	0.60	n/a	Straight	25.9	n/a
LIR24A_SQP_149	0.02	n/a	Straight	-3.8	n/a
LIR24B_SQP_150	0.10	n/a	Straight	11.0	n/a
LIR24B_SQP_150	0.02	n/a	Straight	9.0	n/a
LIR25_0P3_AR10_152	0.30	1.71	10	0.22	111.5
LIR24_0P02_AR10_153	0.02	0.12	10	0.01	123.2
LIR31_0P6_AR10_164	0.61	3.38	10	0.40	123.0
LIR31_0P6_AR10_165	0.50	2.85	10	0.37	114.2
LIR33_0P4_AR10_168	0.40	2.28	10	0.29	93.4
LIR34_0P3_AR10_169	0.30	1.70	10	0.22	115.6
LIR35_0P2_AR10_170	0.20	1.14	10	0.14	84.3
LIR36_0P1_AR10_171	0.10	0.56	10	0.07	77.6
LIR37_0P05_AR10_172	0.05	0.29	10	0.04	67.9

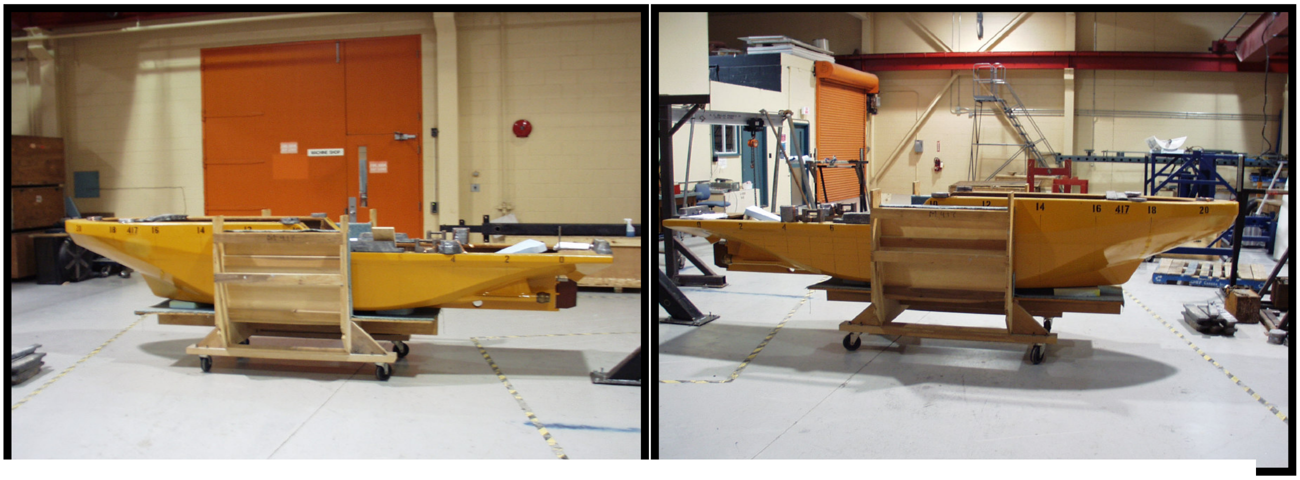

Figure 2.1 a: ***Terry Fox*** **model on the shop floor (model in its wooden cradle)**

Figure 2.1 b: ***Terry Fox*** **model on the swing frame on the shop floor**

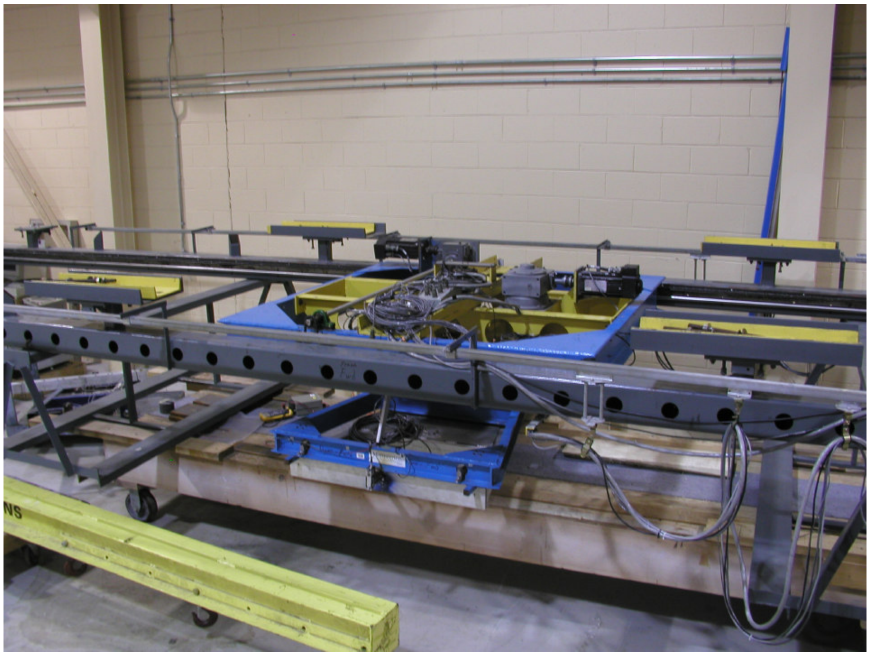

Figure 2.2 a: Actual Planar Motion Mechanism (PMM) on the shop floor

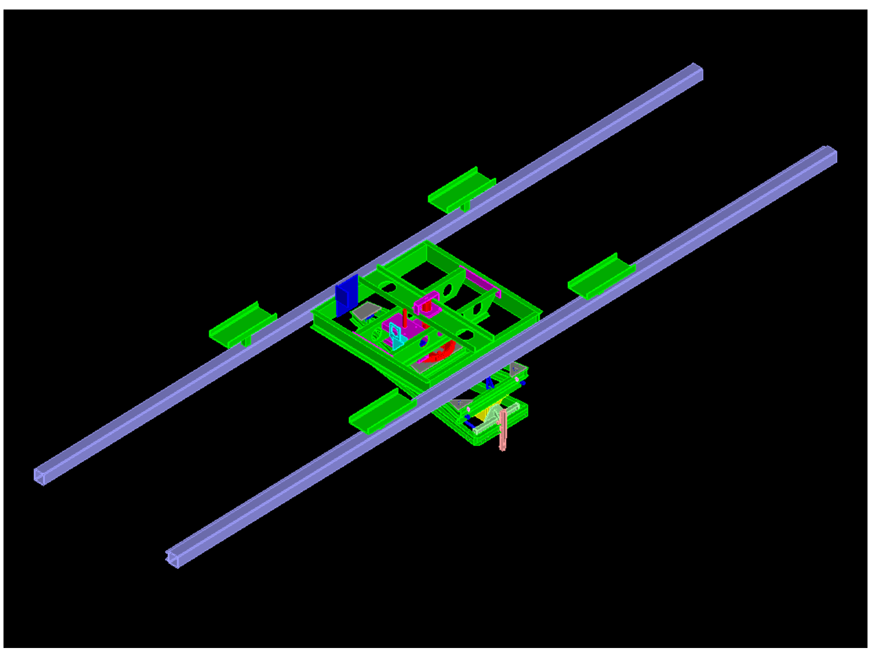

Figure 2.2 b: CAD top isometric view for the PMM

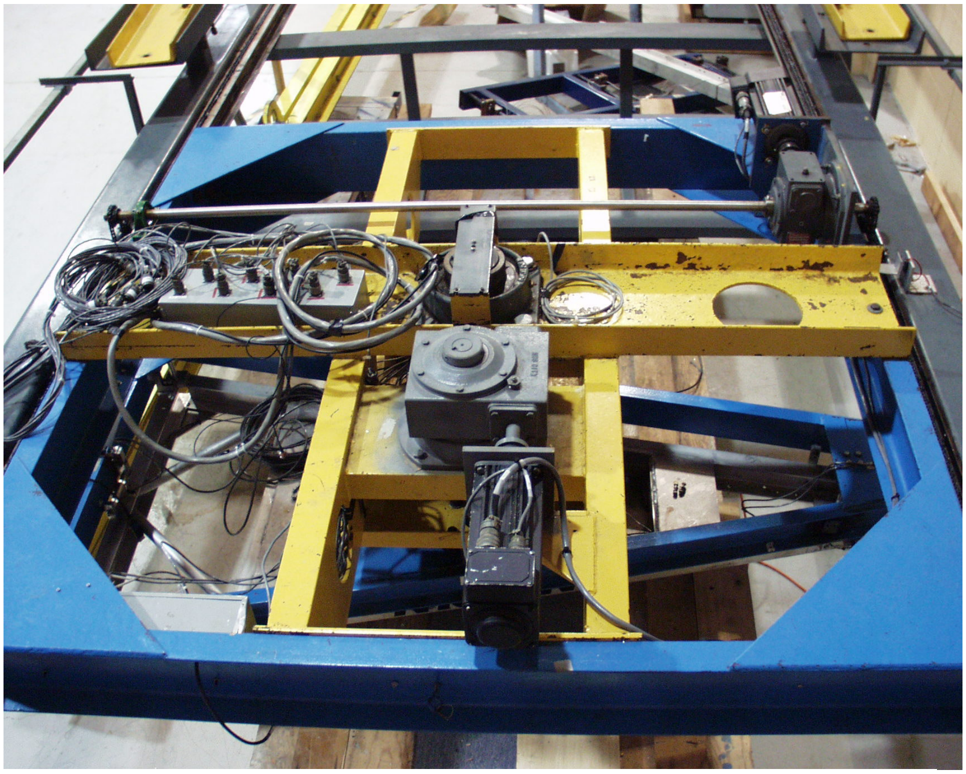

Figure 2.2 c: Actual Planar Motion Mechanism (PMM) (top view)

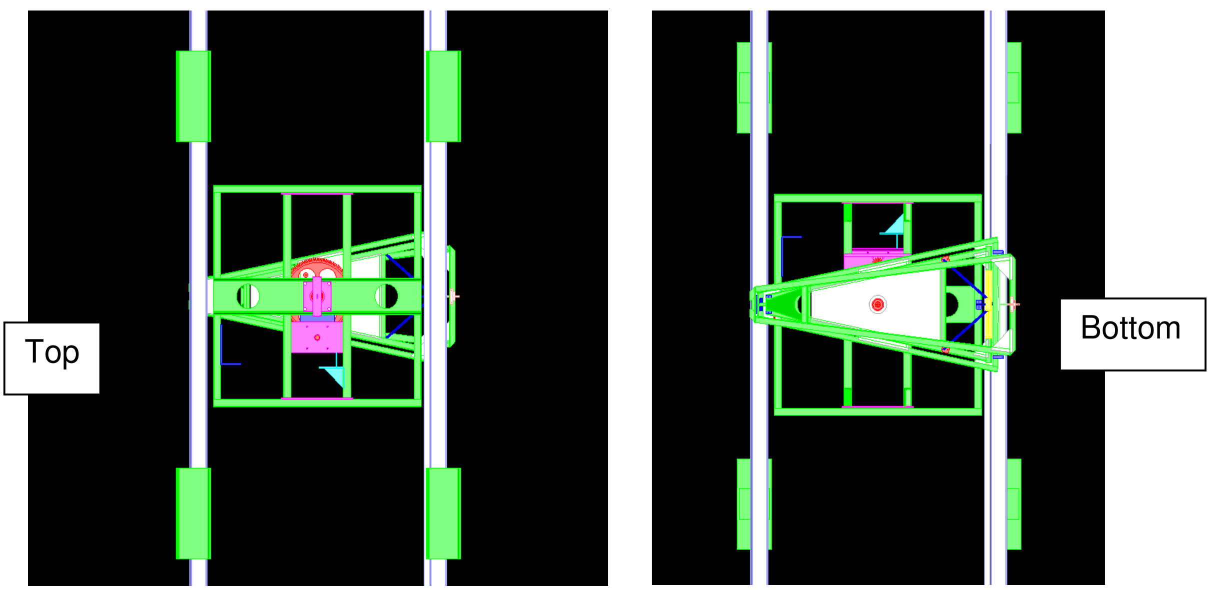

Figure 2.2 d: Top and bottom CAD views of the PMM

Figure 2.3: Typical test run in ice

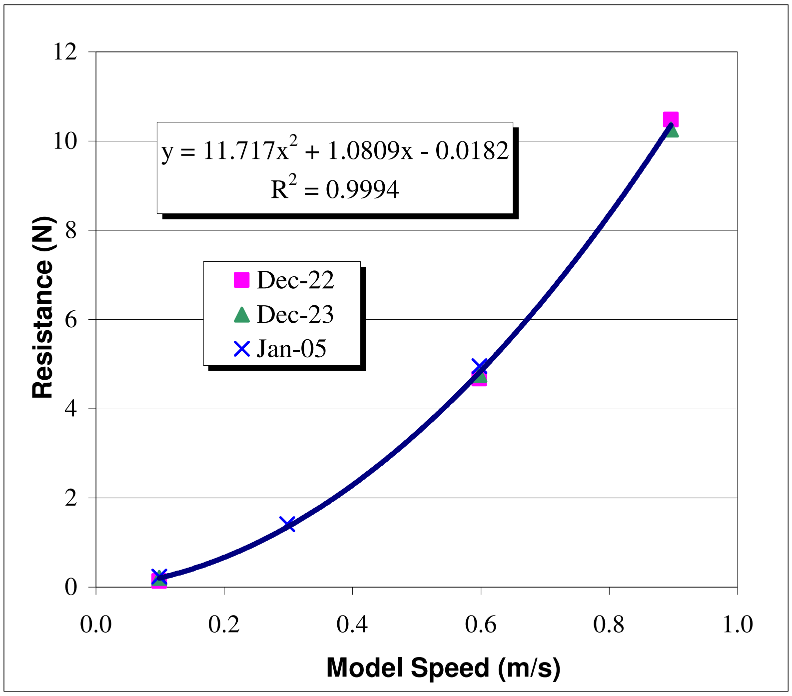

Figure 3.1: Open water resistance tests

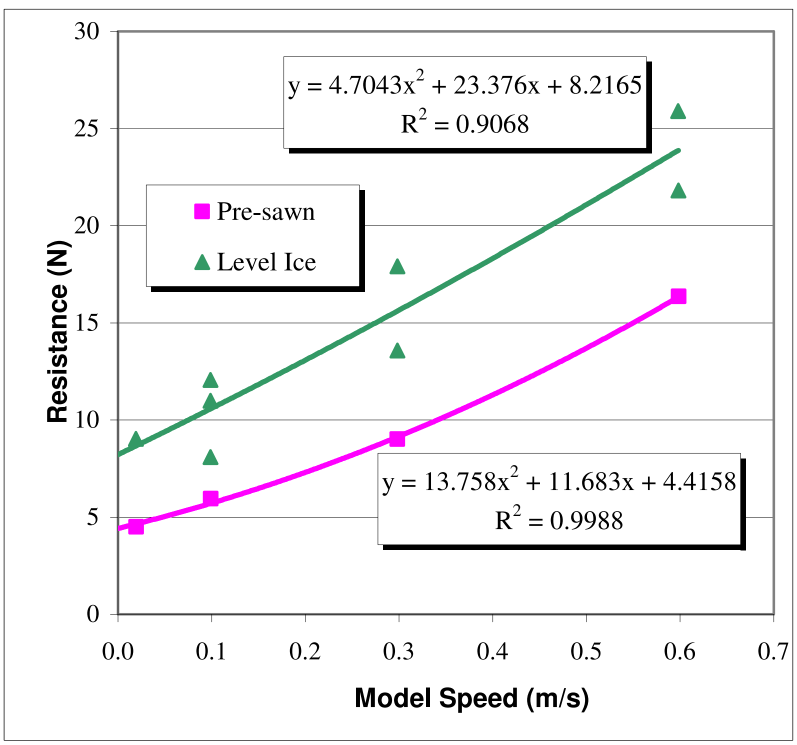

Figure 3.2: Ice resistance tests

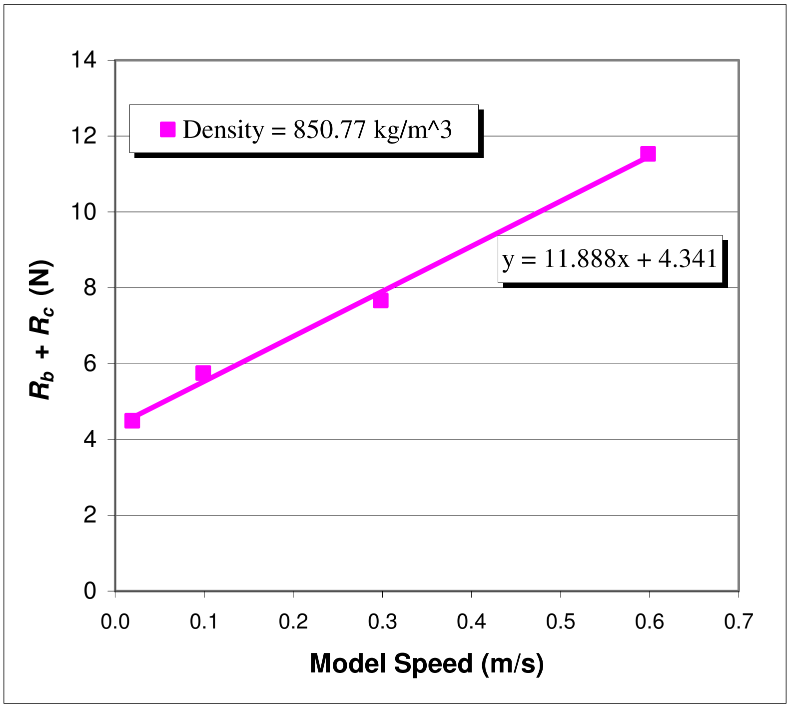

Figure 3.3: Clearing and buoyancy resistance, R_c+R_b, plotted as a function of model speed

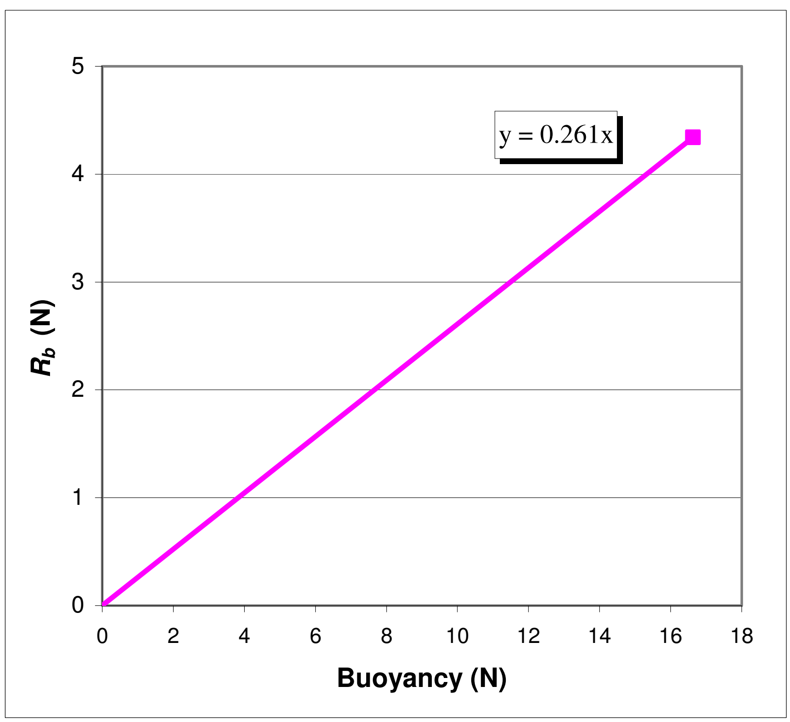

Figure 3.4: The creeping speed buoyancy, R_b, plotted against calculated ice buoyancy, $\Delta\rho_i g B h_i T$. The slope of the least squares regression line through the origin gives C_b

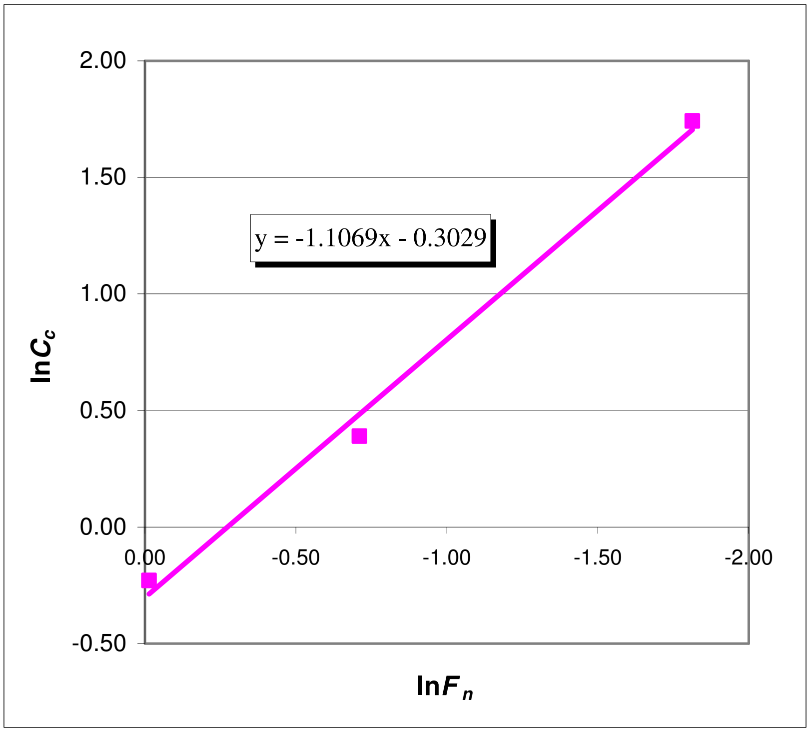

Figure 3.5: An ln-ln plot of clearing coefficient C_c against thickness Froude number, F_n. A least squares regression line and its equation are shown.

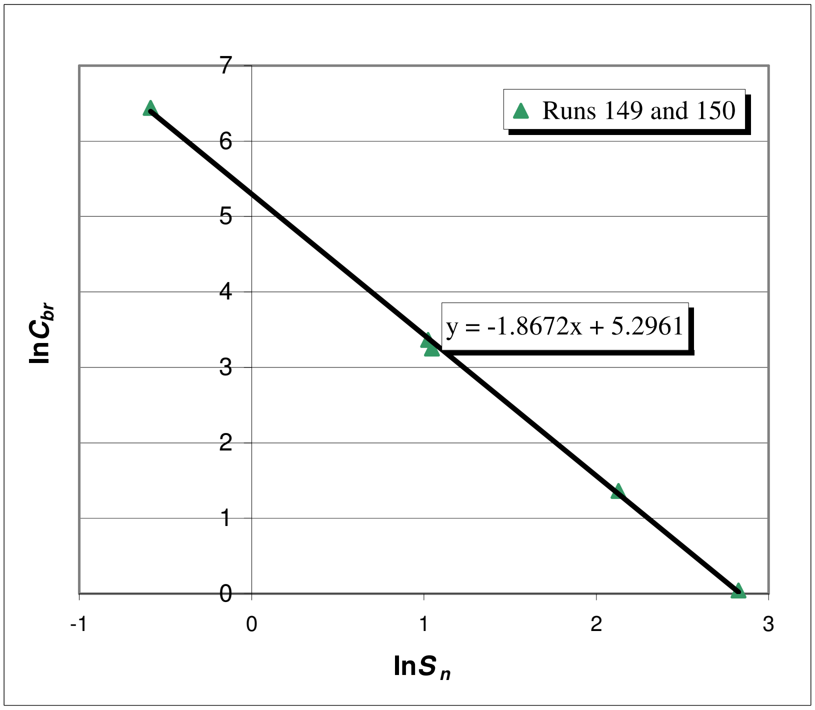

Figure 3.6: A ln-ln plot of the breaking coefficient, C_{br}, against the strength number, S_n

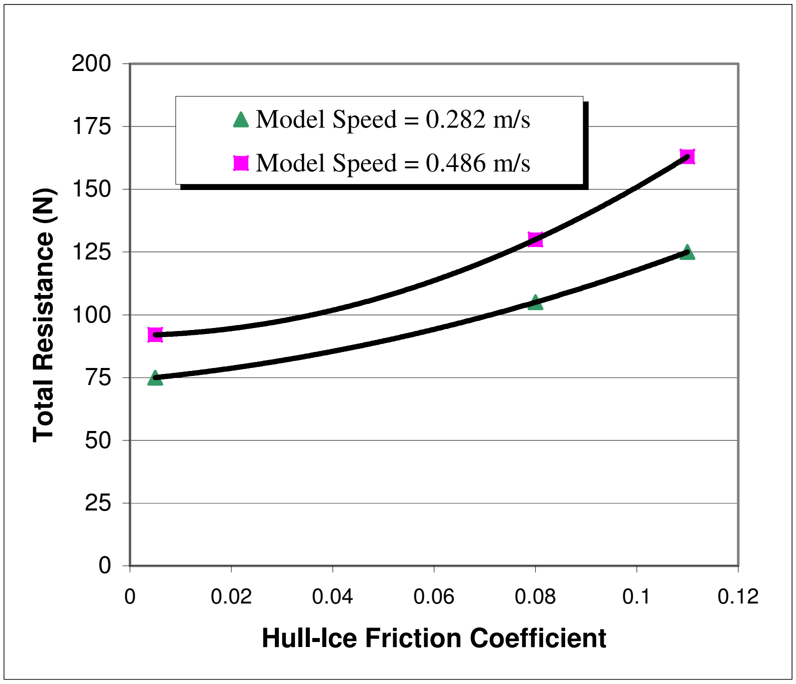

Figure 3.7: Total resistance vs. hull-ice friction coefficient (reproduced from Spencer et al, 1988)

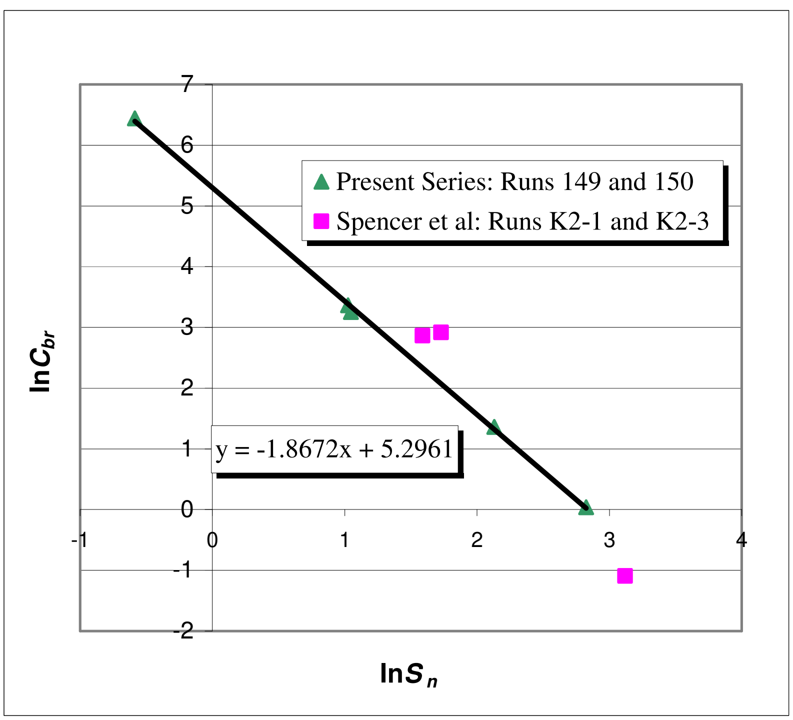

Figure 3.8: Correlation of model test data between Spencer et al (1988) and the present series

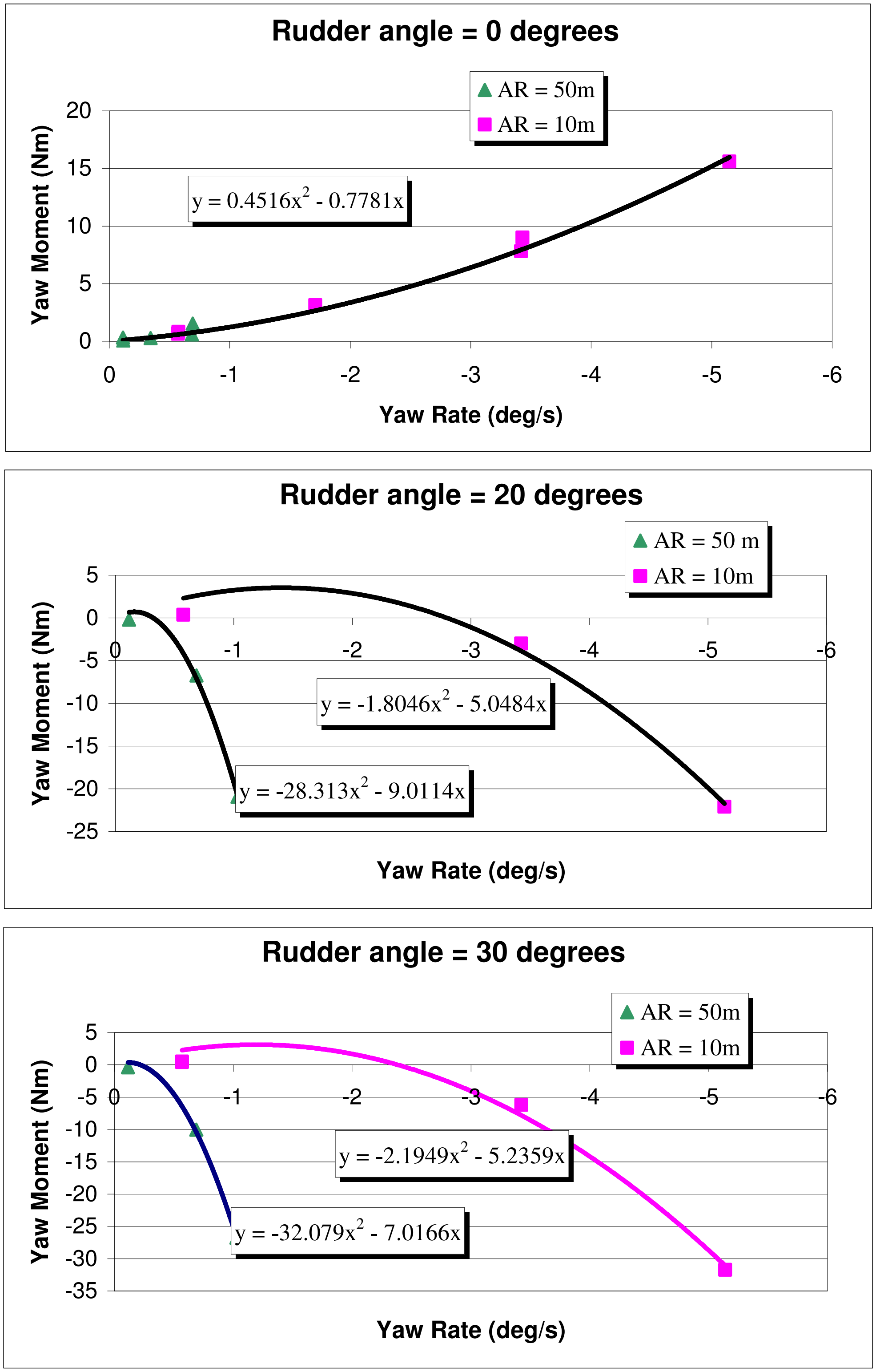

Figure 3.9: Results for open water manoeuvring tests (yaw moment)

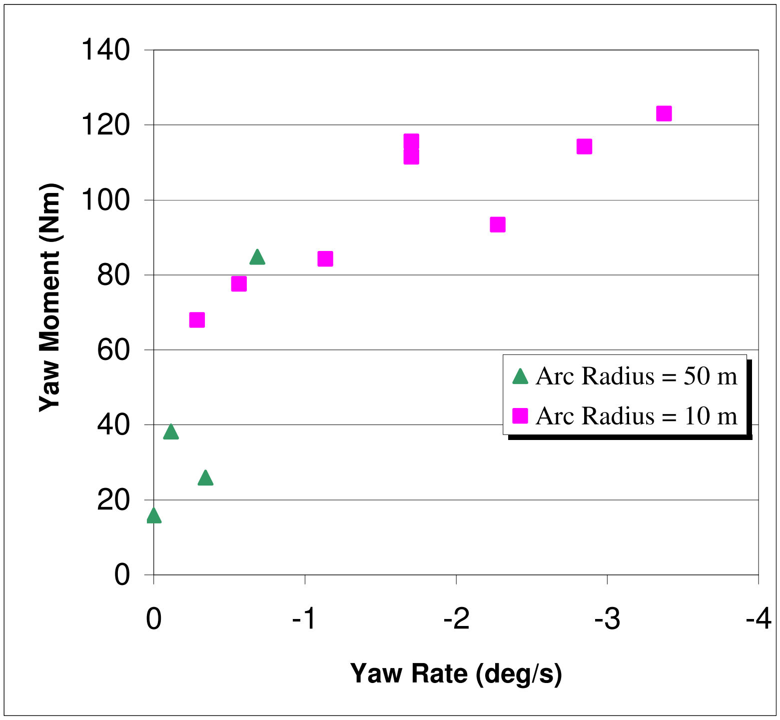

Figure 3.10: Results for ice manoeuvring tests (yaw moment)

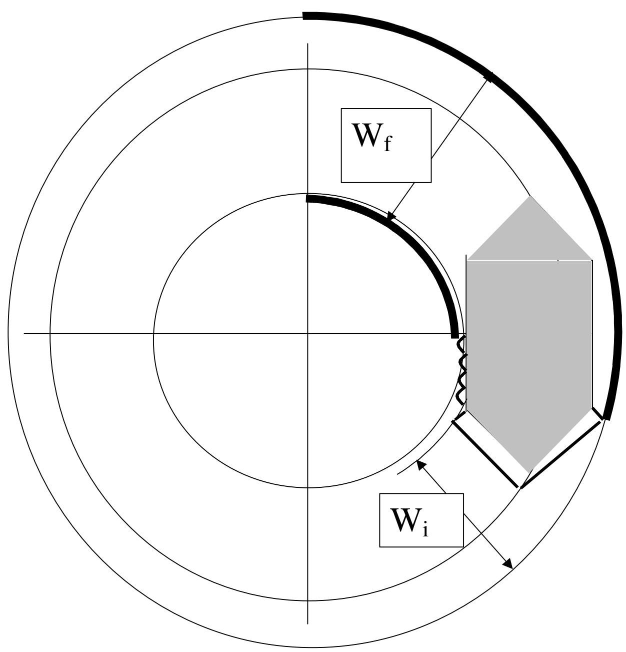

Figure 3.11: The influence of turning motion on channel width, showing the ice breaking at the bow and hull (the piece size is assumed to be 0.2 l_c)

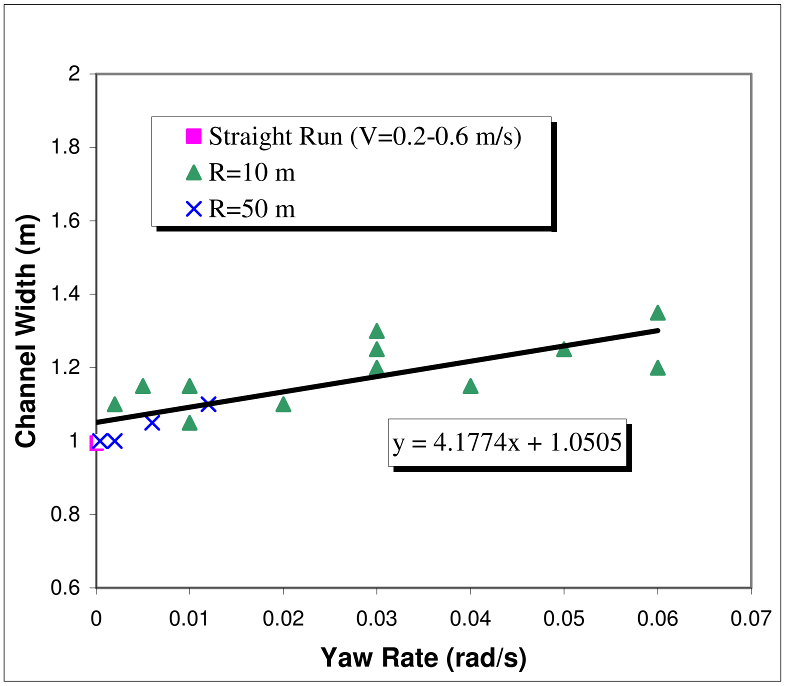

Figure 3. 12: Broken channel width as a function of yaw rate

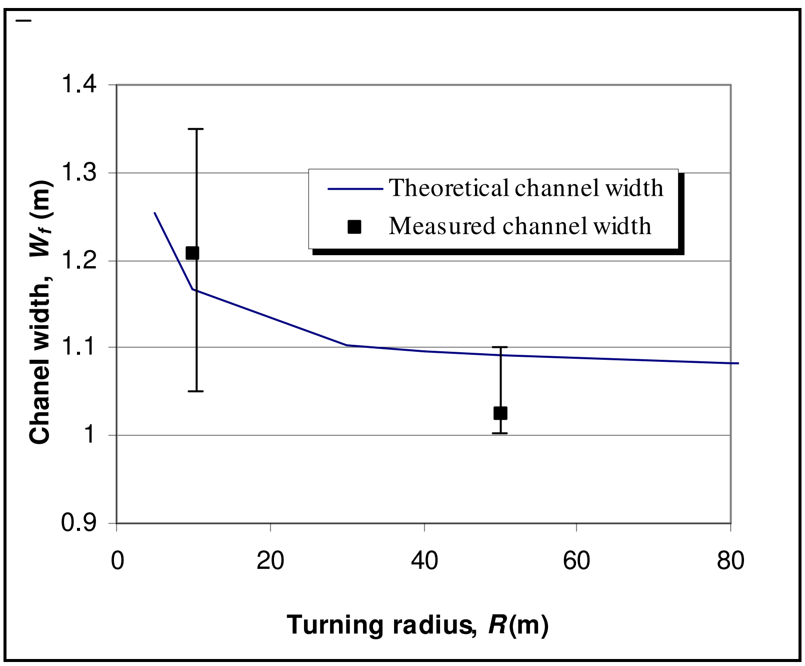

Figure 3. 13: Theoretical and measured channel width as a function of the turning radius (Note: Error bars have ranges of: For R = 10m, W_f = 1.05-1.35m, and for R = 50m, W_f = 1-1.1m).

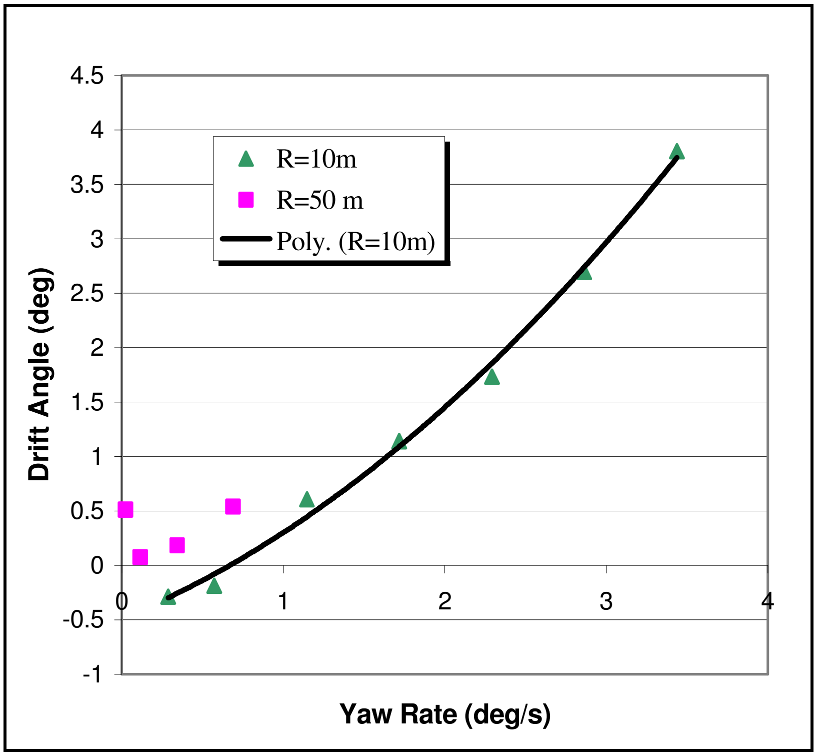

Figure 3. 14: Relative drift angle vs. yaw rate for the 10 and 50 m arc (Assuming drift angle = 0 at beginning of run)

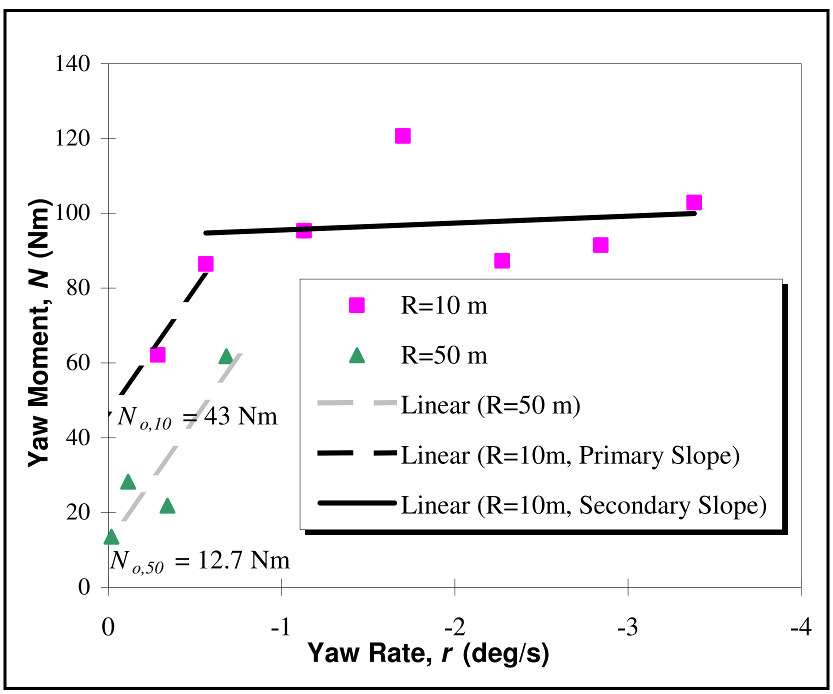

Figure 3. 15: Moment versus yaw rate for the *Terry Fox* model turning in ice with the 10 m and 50 m radii (corrected to 40 mm ice thickness and 31.5 kPa ice flexural strength).

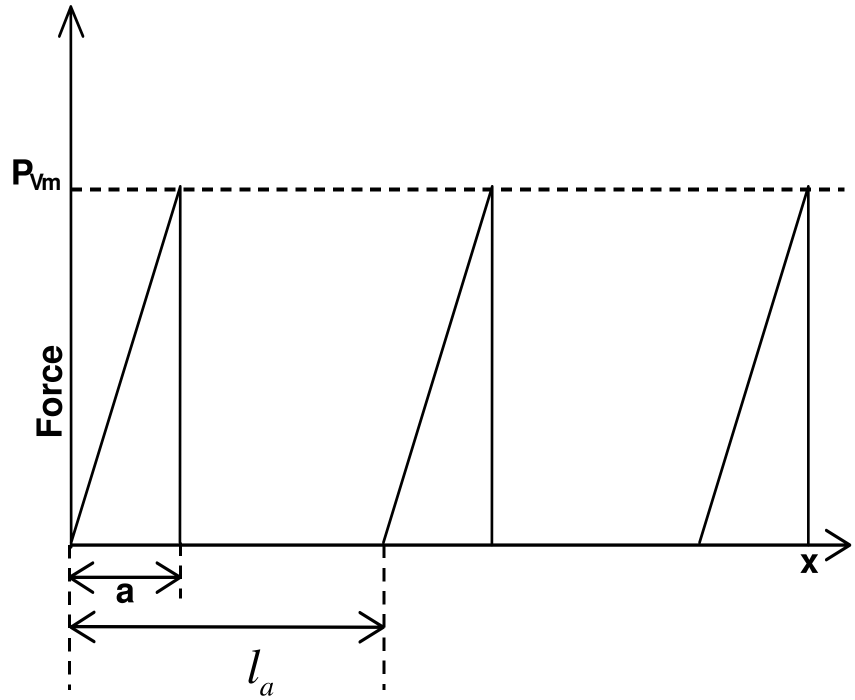

Figure 4.1: The idealized force displacement history when the ship is advancing

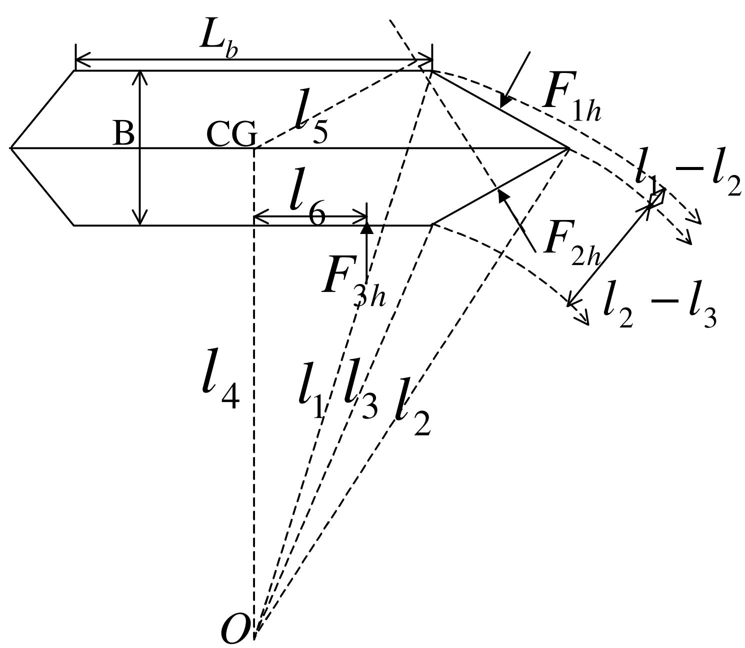

Figure 4.2: Geometry of ship manoeuvres at a constant yaw rate

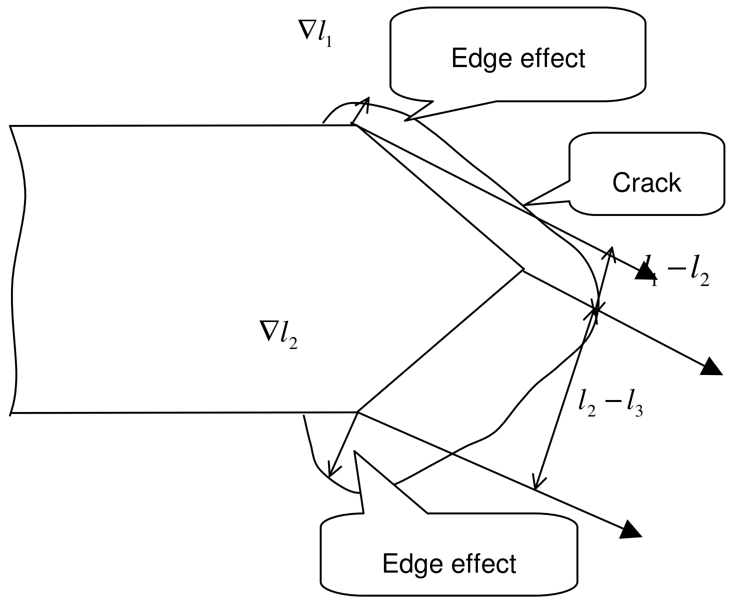

Figure 4.3: Edge effect on ice-breaking pattern at the bow

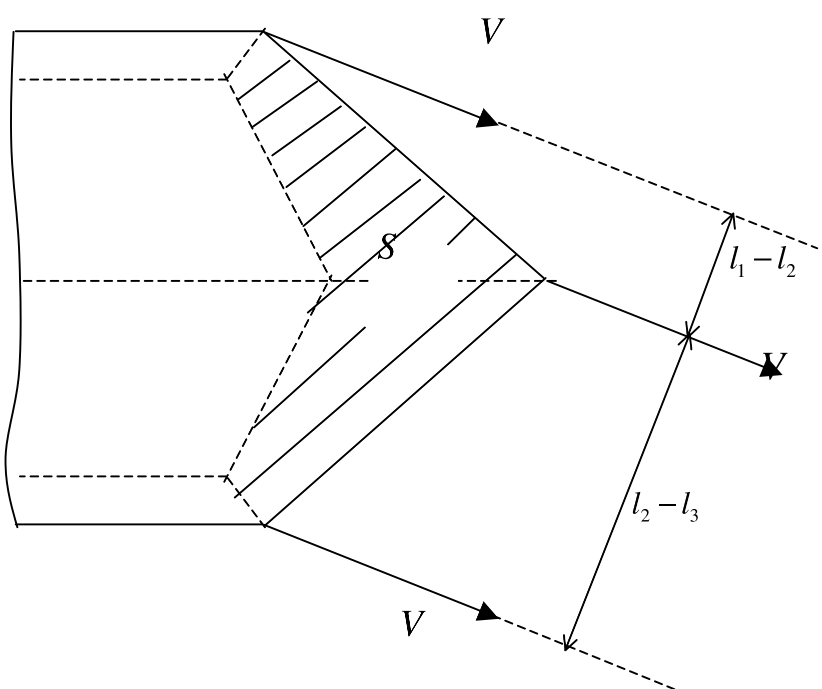

Figure 4.4: Bow geometry, showing amount of ice sliding on bow surface

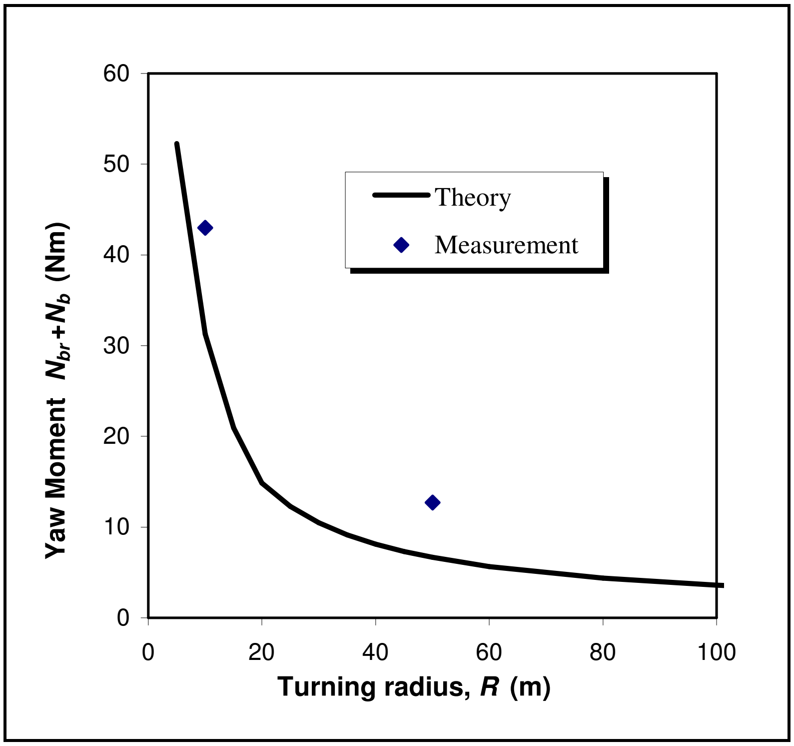

Figure 4. 5 Predicted moment offset as a function of turning radius

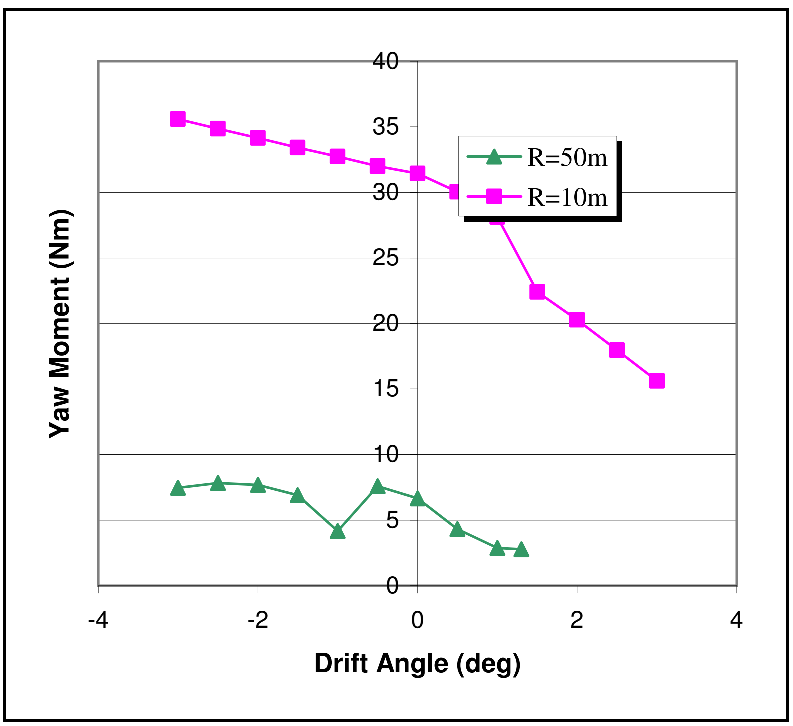

Figure 4. 6: The effect of drift angle on yaw moment offset for the ship and ice conditions

Appendix A

Hydrostatics and Particulars of the *Terry Fox* Model

Hydrostatics

PARAMETER		PROTOTYPE	1/21.8 SCALE MODEL
Length Overall	LOA	86.826m	
	LBP	75.000m	
Beam Overall	BOA	17.494m	802.477064mm
	BWL	17.247 m	
Height Overall	HOA		
Draft	T	8.2m	376.147mm
Volume		6895.791 m^3	
Displacement	Δ	7068.223MT	665.602kg
Waterplane		1250.269 m^2	
Wetted Surface Area	S	2157.345m^2	
Under Water Lateral Plane		570.710 m^2	
Above Water Lateral Plane		137.790 m^2	

COEFFICIENTS (Note: Coefficients calculated based on length of 75.000 m)		
Block Coefficient	CB	0.65
Midship Coefficient	CX	0.906
Prismatic Coefficient	CP	0.718
Waterplane Coefficient	CW	0.967

RATIOS		
Length to Beam Ratio	L/B	4.963
Beam to Draft Ratio	B/T	2.133
Displacement/length		466.923
MT/ cm Immersion		12.815

CENTROIDS		
Buoyancy	LCB	35.218 fwd m
	TCB	0.000 port m
	VCB	4.742 m
Flotation	LCF	33.047 fwd m
Under Water LP		33.218 fwd m of Origin, 3.910 below waterline
Above Water LP		51.279 fwd m of Origin, 1.312 above waterline
TPcm		12.815 MT/cm
MTcm		76.964 MT-m/cm
	GML	81.666 m
GM (Solid)		1.991 m

Draft is from Baseline.
No Trim, No heel, VCG = 6.730
Water Specific Gravity = 1.025. Trim is per 75.00m

Hull Data (with appendages)
Baseline Draft: 8.200
Trim: zero
Heel: zero

Floating Status

Draft FP	8.200 m	Heel	zero	GM(Solid)	1.991 m
Draft MS	8.200 m	Equil	Yes	F/S Corr.	0.000 m
Draft AP	8.200 m	Wind	0.0 kn	GM(Fluid)	1.991 m
Trim	zero	Wave	No	KMT	8.721 m
LCG	35.218f m	VCG	6.730 m	TPcm	12.82

LIST OF TERMINOLOGY
KE = Knife edge
GoBo = Restoring moment of frame without model
GsBs = Restoring moment of frame model, and trimming mass
GcBc = Restoring moment for trimming mass used to level model
GmBm = Restoring moment for the model
Jo = Mass moment of inertia of frame without model
Js = Mass moment of inertia of frame with model, and trimming mass
Jc = Mass moment of inertia of trimming mass used to level model
Jm(ke) = Mass moment of inertia of model about the knife edge
Jm(vcg) = Mass moment of inertia of model about the VCG
K = Radius of Gyration
T = Period

Swung Test Results

CONSTANTS			
Model:			
Description:			
Condition:		Frame used:	Steel Frame
Date:	Nov-26-2003	Frame code:	
Model Length:	3.440m		
Mass of model:	665.602kg	**Frame Constants Used:**	
Model Beam	0.802477064m	G0B0t (Nm)	770.814
Supports (if not used enter 0.0 for mass):		G0b0l (Nm)	772.438
Mass:	3.1kg	l1 (m)	0.750
Length:	2.438m	l2 (m)	0.750
Width	0.609m	a (m)	0.188
Thickness:	0.0508m	d (m)	1.197
		J0t (kg-m^2)	235.098
INCLINOMETER		J0l(kg-m^2)	234.915
Mass:	0kg		
		Frame Constants Corrected for Support	
Height above KE	0m	G0B0t (Nm)	806.433
		G0b0l (Nm)	808.057
INCLINING MASS:	63.5kg	J0t (kg-m^2)	239.450
		J0l (kg-m^2)	240.706
		d (m)	1.146

Pitch Gyradius Only

Inclining Angles (degrees)			Inclining Angles (degrees)		
PITCH BOW DOWN		Theta (deg)	***PITCH BOW UP***		Theta (deg)
Initial	0.0000	0.0000	Initial	0.0000	
Weight Fwd 1	4.3600	4.3600	Weight Aft 1	-4.3600	4.3600
Initial	0.0000	4.3600	Initial	0.0000	4.3600
Weight Fwd 2	4.3600	4.3600	Weight Aft 2	-4.3600	4.3600
Initial	0.0000	4.3600	Initial	0.0000	4.3600
Theta (mean)		4.3600	Theta (mean)		4.3600

Theta (mean) for bow up and bow down= 4.360

	PITCH
TRIMMING MASS (kg)	0
DISTANCE FROM KE (X) (m, + fwd)	0
DISTANCE FROM KE (Y) (m, + stbd)	0
DISTANCE FROM KE (Z) (m, + down)	0
Correction to Inertia of System (kg-m^2):	0
Restoring Moment of System (G1b1) (Nm):	6242.95
Restoring Moment of Frame (G0b0) (Nm):	772.44
Restoring Moment of Inclinometer (Gibi) (Nm):	0.00
Restoring Moment of Model (Gb) (Nm):	5470.51
CG of Model and Trim Weight from KE (m):	0.838
VCG of Model and Trim Weight from keel (m):	0.308
VCG of Model from keel (m):	0.3084

Inertia of Model

PITCH IN AIR		
Cycles	Time (sec)	Period (sec)
10	28.26	2.826
10	28.26	2.826
10	28.26	2.826
	MEAN	**2.826**

	PITCH
Inertia of Entire System about KE (kg-m^2)	1262.92
Inertia of Frame about KE (kg-m^2)	234.92
Inertia of Model about KE (kg-m^2)	1028.00
Parallel Axis Correction (kg-m^2)	467.20
Inertia of Model about own CG (kg-m^2)	560.80
Radius of Gyration (m)	0.918
Radius of Gyration/Length	**0.267**

Roll Gyradius Only

Inclining Mass: 63.5kg

Inclining Angles (degrees)			Inclining Angles (degrees)		
ROLL PORT DOWN		Theta (deg)	***ROLL STBD DOWN***		Theta (deg)
Initial	0.0000		Initial	0.0000	
Weight Fwd 1	4.3700	4.3700	Weight Aft 1	-4.3600	4.3600
Initial	0.0000	4.3700	Initial	0.0000	4.3600
Weight Fwd 2	4.3700	4.3700	Weight Aft 2	-4.3600	4.3600
Initial	0.0000	4.3700	Initial	0.0000	4.3600
Theta (mean)		4.3700	Theta (mean)		4.3600

Theta (mean) for bow up and bow down= 4.365

	ROLL
TRIMMING MASS (kg)	0
DISTANCE FROM KE (X) (m, + fwd)	0
DISTANCE FROM KE (Y) (m, + stbd)	0
DISTANCE FROM KE (Z) (m, + down)	0
Correction to Inertia of System (kg-m^2):	0
Restoring Moment of System (G1b1) (Nm):	6237.81
Restoring Moment of Frame (G0b0t) (Nm):	770.81
Restoring Moment of Inclinometer (Gibi) (Nm):	-1.00
Restoring Moment of Model (Gbt) (Nm):	5468.00
CG of Model and Trim Weight from KE (m):	0.837
VCG of Model and Trim Weight from keel (m):	0.309
VCG of Model from keel (m):	0.3088

Inertia of Model

ROLL IN AIR		
Cycles	Time (sec)	Period (sec)
10	22	2.200
10	22	2.200
10	22	2.200
	MEAN	**2.200**

	ROLL
Inertia of Entire System about KE (kg-m^2)	764.75
Inertia of Frame about KE (kg-m^2)	239.45
Inertia of Model about KE (kg-m^2)	525.30
Parallel Axis Correction (kg-m^2)	466.77
Inertia of Model about own CG (kg-m^2)	58.53
Radius of Gyration (m)	0.297
Radius of Gyration/Beam	**0.370**

FINAL RESULTS	
VCG (Pitch) From keel (m)	**0.308**
VCG (Roll) From keel (m)	**0.309**
Radius of Gyration (Pitch) (m)	**0.918**
Radius of Gyration (Roll) (m)	**0.297**

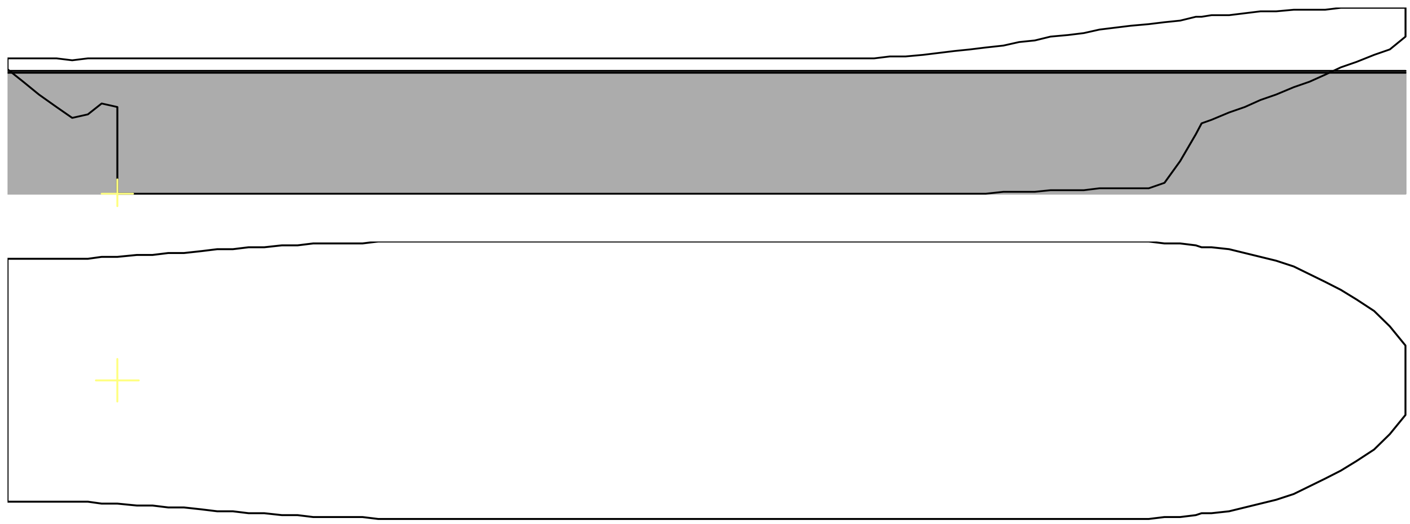

Hull Section Data (with appendages) No Trim, No heel

Location (m)	**Draft (m)**	**Area (m^2)**	**WL Width (m)**	**Girth (m)**
75.000f	8.200	0.077	0.821	0.902
73.125f	8.200	2.234	4.183	4.635
71.250f	8.200	6.838	6.821	7.737
69.375f	8.200	13.997	9.499	10.883
67.500f	8.200	22.830	11.545	13.506
65.625f	8.200	37.399	13.680	20.079
63.750f	8.200	56.009	15.566	23.543
61.875f	8.200	73.126	16.604	24.614
60.000f	8.200	87.952	16.967	25.439
58.125f	8.200	99.829	17.056	26.245
56.250f	8.200	109.806	17.089	27.050
54.375f	8.200	117.199	17.119	27.830
52.500f	8.200	122.555	17.148	28.617
50.625f	8.200	125.838	17.178	29.362
48.750f	8.200	127.696	17.205	30.005
46.875f	8.200	127.994	17.228	30.115
45.000f	8.200	128.106	17.247	30.095
43.125f	8.200	128.106	17.247	30.095
41.250f	8.200	128.106	17.247	30.095
39.375f	8.200	128.106	17.247	30.095
37.500f	8.200	128.106	17.247	30.095
35.625f	8.200	128.106	17.247	30.095
33.750f	8.200	128.106	17.247	30.095
31.875f	8.200	128.106	17.247	30.095
30.000f	8.200	128.106	17.247	30.095
28.125f	8.200	128.106	17.247	30.095
26.250f	8.200	127.578	17.247	30.144

24.375f	8.200	125.502	17.238	30.015
22.500f	8.200	121.670	17.220	29.782
20.625f	8.200	116.211	17.189	29.512
18.750f	8.200	110.112	17.144	29.459
16.875f	8.200	103.832	17.074	29.949
15.000f	8.200	97.408	16.972	31.138
13.125f	8.200	88.881	16.838	32.976
11.250f	8.200	77.287	16.651	35.328
9.375f	8.200	67.885	16.412	37.421
7.500f	8.200	59.068	16.120	40.068
5.625f	8.200	50.782	15.797	42.736
3.750f	8.200	40.063	15.447	47.199
1.875f	8.200	26.329	14.458	26.649
0.000	8.200	20.883	12.797	25.470

Volume = 6895.79m^3 LCG = 35.218f

Section Area Curve (with appendages)

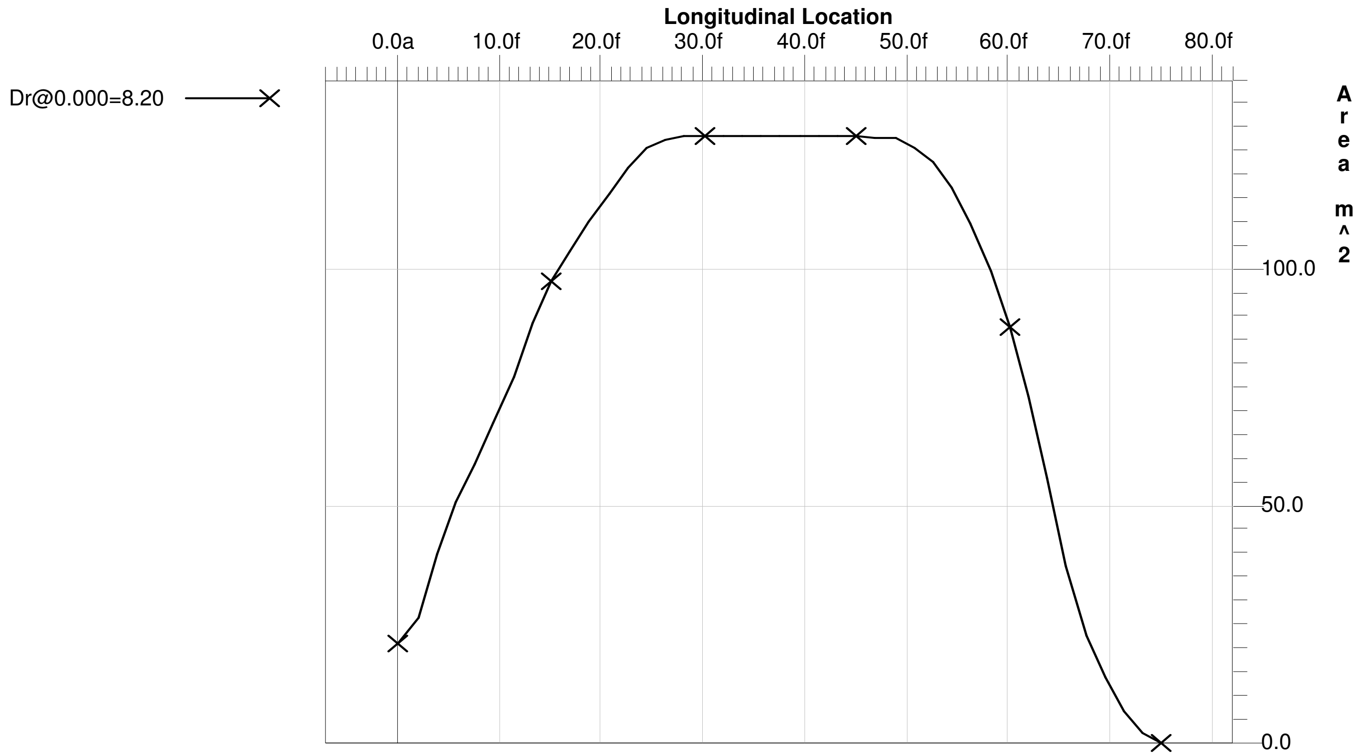

Appendix B

Instrumentation and Calibrations

The test program required measurements of the following 17 items:

i.	Surge Center (N)……………………………………	Channel # 1.
ii.	FWD Sway (N)……………………………………..	Channel # 2.
iii.	AFT Sway (N)…………………….…………………..	Channel # 3.
iv.	X Inline Load cell (N)………………………………	Channel # 4.
v.	Y Inline Load cell (N)………………………………	Channel # 5.
vi.	Yaw (degrees).…………………….………………	Channel # 17.
vii.	Sway Position (m)……….……….………………..	Channel # 19.
viii.	Sway Velocity (m/s).………………………………	Channel # 20.
ix.	FWD Heave (mm).…………………………………	Channel # 21.
x.	AFT Heave (mm)………………………………….	Channel # 22.
xi.	X (m/s^2)……………………………………………	Channel # 25.
xii.	Y (m/s^2)…………………………………………….	Channel # 26.
xiii.	Z (m/s^2)…………………………………………….	Channel # 27.
xiv.	Yaw Rate (deg/s)…..……………………………..	Channel # 28.
xv.	Carriage Position (m)………………………………	Channel # 33.
xvi.	Carriage Velocity (m/s)…………………………….	Channel # 34.
xvii.	Carriage Velocity (F/V) (m/s)……………….………..	Channel # 35.

Test Configuration

DACON File: PJ953_NMS_Dec03
Project: Marine Structural Fragility and Software Validation
Facility: Icetank

Channel No.	Sensor Name	Sensor Model	Serial No.	Data Description
1	SURGE CENTER	SSB-HN-250	B88024	Force (N)
2	FWD Sway	SSB-AJ-500	C65397	Force (N)
3	AFT Sway	SSB-AJ-500	C65391	Force (N)
4	X Inline Load	60001-100	A10501 S/N 683212	Force (N)
5	Y Inline Load cell	60001-100	NRC A10500 S/N 00083211	Force (N)
17	Yaw	DG57-0302-1	IMD20098	Angle (deg)
19	Sway POSITION	DV301-0500-111-1110	NRC168567 A54581	Displacement (m)
20	SWAY Velocity	DV301-0500-111-1110	NRC NRC168567 A54581	Velocity (m/s)
21	FWD HEAVE	pt-101-0010-111-1110	A55549 nrc# 168628	Displacement (mm)
22	AFT HEAVE	PT-101-0010-111-1110	A56015 NRC# 168630	Displacement (mm)
25	X	QFLEX QA700 9790700001	13702	Acceleration (m/s^2)
26	Y	QFLEX QA1400 979-1400-001	942 8710	Acceleration (m/s^2)
27	Z	QFLEX QA1400-AA01-01,9791400001	2149	Acceleration (m/s^2)
28	Yaw Rate	Northrop dac7836978	28 nrc 166870	Angular Velocity (deg/s)
33	Carriage position	ITC Carriage A/D output (CnE)	N/A	Displacement (m)
34	Carriage Velocity	Carriage A/D output (CnE)	N/A	Velocity (m/s)
35	Carriage Speed (F/V)	Ono Sokki 132 Wheel en fv801	60302876	Velocity (m/s)

Calibration of ICEDAS Channel 1   15:13   09 December 2003

Project: Marine Structural Fragility and Software Validation   **Facility:** Ice Tank

Sensor: SURGE CENTER   **Model:** SSB-HN-250   **Serial Number:** B88024

Programmable Gain: 1   **Plug-In Gain:** 200   **Filter Frequency:** 10.0 Hz

Data Point No.	Input Signal (volts)	Physical Value (N)	Fitted Curve Value (N)	Error (N)	
1	5.359	1000.8	1000.9	0.09186	
2	2.971	556.0	555.9	−0.12476	⇐ Maximum Error
3	−0.013	0.0	0.0	−0.02280	
4	−2.996	−556.0	−556.0	0.07465	
5	−5.384	−1000.8	−1000.9	−0.01892	
Maximum Error = −0.00623 % of Calibration Range.					

Definition of Calibration Curve

Polynomial Degree = 1 (Linear Fit)

$$Y = C_0 + C_1 \cdot V$$

where $Y(t)$ = Force (N),

$V(t)$ = input signal at A/D converter (volts),

C_0 = 2.33367 N,

and C_1 = 186.331 N/volt .

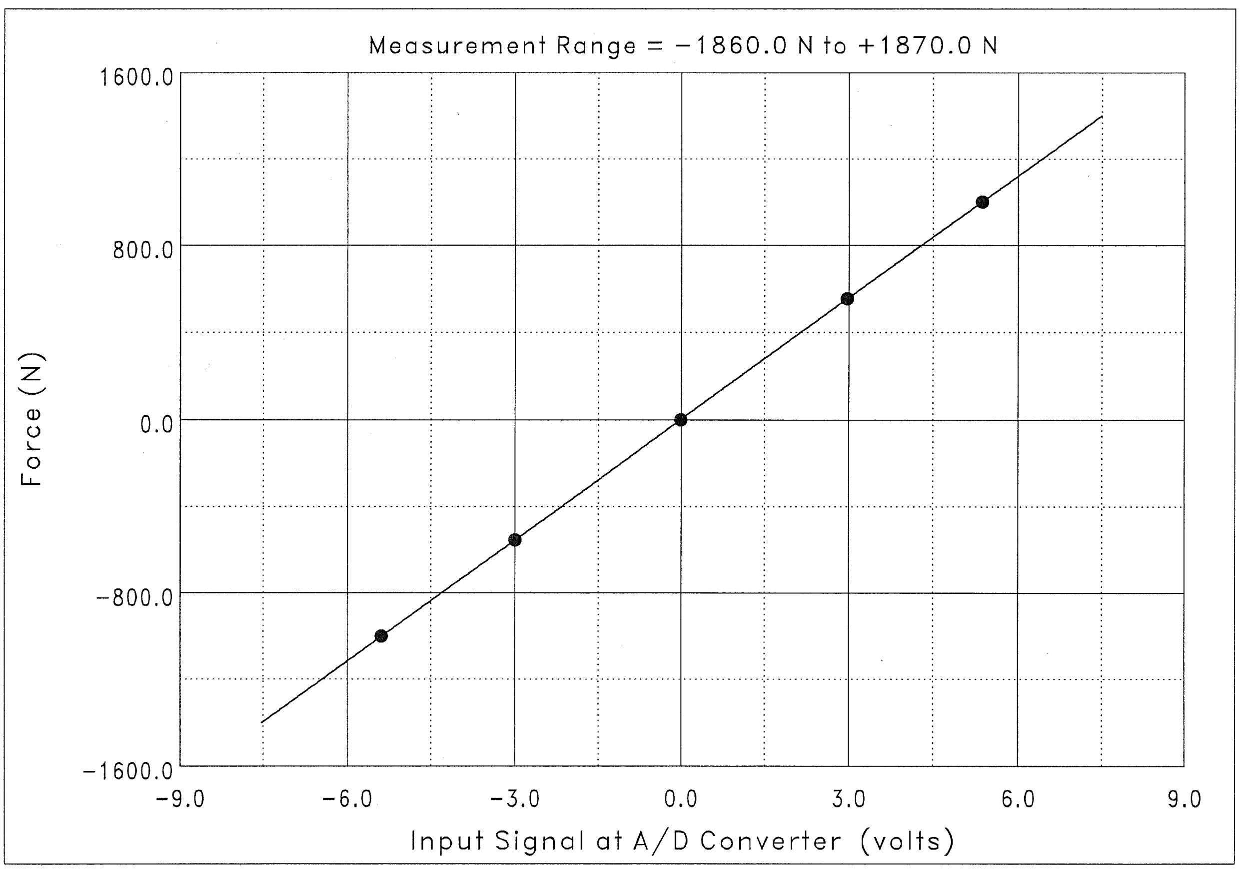

Calibration of ICEDAS Channel 2 15:18 09 December 2003

Project: Marine Structural Fragility and Software Validation **Facility:** Ice Tank

Sensor: FWD. Sway **Model:** SSB-AJ-500 **Serial Number:** C65397

Programmable Gain: 1 **Plug-In Gain:** 1000 **Filter Frequency:** 10.0 Hz

Data Point No.	Input Signal (volts)	Physical Value (N)	Fitted Curve Value (N)	Error (N)	
1	−5.476	−2001.7	−2001.8	−0.11694	
2	−3.052	−1112.1	−1112.1	−0.01477	
3	−0.021	0.0	0.3	0.30813	⇐ Maximum Error
4	3.007	1112.1	1111.9	−0.11487	
5	5.431	2001.7	2001.6	−0.06152	
Maximum Error = 0.00770 % of Calibration Range.					

Definition of Calibration Curve

Polynomial Degree = 1 (Linear Fit)

$$Y = C_0 + C_1 \cdot V$$

where $Y(t)$ = Force (N),
$V(t)$ = input signal at A/D converter (volts),
C_0 = 8.09692 N,
and C_1 = 367.037 N/volt .

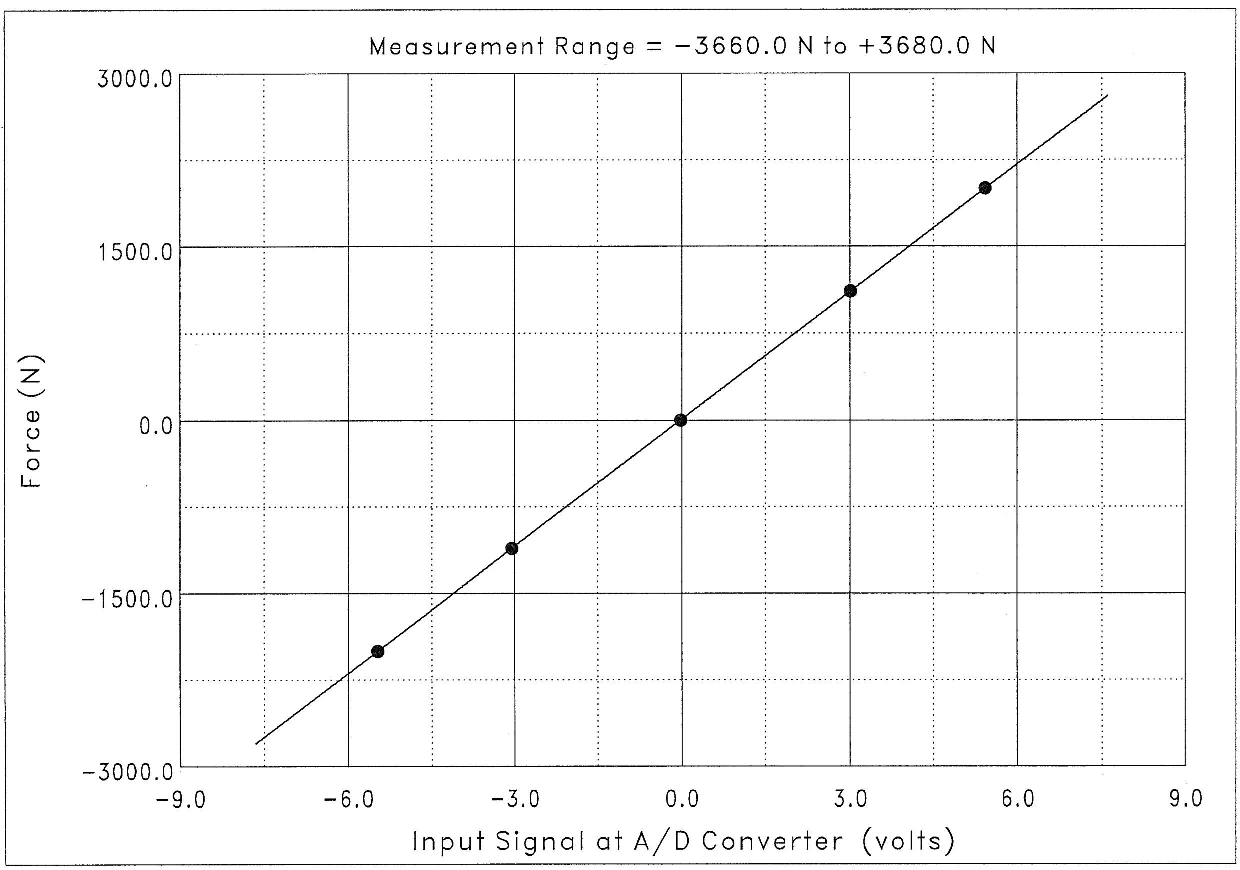

Calibration of ICEDAS Channel 3 15:25 09 December 2003

Project: Marine Structural Fragility and Software Validation **Facility:** Ice Tank

Sensor: AFT.Sway **Model:** SSB-AJ-500 **Serial Number:** C65391

Programmable Gain: 1 **Plug-In Gain:** 1000 **Filter Frequency:** 10.0 Hz

Data Point No.	Input Signal (volts)	Physical Value (N)	Fitted Curve Value (N)	Error (N)	
1	−5.673	2001.7	2001.7	−0.036499	
2	−3.157	1112.1	1112.1	0.023315	
3	−0.011	0.0	0.0	0.042977	⇐ Maximum Error
4	3.134	−1112.1	−1112.1	−0.013672	
5	5.650	−2001.7	−2001.7	−0.015991	
Maximum Error = 0.00107 % of Calibration Range.					

Definition of Calibration Curve
Polynomial Degree = 1 (Linear Fit)

$$Y = C_0 + C_1 \cdot V$$

where $Y(t)$ = Force (N),
$V(t)$ = input signal at A/D converter (volts),
C_0 = −3.99404 N,
and C_1 = −353.556 N/volt .

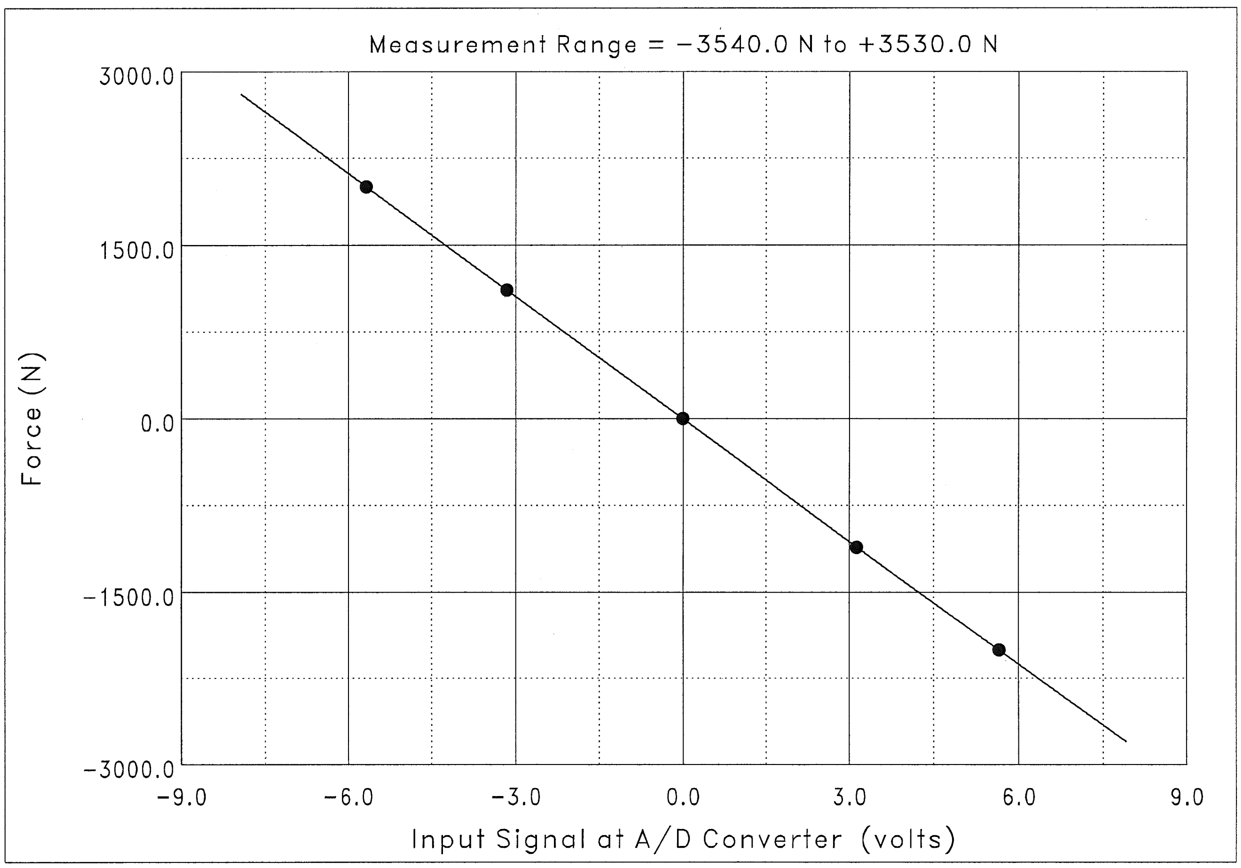

Calibration of ICEDAS Channel 4 16:00 09 December 2003

Project: Marine Structural Fragility and Software Validation **Facility:** Ice Tank

Sensor: X Inline Load **Model:** 60001-100 **Serial Number:** A10501 S/N 683212

Programmable Gain: 1 **Plug-In Gain:** 200 **Filter Frequency:** 10.0 Hz

Data Point No.	Input Signal (volts)	Physical Value (N)	Fitted Curve Value (N)	Error (N)	
1	0.682	0.00	−0.08	−0.08144	
2	1.369	49.03	48.89	−0.14052	
3	2.060	98.07	98.10	0.03813	
4	2.746	147.10	147.00	−0.09511	
5	3.436	196.13	196.18	0.04904	
6	4.129	245.17	245.53	0.36099	
7	4.818	294.20	294.68	0.48422	⇐ Maximum Error
8	5.495	343.23	342.88	−0.35342	
9	6.184	392.27	392.00	−0.26187	
Maximum Error = 0.123 % of Calibration Range.					

Definition of Calibration Curve

Polynomial Degree = 1 (Linear Fit)

$$Y = C_0 + C_1 \cdot V$$

where $Y(t)$ = Force (N),
$V(t)$ = input signal at A/D converter (volts),
C_0 = −48.7054 N,
and C_1 = 71.2668 N/volt .

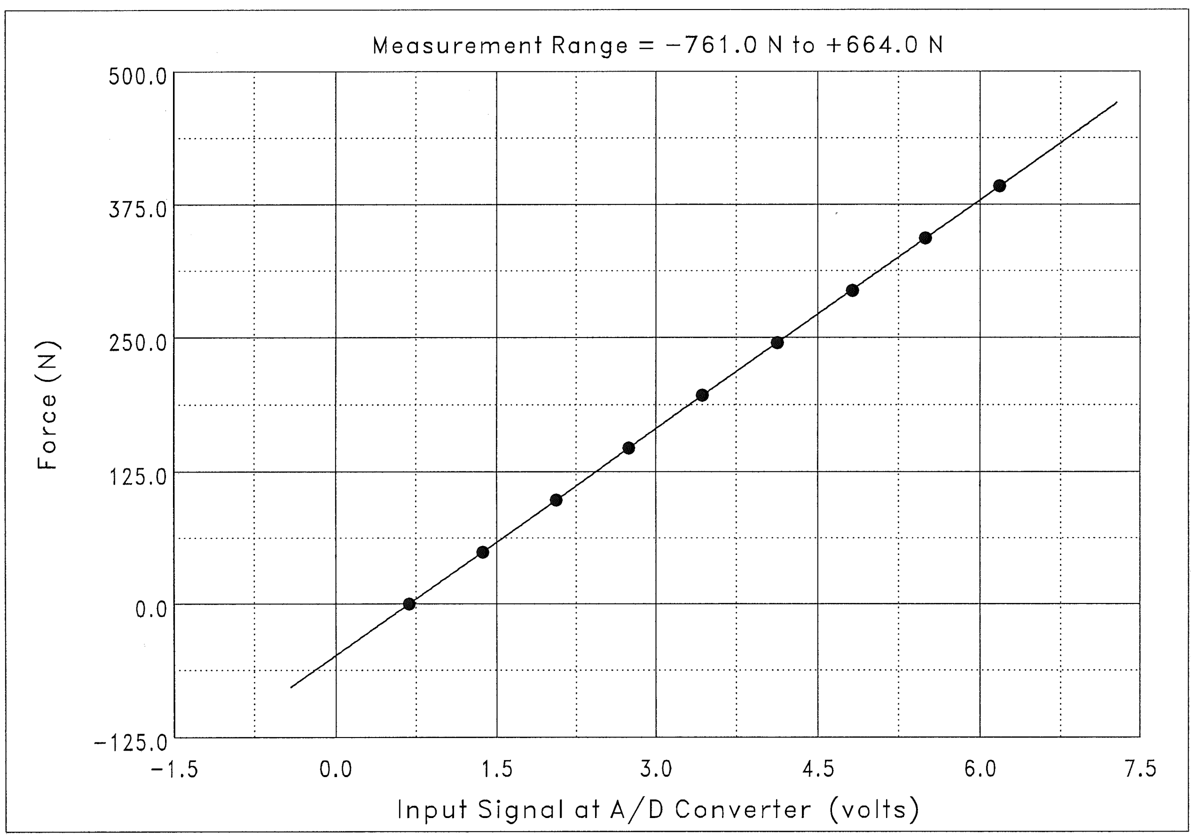

Calibration of ICEDAS Channel 5 16:00 09 December 2003

Project: Marine Structural Fragility and Software Validation **Facility:** Ice Tank

Sensor: Y Inline Load cell **Model:** 6001-100 **Serial Number:** NRC A10500 S/N 00083211

Programmable Gain: 1 **Plug-In Gain:** 200 **Filter Frequency:** 10.0 Hz

Data Point No.	Input Signal (volts)	Physical Value (N)	Fitted Curve Value (N)	Error (N)	
1	0.403	0.00	−0.03	−0.03161	
2	1.043	49.03	49.49	0.45797	⇐ Maximum Error
3	1.668	98.07	97.88	−0.19124	
4	2.301	147.10	146.83	−0.26707	
5	2.935	196.13	195.86	−0.27354	
6	3.573	245.17	245.26	0.09845	
7	4.209	294.20	294.51	0.30521	
8	4.836	343.23	342.96	−0.26959	
9	5.475	392.27	392.44	0.17136	
Maximum Error = 0.117 % of Calibration Range.					

Definition of Calibration Curve

Polynomial Degree = 1 (Linear Fit)

$$Y = C_0 + C_1 \cdot V$$

where $Y(t)$ = Force (N),
$V(t)$ = input signal at A/D converter (volts),
C_0 = -31.2063 N,
and C_1 = 77.3780 N/volt.

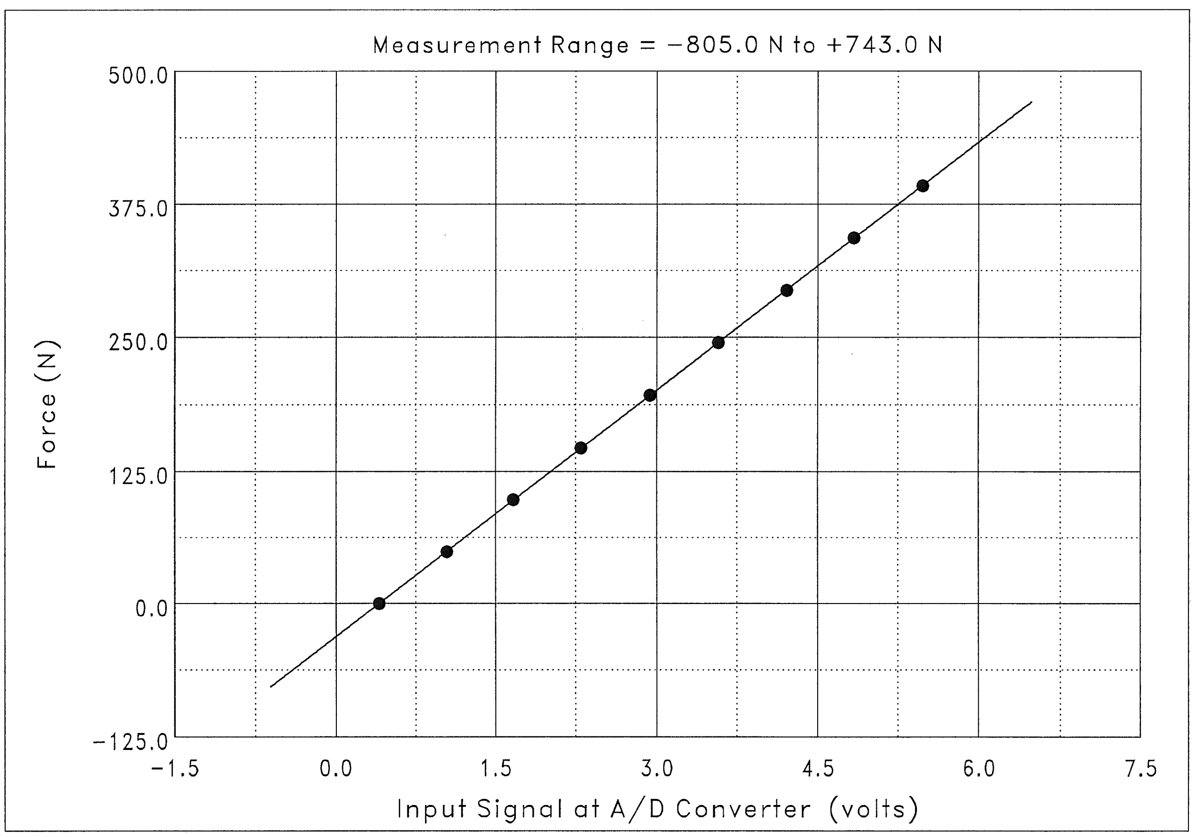

Calibration of ICEDAS Channel 17 16:58 11 December 2003

Project: Marine Structural Fragility and Software Validation **Facility:** Ice Tank

Sensor: Yaw **Model:** DG57-0302-1 **Serial Number:** IMD20098

Programmable Gain: 1 **Plug-In Gain:** 1 **Filter Frequency:** 10.0 Hz

Data Point No.	Input Signal (volts)	Physical Value (deg)	Fitted Curve Value (deg)	Error (deg)	
1	2.895	−90.000	−90.025	−0.02460	
2	4.180	−45.000	−44.884	0.11562	⇐ Maximum Error
3	5.455	0.000	−0.094	−0.09433	
4	6.737	45.000	44.941	−0.05917	
5	8.021	90.000	90.062	0.06245	
Maximum Error = 0.0642 % of Calibration Range.					

Definition of Calibration Curve

Polynomial Degree = 1 (Linear Fit)

$$Y = C_0 + C_1 \cdot V$$

where $Y(t)$ = Angle (deg),
$V(t)$ = input signal at A/D converter (volts),
C_0 = -191.706 deg,
and C_1 = 35.1274 deg/volt .

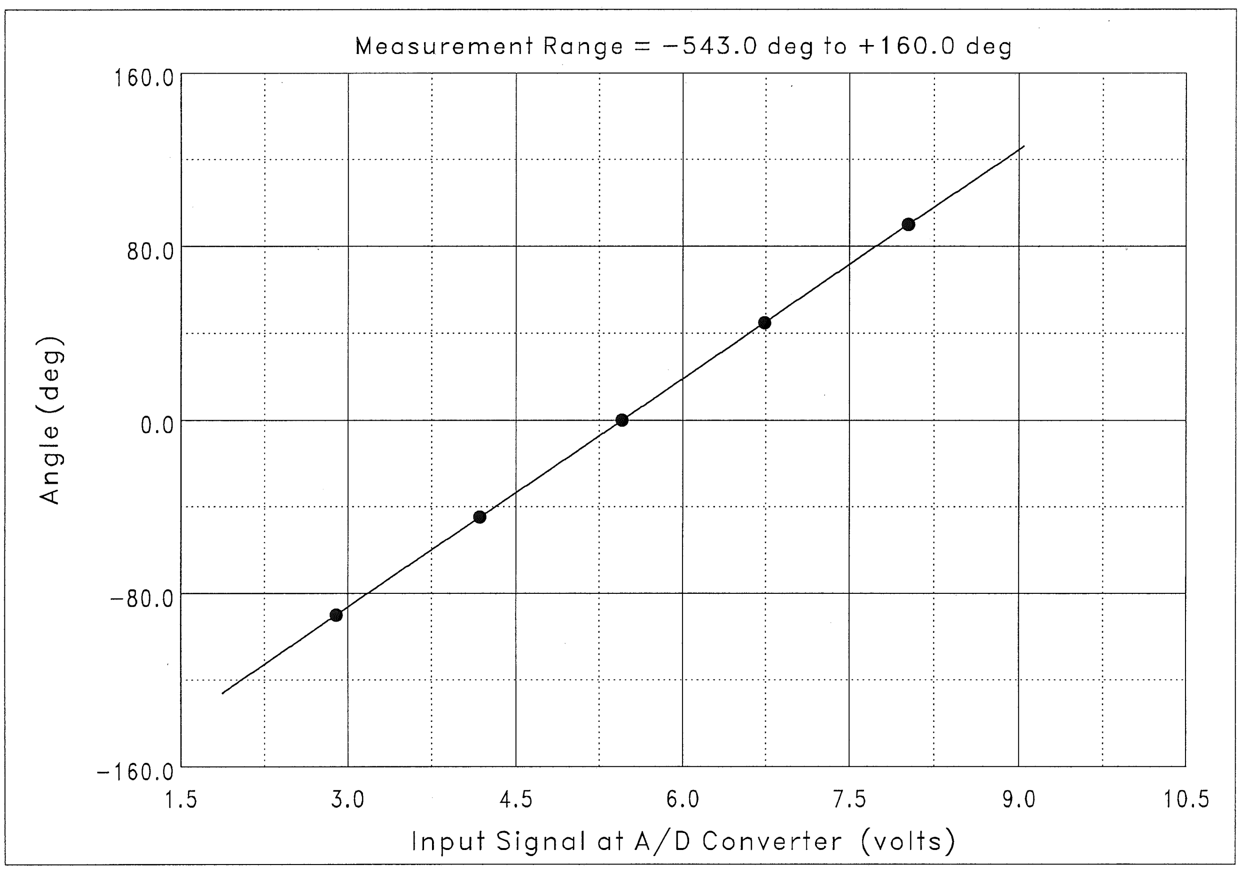

Calibration of ICEDAS Channel 19 09:50 10 December 2003

Project: Marine Structural Fragility and Software Validation **Facility:** Ice Tank

Sensor: Sway POSITION **Model:** DV301-0500-111-1110 **Serial Number:** NRC168567 A54581

Programmable Gain: 1

Data Point No.	Input Signal (volts)	Physical Value (m)	Fitted Curve Value (m)	Error (m)	
1	0.538	−3.5000	−3.4997	0.0003138	
2	0.920	−3.0000	−3.0016	−0.0016077	
3	2.073	−1.5000	−1.4982	0.0018070	⇐ Maximum Error
4	3.222	0.0000	−0.0008	−0.0008292	
5	4.374	1.5000	1.5007	0.0006876	
6	4.758	2.0000	2.0013	0.0013289	
7	5.140	2.5000	2.4988	−0.0012407	
8	5.907	3.5000	3.4995	−0.0004606	
Maximum Error = 0.0258 % of Calibration Range.					

Definition of Calibration Curve
Polynomial Degree = 1 (Linear Fit)

$$Y = C_0 + C_1 \cdot V$$

where $Y(t)$ = Displacement (m),
$V(t)$ = input signal at A/D converter (volts),
C_0 = −4.20079 m,
and C_1 = 1.30351 m/volt.

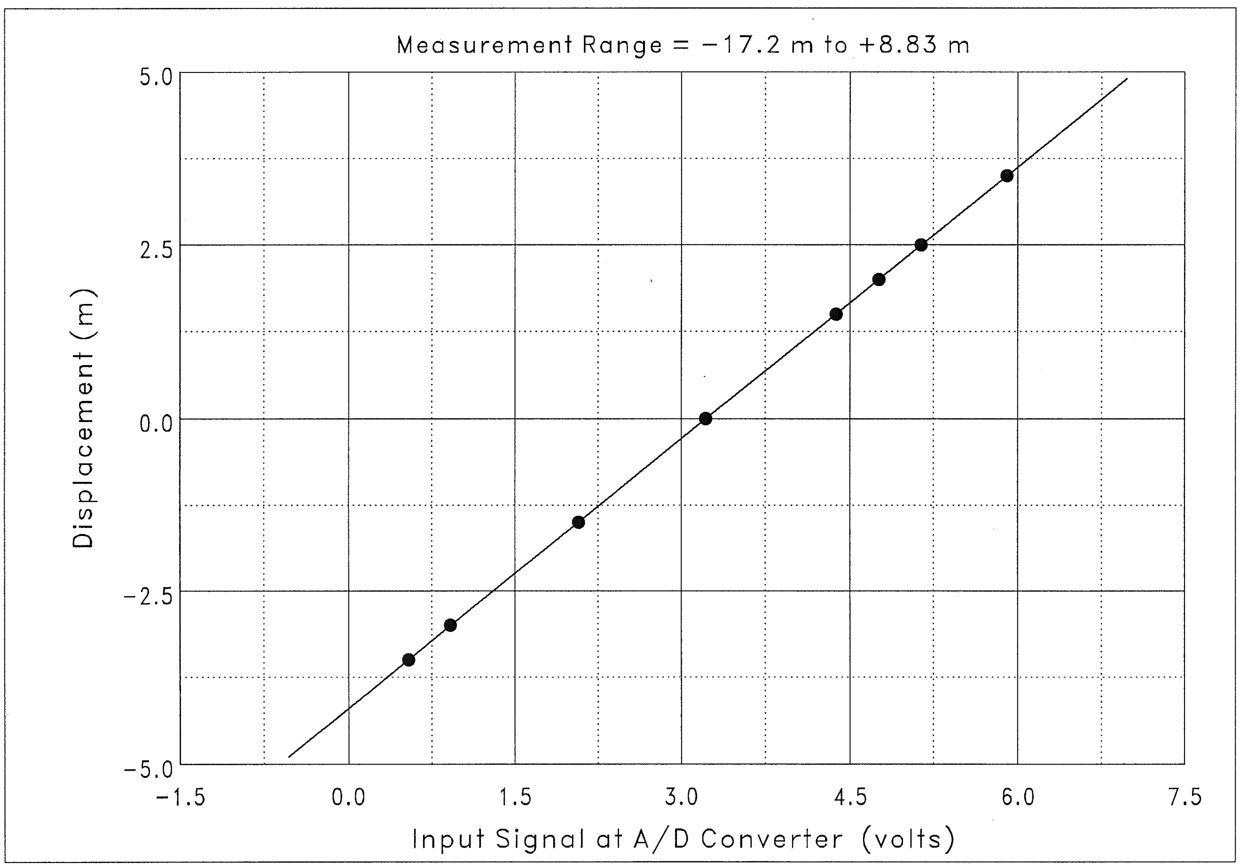

Calibration of ICEDAS Channel 20 10:20 03 November 2003

Project: Marine Structural Fragility and Software Validation **Facility:** Ice Tank

Sensor: SWAY Velocity **Model:** DV301-0500-111-1110 **Serial Number:** NRC NRC168567 A54581

Programmable Gain: 1

Data Point No.	Input Signal (volts)	Physical Value (m/s)	Fitted Curve Value (m/s)	Error (m/s)	
1	−0.008	0.00000	0.00015	0.00014710	
2	−0.850	−0.10000	−0.10049	−0.00048641	
3	0.830	0.10000	0.10043	0.00042554	
4	−0.175	−0.02000	−0.01981	0.00018959	
5	−0.566	−0.06700	−0.06657	0.00043124	
6	0.185	0.02300	0.02324	0.00023602	
7	0.563	0.06950	0.06856	−0.00094309	⇐ Maximum Error
Maximum Error = −0.472 % of Calibration Range.					

Definition of Calibration Curve
Polynomial Degree = 1 (Linear Fit)

$$Y = C_0 + C_1 \cdot V$$

where $Y(t)$ = Velocity (m/s),
$V(t)$ = input signal at A/D converter (volts),
C_0 = 0.00116103 m/s,
and C_1 = 0.119639 (m/s)/volt.

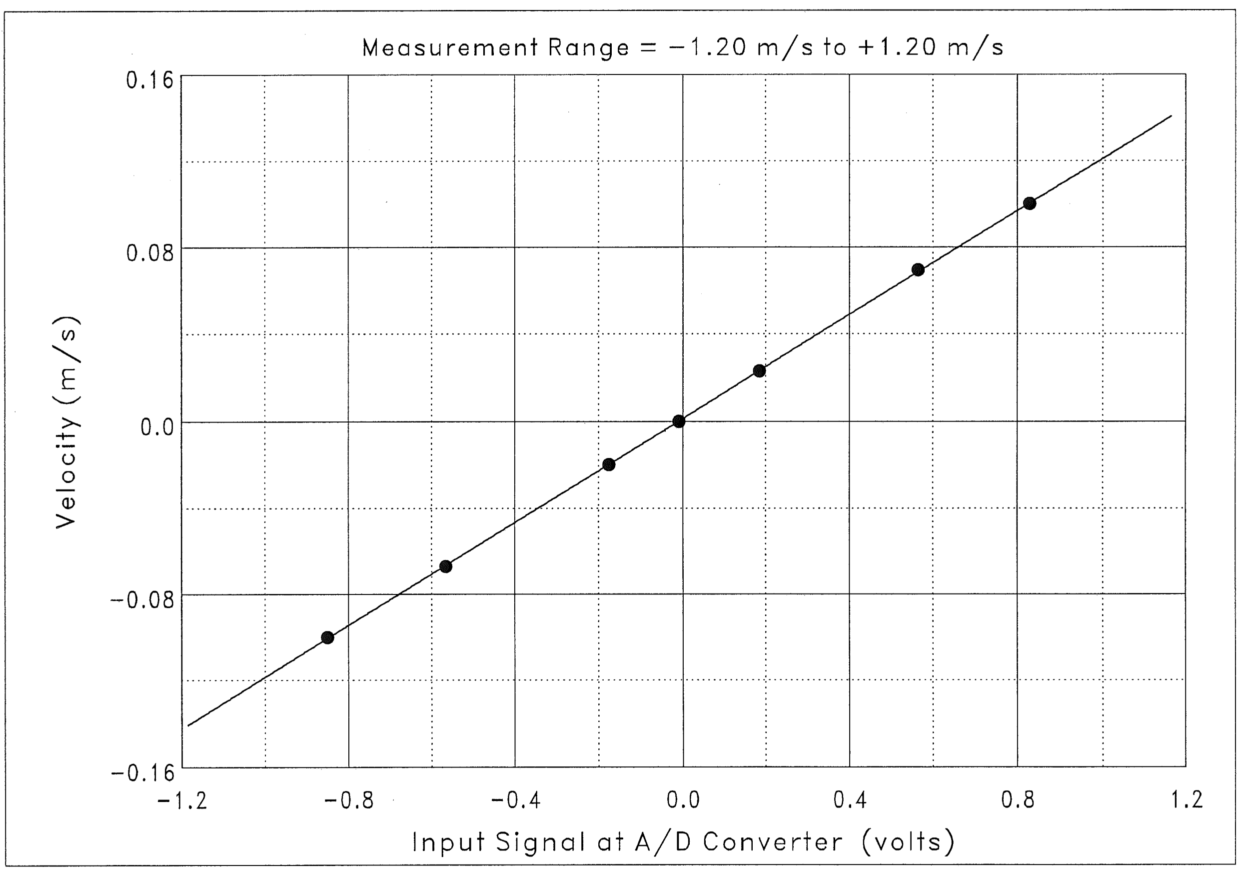

Calibration of ICEDAS Channel 21 08:48 10 December 2003

Project: Marine Structural Fragility and Software Validation **Facility:** Ice Tank

Sensor: FWD HEAVE **Model:** pt-101-0010-111-1110 **Serial Number:** a55549 nrc# 168628

Programmable Gain: 1 **Plug-In Gain:** 1 **Filter Frequency:** 10.0 Hz

Data Point No.	Input Signal (volts)	Physical Value (mm)	Fitted Curve Value (mm)	Error (mm)	
1	0.828	0.00	0.17	0.17174	
2	1.734	50.00	49.94	−0.05975	
3	2.652	100.00	100.29	0.29124	
4	3.551	150.00	149.65	−0.34860	
5	4.455	200.00	199.23	−0.76944	⇐ Maximum Error
6	5.393	250.00	250.71	0.71478	
Maximum Error = −0.308 % of Calibration Range.					

Definition of Calibration Curve

Polynomial Degree = 1 (Linear Fit)

$$Y = C_0 + C_1 \cdot V$$

where $Y(t)$ = Displacement (mm),
$V(t)$ = input signal at A/D converter (volts),
C_0 = -45.2486 mm,
and C_1 = 54.8830 mm/volt .

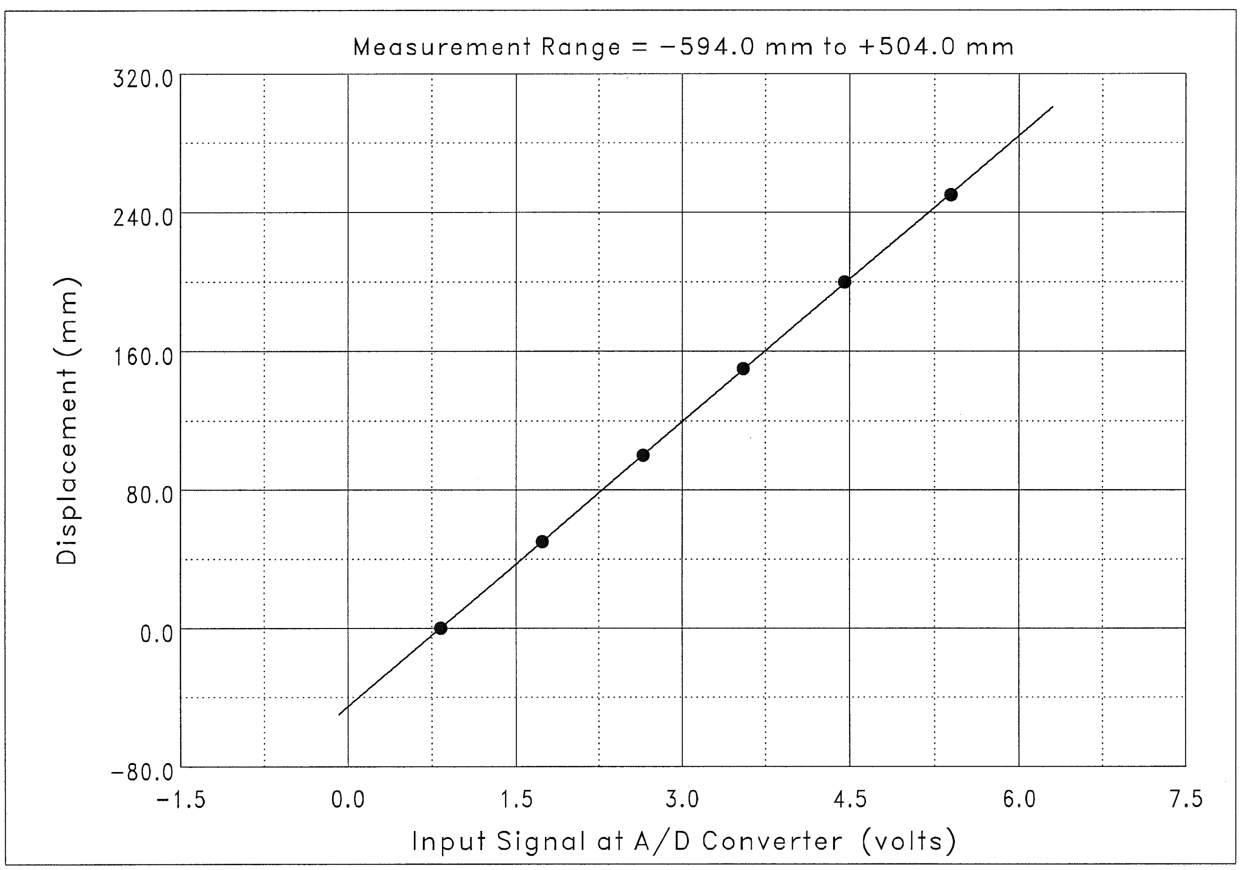

Calibration of ICEDAS Channel 22 08:51 10 December 2003

Project: Marine Structural Fragility and Software Validation **Facility:** Ice Tank

Sensor: AFT HEAVE **Model:** PT101-0010-111-1110 **Serial Number:** A56015 NRC# 168630

Programmable Gain: 1 **Plug-In Gain:** 1 **Filter Frequency:** 10.0 Hz

Data Point No.	Input Signal (volts)	Physical Value (mm)	Fitted Curve Value (mm)	Error (mm)	
1	0.765	0.00	0.69	0.6947	
2	1.674	50.00	50.00	0.0023	
3	2.591	100.00	99.71	−0.2868	
4	3.509	150.00	149.52	−0.4821	
5	4.411	200.00	198.46	−1.5424	
6	5.391	250.00	251.61	1.6143	⇐ Maximum Error
Maximum Error = 0.646 % of Calibration Range.					

Definition of Calibration Curve
Polynomial Degree = 1 (Linear Fit)

$$Y = C_0 + C_1 \cdot V$$

where $Y(t)$ = Displacement (mm),
$V(t)$ = input signal at A/D converter (volts),
C_0 = -40.7959 mm,
and C_1 = 54.2361 mm/volt .

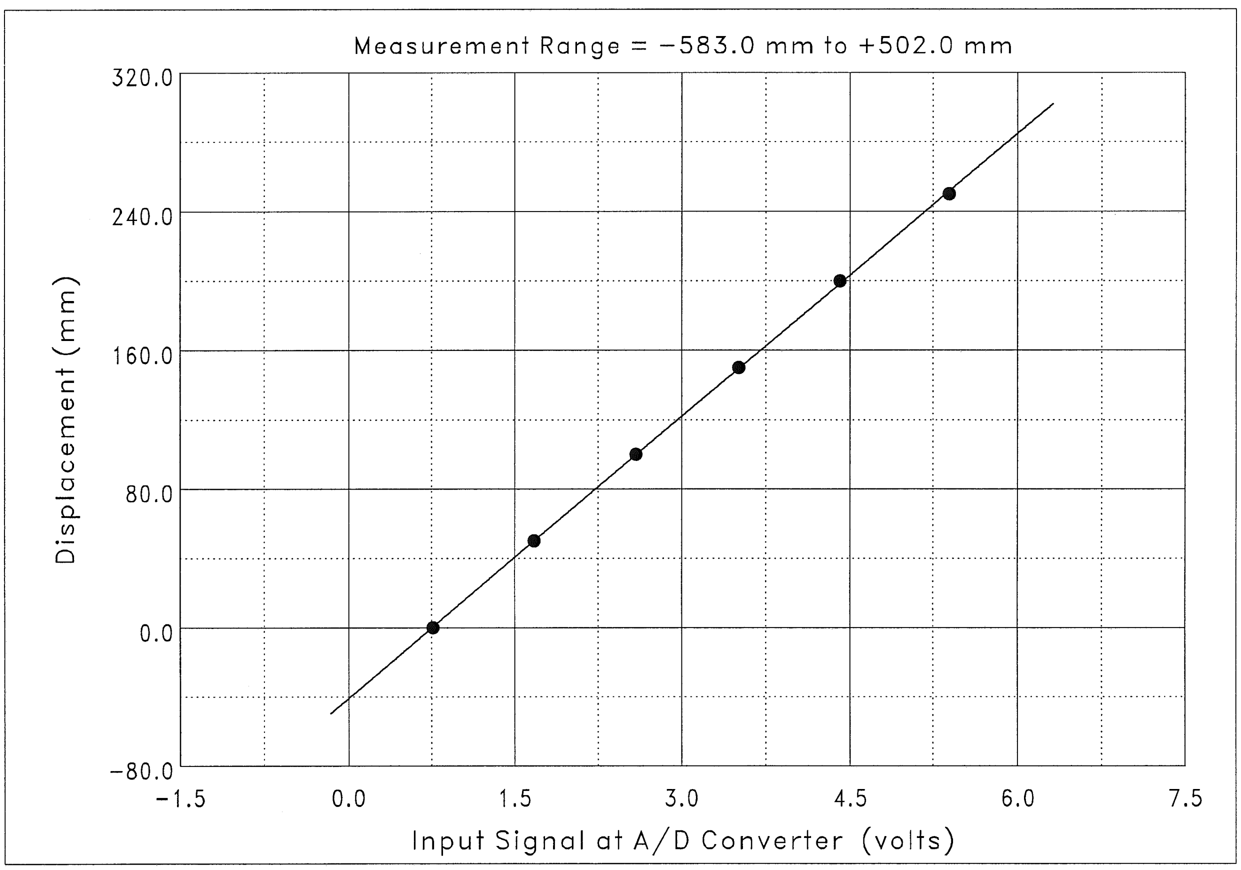

Calibration of ICEDAS Channel 25 — 14:19 09 December 2003

Project: Marine Structural Fragility and Software Validation **Facility:** Ice Tank

Sensor: X **Model:** QFLEX QA700 9790700001 **Serial Number:** 13702

Programmable Gain: 1 **Plug-In Gain:** 1 **Filter Frequency:** 10.0 Hz

Data Point No.	Input Signal (volts)	Physical Value (m/s**2)	Fitted Curve Value (m/s**2)	Error (m/s**2)	
1	−0.016	0.0000	0.0033	0.0033010	⇐ Maximum Error
2	−4.486	9.8080	9.8063	−0.0016508	
3	4.458	−9.8080	−9.8096	−0.0016499	
Maximum Error = 0.0168 % of Calibration Range.					

Definition of Calibration Curve

Polynomial Degree = 1 (Linear Fit)

$$Y = C_0 + C_1 \cdot V$$

where $Y(t)$ = Acceleration (m/s**2),
$V(t)$ = input signal at A/D converter (volts),
C_0 = −0.0326240 m/s**2,
and C_1 = −2.19335 (m/s**2)/volt .

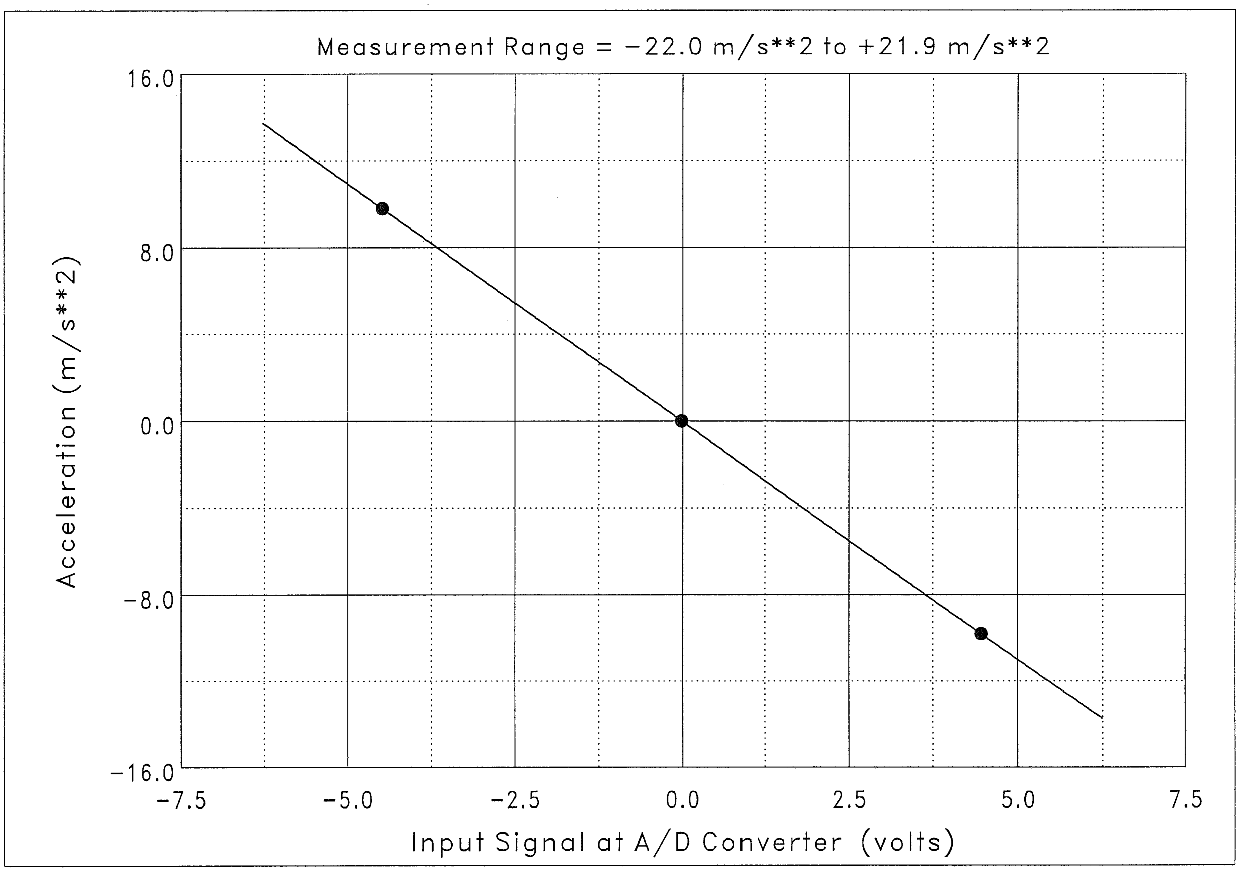

Calibration of ICEDAS Channel 26 14:15 09 December 2003

Project: Marine Structural Fragility and Software Validation **Facility:** Ice Tank

Sensor: Y **Model:** QFLEX QA1400 979-1400-001 **Serial Number:** 942 8710

Programmable Gain: 1 **Plug-In Gain:** 1 **Filter Frequency:** 10.0 Hz

Data Point No.	Input Signal (volts)	Physical Value (m/s**2)	Fitted Curve Value (m/s**2)	Error (m/s**2)	
1	−0.013	0.0000	−0.0043	−0.0043424	⇐ Maximum Error
2	4.507	9.8080	9.8102	0.0021696	
3	−4.526	−9.8080	−9.8058	0.0021734	
Maximum Error = −0.0221 % of Calibration Range.					

Definition of Calibration Curve
Polynomial Degree = 1 (Linear Fit)

$$Y = C_0 + C_1 \cdot V$$

where $Y(t)$ = Acceleration (m/s**2),
$V(t)$ = input signal at A/D converter (volts),
C_0 = 0.0230729 m/s**2,
and C_1 = 2.17172 (m/s**2)/volt .

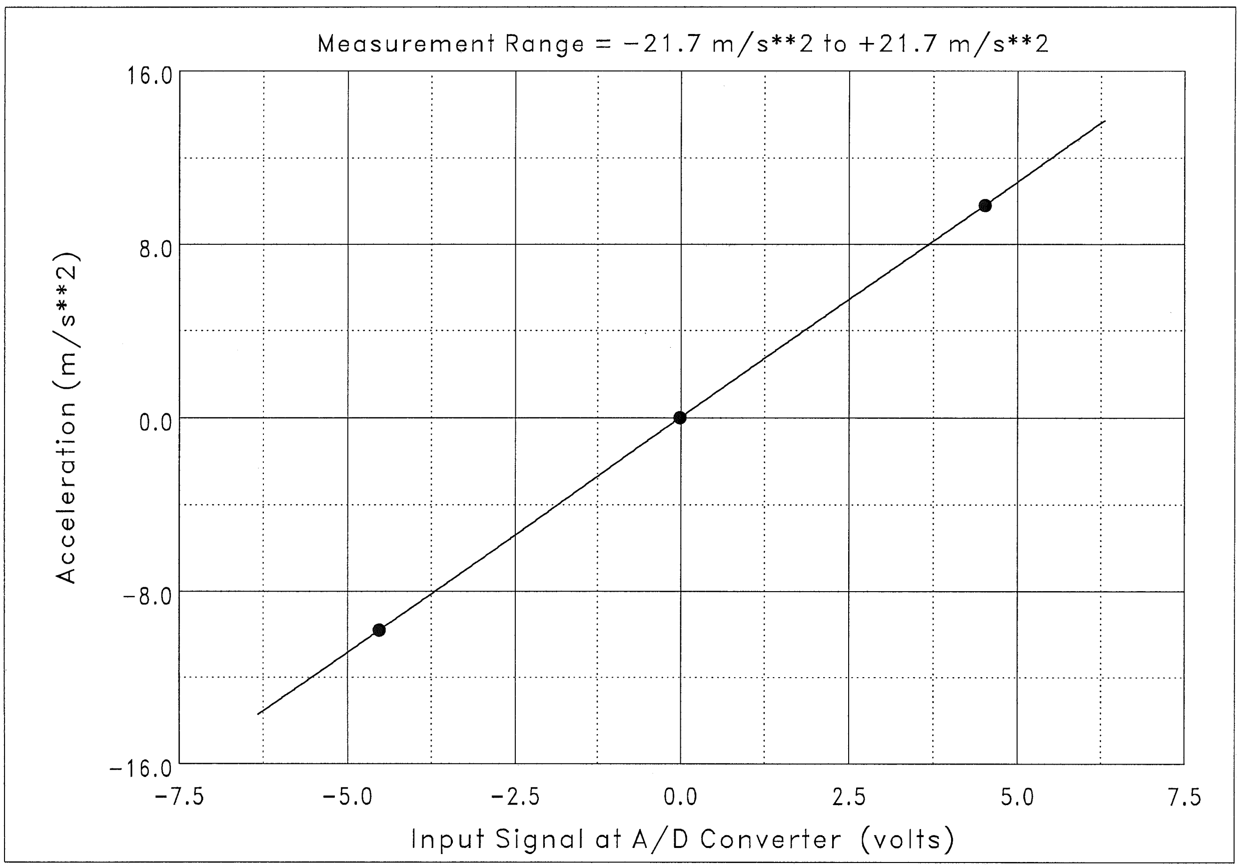

Calibration of ICEDAS Channel 27 — 14:30 09 December 2003

Project: Marine Structural Fragility and Software Validation **Facility:** Ice Tank

Sensor: Z **Model:** QFLEX QA1400-AA01-01,9791400001 **Serial Number:** 2149

Programmable Gain: 1 **Plug-In Gain:** 1 **Filter Frequency:** 10.0 Hz

Data Point No.	Input Signal (volts)	Physical Value (m/s**2)	Fitted Curve Value (m/s**2)	Error (m/s**2)	
1	−0.007	0.0000	−0.0070	−0.0070275	⇐ Maximum Error
2	4.514	9.8080	9.8115	0.0035105	
3	−4.519	−9.8080	−9.8045	0.0035181	
Maximum Error = −0.0358 % of Calibration Range.					

Definition of Calibration Curve
Polynomial Degree = 1 (Linear Fit)

$$Y = C_0 + C_1 \cdot V$$

where $Y(t)$ = Acceleration (m/s**2),
$V(t)$ = input signal at A/D converter (volts),
C_0 = 0.00879919 m/s**2,
and C_1 = 2.17170 (m/s**2)/volt .

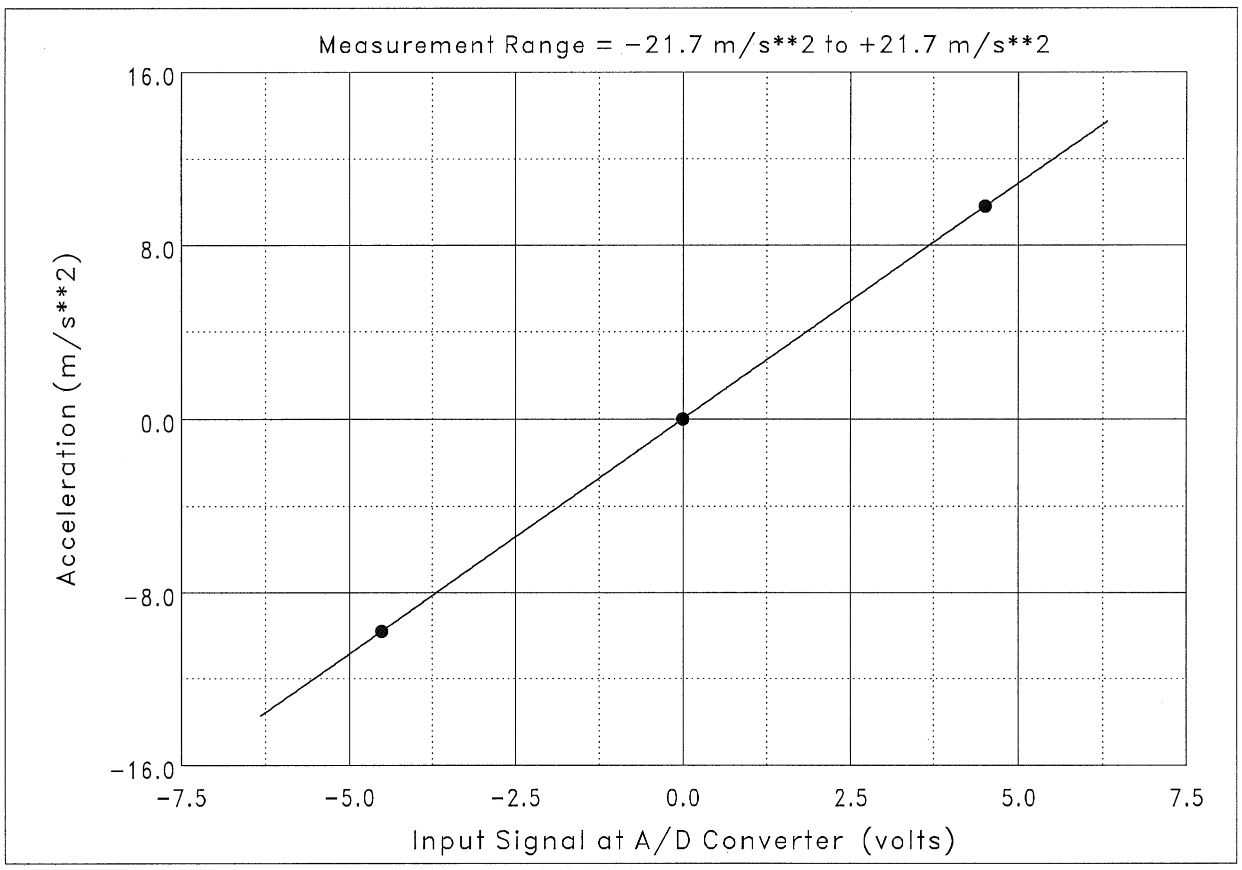

Calibration of ICEDAS Channel 28 16:29 12 December 2003

Project: Marine Structural Fragility and Software Validation **Facility:** Ice Tank

Sensor: Yaw Rate **Model:** Northrop dac7836978 **Serial Number:** 28 nrc 166870

Programmable Gain: 2 **Plug-In Gain:** 1 **Filter Frequency:** 10.0 Hz

Data Point No.	Input Signal (volts)	Physical Value (deg/s)	Fitted Curve Value (deg/s)	Error (deg/s)	
1	4.980	0.0000	0.0104	0.010433	
2	5.031	0.2000	0.2175	0.017508	
3	5.106	0.5000	0.5217	0.021727	
4	5.234	1.0000	1.0474	0.047403	
5	4.720	−1.0000	−1.0509	−0.050898	⇐ Maximum Error
6	4.849	−0.5000	−0.5270	−0.027029	
7	4.926	−0.2000	−0.2132	−0.013173	
8	4.489	−2.0000	−1.9942	0.005789	
9	5.464	2.0000	1.9860	−0.013994	
10	4.618	−1.5000	−1.4661	0.033871	
11	5.338	1.5000	1.4684	−0.031631	
Maximum Error = −1.27 % of Calibration Range.					

Definition of Calibration Curve
Polynomial Degree = 1 (Linear Fit)

$$Y = C_0 + C_1 \cdot V$$

where $Y(t)$ = Angular Velocity (deg/s),
$V(t)$ = input signal at A/D converter (volts),
C_0 = −20.3109 deg/s,
and C_1 = 4.08033 (deg/s)/volt .

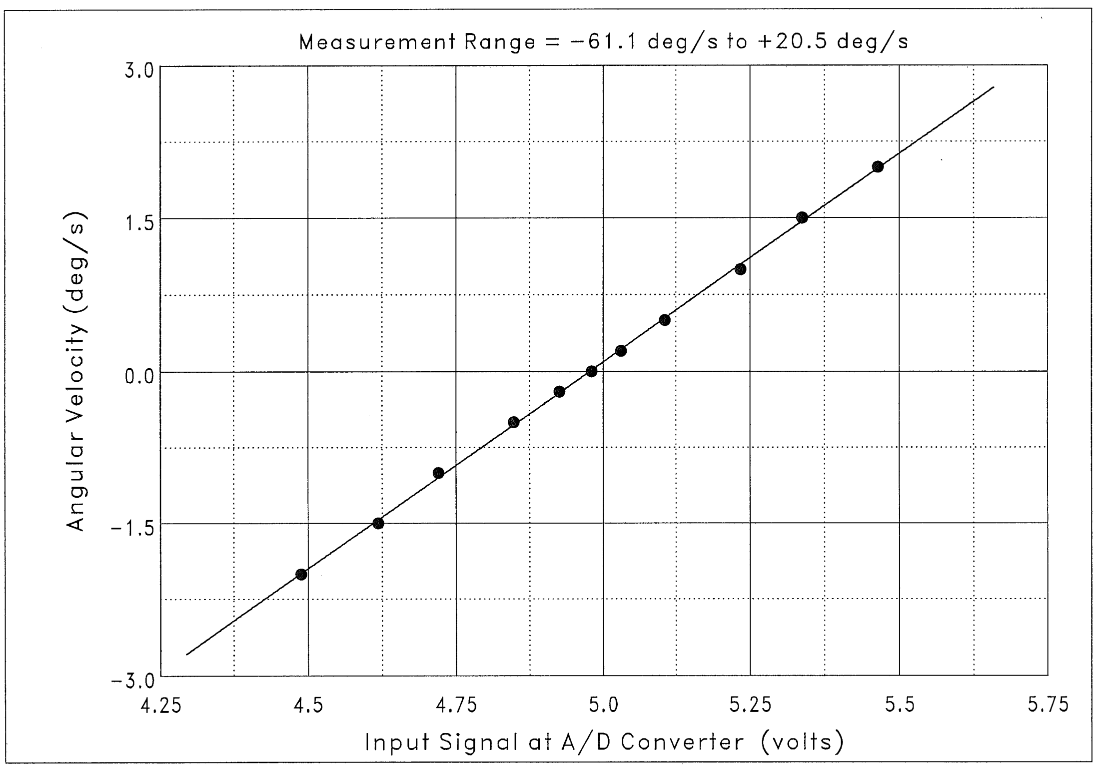

Calibration of ICEDAS Channel 33 — 12:10 — 19 November 2003

Project: Marine Structural Fragility and Software Validation **Facility:** Ice Tank

Sensor: Carriage position **Model:** ITC Carriage A/D output (CnE) **Serial Number:** N/A

Programmable Gain: 1 **Plug-In Gain:** 1 **Filter Frequency:** 10.0 Hz

Data Point No.	Input Signal (volts)	Physical Value (m)	Fitted Curve Value (m)	Error (m)	
1	−7.319	9.999	9.993	−0.0063848	
2	−4.664	19.996	20.006	0.0095901	⇐ Maximum Error
3	0.632	39.986	39.983	−0.0032005	
Maximum Error = 0.0320 % of Calibration Range.					

Definition of Calibration Curve

Polynomial Degree = 1 (Linear Fit)

$$Y = C_0 + C_1 \cdot V$$

where $Y(t)$ = Displacement (m),
$V(t)$ = input signal at A/D converter (volts),
C_0 = 37.6003 m,
and C_1 = 3.77227 m/volt .

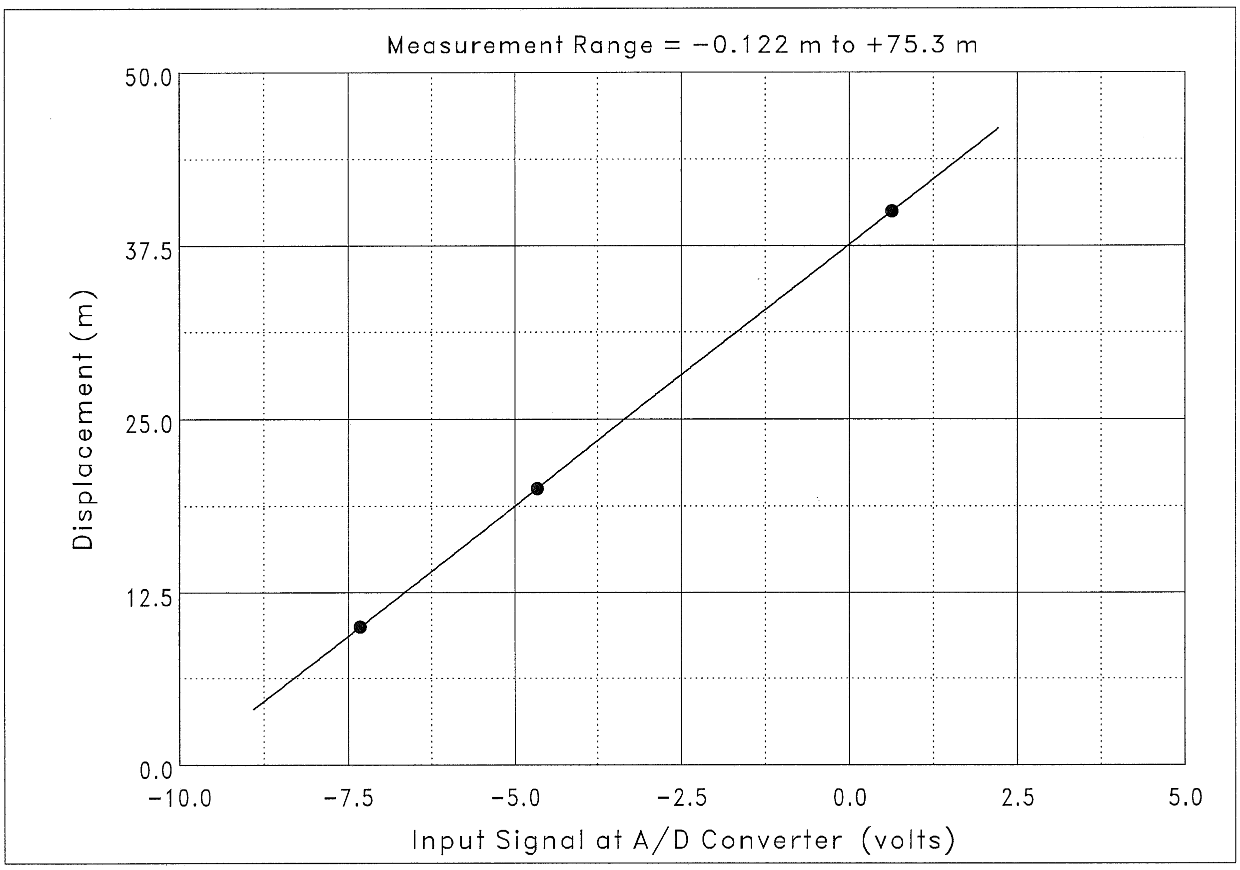

Calibration of ICEDAS Channel 34 15:54 10 December 2003

Project: Marine Structural Fragility and Software Validation **Facility:** Ice Tank

Sensor: Carriage Velocity **Model:** Carriage A/D Output (CnE) **Serial Number:** N/A

Programmable Gain: 1 **Plug-In Gain:** 1 **Filter Frequency:** 10.0 Hz

Data Point No.	Input Signal (volts)	Physical Value (m/s)
1	−6.010	0.0000
2	−0.011	1.5000

Definition of Calibration Curve
Polynomial Degree = 1 (Linear Fit)

$$Y = C_0 + C_1 \cdot V$$

where $Y(t)$ = Velocity (m/s),
$V(t)$ = input signal at A/D converter (volts),
C_0 = 1.50263 m/s,
and C_1 = 0.250007 (m/s)/volt.

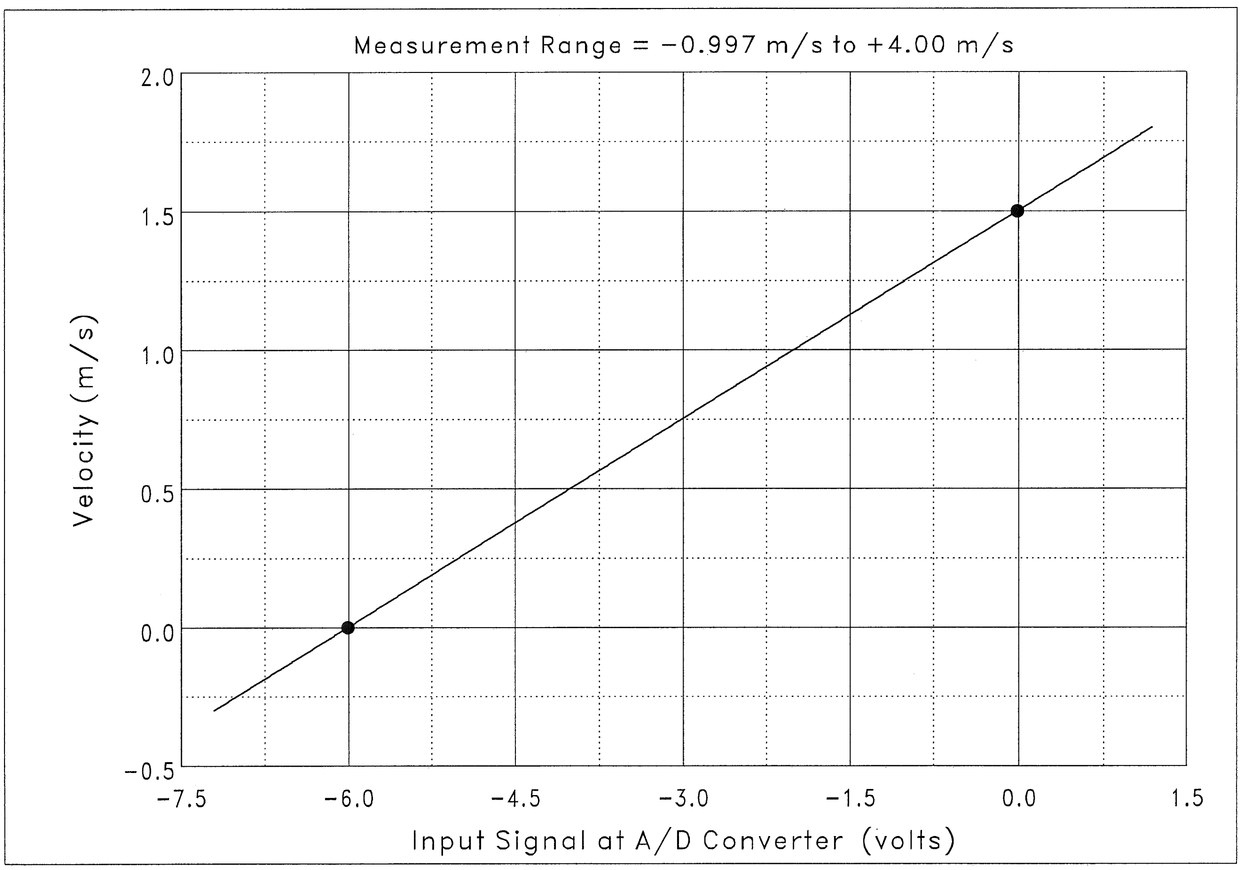

Calibration of ICEDAS Channel 35 11:24 27 November 2003

Project: Marine Structural Fragility and Software Validation **Facility:** Ice Tank

Sensor: Carriage Speed (F/V) **Model:** Ono Sokki 132 Wheel en fv801 **Serial Number:** 60302876

Programmable Gain: 1 **Plug-In Gain:** 1 **Filter Frequency:** 100.0 Hz

Data Point No.	Input Signal (volts)	Physical Value (m/s)	Fitted Curve Value (m/s)	Error (m/s)	
1	0.095	0.0250	0.0253	0.00026187	
2	4.979	1.0000	1.0001	0.00012660	
3	2.471	0.5000	0.4996	−0.00044927	⇐ Maximum Error
4	7.484	1.5000	1.5001	0.00006080	
Maximum Error = −0.0305 % of Calibration Range.					

Definition of Calibration Curve
Polynomial Degree = 1 (Linear Fit)

$$Y = C_0 + C_1 \cdot V$$

where $Y(t)$ = Velocity (m/s),
$V(t)$ = input signal at A/D converter (volts),
C_0 = 0.00628002 m/s,
and C_1 = 0.199592 (m/s)/volt .

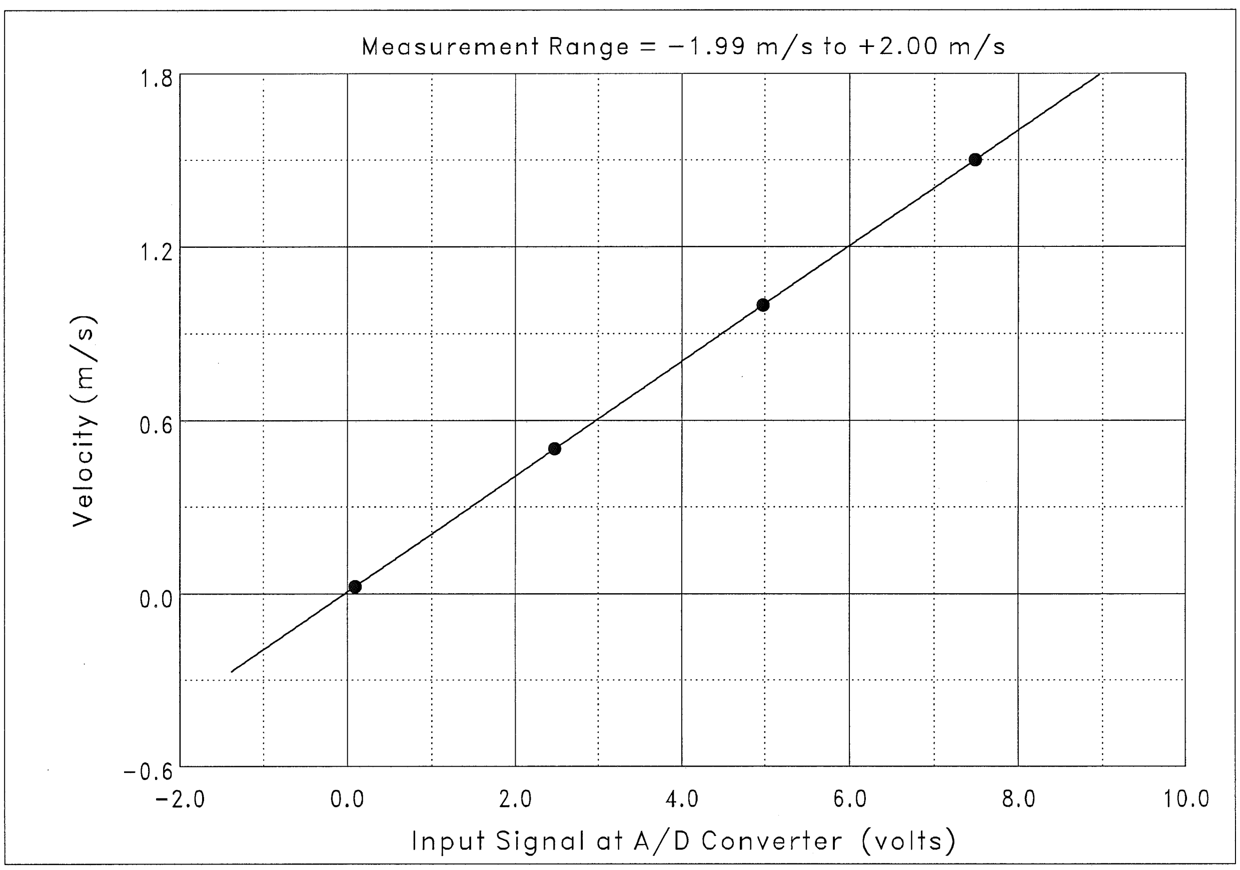

Appendix C

Ice Sheet Summaries

NRC - INSTITUTE FOR MARINE DYNAMICS

ARCTIC VESSEL RESEARCH SECTION

ICE MECHANICAL PROPERTIES SUMMARY

Test Name: NMS1 Project Number: 953

Warm up commenced: 23:00 14-DEC-2003

Time	Warm-up hrs	Loc	hi mm	Sf kPa	Lc cm	E MPa	E/Sf	Lc/hi	K1c N/m	Sf/K1c m-.5	Sc/s kPa	Rhoi Mg/m3
0820	9.33	N	39.3± 0.6 n= 3									
		S	40.5± 3.8 n= 3									
0834	9.57	40N	40.4		63.	258.6	3881	15.7				
0855	9.92	40S	38.8	49.± 4.7								
			38.5	30.(u/d 61%)								
0905	10.08	40N	39.4	64.± 1.4								
			39.4	41.(u/d 63%)								
1025	11.42	38N	39.9	53.± 3.3								
			40.5	29.(u/d 54%)								
1030	11.50	38S	39.1	48.± 3.0								
			38.3	34.(u/d 70%)								
1138	12.63	39N	40.1	47.± 6.3								
			39.9	24.(u/d 50%)								
1142	12.70	39S	38.5	37.± 1.3								
			38.5	28.(u/d 74%)								
1215	13.25	N	40.9± 1.3 n=32									
		S	40.2± 1.2 n=32									
1355	14.92	N	39.3± 1.5 n=33									
		S	39.1± 1.4 n=33									
1415	15.25	35N	40.0	42.±10.6								
			40.0	18.(u/d 43%)								
1420	15.33	35S	37.8	24.± 3.4								
			38.8	12.(u/d 48%)								
1433	15.55	66N	36.4									.841
1435	15.58	66S	35.7									.906

Run #	Date	Time	Hours from Warm-up	Flexural Strength north	south	mean
LIR_022	12/15/2003	1204	13.07	45.8	35.2	40.5
PS_LIR_023	12/15/2003	1327	14.45	45.1	27.0	36.1
AR_R10_V0P02_024	12/15/2003	1457	15.95	40.2	21.9	31.1
AR_R10_V0P1_025	12/15/2003	1521	16.35	39.0	20.7	29.9
AR_R10_V0P6_026	12/15/2003	1539	16.65	38.2	19.9	29.0
CR_R10_V0P6_027	12/15/2003	1547	16.78	37.8	19.5	28.6
CR_R10_V0P9_028	12/15/2003	1600	17.00	37.1	18.9	28.0

NRC - INSTITUTE FOR MARINE DYNAMICS

ARCTIC VESSEL RESEARCH SECTION

ICE MECHANICAL PROPERTIES SUMMARY

Test Name: NMS2 Project Number: 04953

Warm up commenced: 00:37 7-JAN-2004

Time	Warm-up hrs	Loc	hi mm	Sf kPa	Lc cm	E MPa	E/Sf	Lc/hi	K1c N/m	Sf/K1c m-.5	Sc/s kPa	Rhoi Mg/m3
0805	7.45	N	39.2± 4.3 n= 3									
		S	35.1± 0.8 n= 3									
0830	7.87	40S	36.8		50.	136.4	1629	13.7				
0900	8.37	40N	37.1	69.± 2.2								
			37.1	67.(u/d 97%)								
0903	8.42	40S	36.7	76.± 3.5								
			36.2	40.(u/d 52%)								
1031	9.89	39N	37.0	53.± 1.2								
			37.1	57.(u/d108%)								
1035	9.95	39S	37.0	54.± 7.0								
			36.4	37.(u/d 68%)								
1114	10.60	39S	37.6							s	50.4± 6.4	
1120	10.70	39N	37.6							s	40.0_ 2.9	
1129	10.85	38S	36.9	36.± 2.4								
			36.3	32.(u/d 89%)								
1137	10.99	38N	36.3	40.± 1.8								
			35.6	34.(u/d 83%)								
1220	11.70	N	38.2± 1.6 n=31									
		S	38.8± 1.5 n=31									
1318	12.67	62S	40.9									.819
1400	13.37	N	38.2± 1.3 n=31									
		S	36.9± 1.1 n=31									
1420	13.70	70S	39.1									.888
1432	13.90	66N	40.3									.845
1435	13.95	N	38.0± 2.0 n=32									
		S	38.2± 2.0 n=32									
1500	14.37	42S	36.6	27.± 2.2								

			36.2	21.(u/d 78%)
1501	14.39	42N	37.2	39.± 4.5
			37.3	32.(u/d 82%)

Run #	Date	Time	Hours from Warm-up	Flexural Strength north	south	mean
LIR_CC_111	01/07/2004	1202	11.40	39.0	32.6	35.8

NRC - INSTITUTE FOR MARINE DYNAMICS

ARCTIC VESSEL RESEARCH SECTION

ICE MECHANICAL PROPERTIES SUMMARY

Test Name: NMS3 Project Number: 04953

Warm up commenced: 22:34 8-JAN-2004

Time	Warm-up hrs	Loc	hi mm	Sf kPa	Lc cm	E MPa	E/Sf	Lc/hi	K1c N/m	Sf/K1c m-.5	Sc/s kPa	Rhoi Mg/m3
0836	10.02	N	39.3± 2.2 n= 3									
		S	39.4± 1.9 n= 3									
0846	10.19	40S	38.7		47.	90.1	1658	12.2				
0913	10.64	40N	39.8	74.± 4.3								
			40.1	44.(u/d 60%)								
0917	10.70	40S	39.1	51.± 4.8								
			39.0	36.(u/d 70%)								
1054	12.32	39N	39.8	65.± 3.7								
			39.5	36.(u/d 55%)								
1058	12.39	39S	39.6	46.± 4.4								
			40.1	31.(u/d 65%)								
1106	12.52	39N	39.3									.844
1112	12.62	39S	39.9									.850
1121	12.77	39S	39.8							s	63.2± 9.8	
1208	13.55	38N	40.2	52.± 4.0								
			40.3	32.(u/d 61%)								
1212	13.62	38S	40.1	43.± 1.2								
1317	14.70	N	40.3± 1.8 n=12									
		S	39.8± 1.8 n=12									
1418	15.72	37N	40.8	45.± 3.1								
			40.8	32.(u/d 71%)								
1420	15.75	37S	39.9	32.± 4.1								
			40.1	26.(u/d 81%)								
1430	15.92m	N	41.4± 1.9 n=19									
		S	40.8± 1.2 n=19									
1535	17.00	N	40.1± 1.0 n=13									

		S	39.7± 0.8 n=13	
1623	17.80	N	40.5± 1.8 n= 5	
		S	40.3± 1.9 n= 5	
1642	18.12	41N	40.2	26.± 4.0
			40.1	19.(u/d 71%)
1644	18.15	41S	40.0	20.± 1.9
			39.9	15.(u/d 76%)
1650	18.25	N	38.9± 2.0 n=20	
		S	38.8± 0.9 n=20	

Run #	Date	Time	Hours from Warm-up	Flexural Strength north	south	mean
LIR CC 128	01/09/2004	1245	14.17	48.2	39.8	44.0
LIR CC 129	01/09/2004	1342	15.12	48.3	34.4	41.3
LIR CC 130	01/09/2004	1351	15.27	47.3	33.7	40.5
LIR CC 131	01/09/2004	1451	16.27	41.3	29.8	35.5
LIR CC 132	01/09/2004	1502	16.45	40.3	29.1	34.7
LIR CC 133	01/09/2004	1554	17.32	28.9	22.4	25.6

NRC - INSTITUTE FOR MARINE DYNAMICS

ARCTIC VESSEL RESEARCH SECTION

ICE MECHANICAL PROPERTIES SUMMARY

Test Name: NMS4 Project Number: O4953

Warm up commenced: 22:37 11-JAN-2004

Time	Warm-up hrs	Loc	hi mm	Sf kPa	Lc cm	E MPa	E/Sf	Lc/hi	K1c N/m	Sf/K1c m-.5	Sc/s kPa	Rhoi Mg/m3
0823	9.75	N	39.4± 3.0 n= 3									
		S	40.6± 2.3 n= 3									
0837	9.99	40S	39.1		48.	90.9	1467	12.2				
0855	10.29	40N	39.2	64.± 1.3								
			39.4	42.(u/d 65%)								
0904	10.44	40S	39.6	57.± 2.9								
			39.6	42.(u/d 74%)								
0943	11.09	39N	39.3	56.± 3.6								
			39.7	105.(u/d187%)								
0959	11.35	39S	39.8	55.± 2.9								
			40.0	40.(u/d 73%)								
1047	12.15	39S	40.1							s	60.9±11.4	
1102	12.40	39S	40.1									.844
1110	12.54	39N	41.1									.809
1119	12.69	38N	39.9	54.± 4.0								
			40.4	40.(u/d 74%)								
1122	12.74	38S	40.2	47.± 4.8								
			40.7	33.(u/d 70%)								
1330	14.87	N	41.0± 2.1 n=14									
		S	40.9± 2.1 n=14									
1351	15.22	37N	40.6	41.± 1.7								
			41.0	28.(u/d 68%)								
1352	15.24	37S	40.3	34.± 2.1								
			40.5	25.(u/d 72%)								
1432	15.90	N	41.7± 1.8 n=12									
		S	41.2± 1.0 n=12									

1511	16.55	N	40.3± 0.4 n= 5	
		S	40.5± 0.4 n= 5	
1536	16.97	N	39.7± 0.5 n= 5	
		S	39.8± 0.5 n= 5	
1655	18.29	N	39.0± 0.9 n= 4	
		S	39.4± 0.2 n= 4	
1717	18.65	N	39.2± 0.2 n= 4	
		S	39.3± 0.4 n= 4	
1732	18.90	35N	40.1	16.± 2.0
1735	18.95	35S	40.5	11.± 0.8
			40.8	10.(u/d 87%)

Run #	Date	Time	Hours from Warm-up	Flexural Strength north	south	mean
LIR CC 144	01/12/2004	1309	14.52	45.5	39.1	42.3
LIR CC 145	01/12/2004	1356	15.30	40.3	33.6	36.9
LIR CC 146	01/12/2004	1408	15.50	39.1	32.3	35.7
LIR CC 147	01/12/2004	1446	16.14	35.4	28.6	32.0
LIR CC 148	01/12/2004	1528	16.84	31.8	25.0	28.4

NRC - INSTITUTE FOR OCEAN TECHNOLOGY

ICE TANK FACILITIES

ICE MECHANICAL PROPERTIES SUMMARY

Test Name: NMS5 Project Number: 04953

Warm up commenced: 22:40 13-JAN-2004

Time	Warm-up hrs	Loc	hi mm	Sf kPa	Lc cm	E MPa	E/Sf	Lc/hi	K1c N/m	Sf/K1c m-.5	Sc/s kPa	Rhoi Mg/m3
0823	9.70	N	38.5± 1.4 n= 3									
		S	40.3± 1.4 n= 3									
0832	9.85	40N	38.2		41.	51.2	1448	10.6				
0854	10.22	40N	39.4	34.± 0.6								
			39.4	25.(u/d 73%)								
0858	10.29	40S	39.1	37.± 5.5								
			39.5	28.(u/d 74%)								
1028	11.79	N	39.4± 1.5 n= 4									
		S	40.0± 1.2 n= 4									
1051	12.17	N	38.5± 0.9 n= 4									
		S	38.2± 0.8 n= 4									
1105	12.40	N	39.0± 1.8 n= 4									
		S	39.1± 2.3 n= 4									
1122	12.69	38N	40.9	38.± 5.0								
			41.1	32.(u/d 83%)								
1129	12.80	38N	40.1	32.± 1.3								
			39.1	17.(u/d 54%)								
1138	12.95	38S	40.0							s	44.2± 5.8	
1222	13.69	N	41.8± 0.7 n= 5									
		S	41.1± 0.8 n= 5									
1316	14.59	37N	39.1	28.± 3.6								
			38.7	18.(u/d 63%)								
1317	14.60	37S	40.4	29.± 4.2								
			40.5	20.(u/d 70%)								
1324	14.72	N	41.2± 0.7 n= 5									
		S	40.9± 1.7 n= 5									
1437	15.94	N	40.3± 0.7 n= 5									

		S	41.0± 0.7 n= 5		
1508	16.45	36N	41.0		.867
1511	16.50	37S	40.4		.915
1514	16.55	N	40.4± 0.2 n= 5		
		S	40.4_ 0.4 n= 5		
1523	16.70	34N	39.0	18.± 2.6	
			39.1	10.(u/d 57%)	
1525	16.74	34S	40.2	16.± 0.6	
			40.0	12.(u/d 71%)	
1559	17.30	N	38.6± 0.5 n= 5		
		S	39.6± 0.5 n= 5		
1623	17.70	N	38.8± 0.8 n= 5		
		S	39.2± 0.7 n= 5		
1648	18.12	N	39.8± 0.7 n= 6		
		S	40.4± 1.2 n= 6		
1703	18.37	41N	39.0	18.± 1.3	
			39.3	13.(u/d 70%)	
1708	18.45	41S	39.1	15.± 0.9	
			39.0	7.(u/d 50%)	

Run #	Date	Time	Hours from Warm-up	Flexural Strength north	south	mean
LIR_YAW00_0P6_CC_156	01/14/2004	1050	12.15	33.0	31.7	32.3
LIR_YAW2_0P6_SQP_157	01/14/2004	1050	12.15	33.0	31.7	32.3
LIR_YAWM2_0P6_NQP_158	01/14/2004	1050	12.15	33.0	31.7	32.3
LIR31_0P6_AR10_164	01/14/2004	1206	13.42	29.1	27.1	28.1
LIR31_0P6_AR10_165	01/14/2004	1236	13.92	27.7	25.5	26.6
LIR33_0P4_AR10_168	01/14/2004	1424	15.72	23.1	20.5	21.8
LIR34_0P3_AR10_169	01/14/2004	1457	16.27	21.8	19.2	20.5
LIR35_0P2_AR10_170	01/14/2004	1543	17.04	20.2	17.4	18.8
LIR36_0P1_AR10_171	01/14/2004	1613	17.54	19.2	16.4	17.8
LIR37_0P05_AR10_172	01/14/2004	1635	17.90	18.5	15.7	17.1

Appendix D

Test Matrix

<table>
<tr><th>Test type</th><th>Name</th></tr>
<tr><td>Level Ice Resistance Runs</td><td>

Name: LIR_'Channel'_Inc.dac

- LIR = Level Ice Resistance
- Channel = test location (CC, NQP, or SQP) If not stated assume CC
- Inc = Incremented File Number (automatically)
- dac = extension for GEDAP files.

Example: LIR_CC_111

- Level ice resistance, Center Channel, 111^{th} run sequence.

</td></tr>
<tr><td>Pre-sawn Resistance Runs</td><td>

Name: PS_'SQP'_'Cut'_Inc.dac

- PS = Pre-sawn Ice Resistance
- SQP = test performed in South Quarter Point
- Cut = HB or SC. If not stated assume HB
    - HB = Herring Bone
    - SC = Straight Cut
- Inc = Incremented File Number (automatically)
- dac = extension for GEDAP files.

Example: PRESAWN_SQP_HB_112

- Pre-sawn ice resistance, South Quarter Point, Herring Bone, 112^{th} run sequence.

</td></tr>
<tr><td>Arc Ice Runs</td><td>

Name: 'LIR##'_'V_m'_'AR#'_Inc.dac

- LIR = Level Ice Resistance
- ## = Ice sheet #, Arc #
- V_m = Velocity of the model (example: 0P1 = 0.1 m/s)
- RA# = Rudder Angle (degrees)
- AR# = Arc Radius (m)
- Inc = Incremented File Number (automatically)
- dac = extension for GEDAP files.

Example: LIR23_OP6_AR10_147

- Level ice test, Ice Sheet # 2, Run # 3, Model Speed = 0.6 m/s, Arc radius = 10 m, 147^{th} run sequence.

</td></tr>
<tr><td>Open Water Runs</td><td>

Name: 'OW#'_'V_m'_'RA#'_'AR#'_inc.dac

- OW = Open Water
- V_m = Model Speed
- Inc = Incremented File Number

Example: OW1_OP1_RA0_AR999_053

- Open Water Test, Speed of 0.1m/s, Rudder Angle of 0°, and Arc radius of 999 m, 53^{rd} run sequence

</td></tr>
</table>

Experiments in Level Ice:

Run name	Test Date	Test Time	Model Velocity (m/s)	Arc Radius (m)
LIR_022	15-Dec-03	12:04:34	0.1	Straight
LIR_022	15-Dec-03	12:04:34	0.6	Straight
LIR_022	15-Dec-03	12:04:34	0.9	Straight
LIR_022	15-Dec-03	12:04:34	0.02	Straight
LIR_CC_111	7-JAN-2004	12:02:05	0.1	Straight
LIR_CC_111	7-JAN-2004	12:02:05	0.3	Straight
LIR_CC_111	7-JAN-2004	12:02:05	0.6	Straight
LIR_CC_111	7-JAN-2004	12:02:05	0.02	Straight
LIR_NQP_114	7-JAN-2004	14:20:35	0.1	Straight
LIR_NQP_114	7-JAN-2004	14:20:35	0.6	Straight
LIR_NQP_114	7-JAN-2004	14:20:35	0.9	Straight
LIR_NQP_114	7-JAN-2004	14:20:35	0.02	Straight
LIR11_0P1_AR50_128	9-JAN-2004	12:45:07	0.1	50
LIR11A_0P1_129	9-JAN-2004	13:42:14	0.1	Straight
LIR12_0P3_AR50_130	9-JAN-2004	13:51:13	0.3	50
LIR12A_0P3_131	9-JAN-2004	14:51:09	0.3	Straight
LIR13_0P3_AR10_132	9-JAN-2004	15:02:01	0.3	10
LIR14_0P1_AR10_133	9-JAN-2004	15:54:43	0.1	10
LIR_SQP_134	9-JAN-2004	16:29:41	0.1	Straight
LIR_SQP_134	9-JAN-2004	16:29:41	0.3	Straight
LIR_SQP_134	9-JAN-2004	16:29:41	0.6	Straight
LIR21_OP6_AR50_144	12-Jan-04	13:09:49	0.6	50
LIR21A_OP6_145	12-Jan-04	13:56:30	0.6	Straight
LIR22_OP02_AR50_146	12-Jan-04	14:08:37	0.02	10
LIR23A_OP6_AR10_148	12-Jan-04	15:26:37	0.6	10
LIR24A_SQP_149	12-Jan-04	16:13:52	0.1	Straight
LIR24A_SQP_149	12-Jan-04	16:13:52	0.3	Straight
LIR24A_SQP_149	12-Jan-04	16:13:52	0.6	Straight
LIR24A_SQP_149	12-Jan-04	16:13:52	0.02	Straight
LIR24B_SQP_150	12-Jan-04	16:20:47	0.1	Straight
LIR24B_SQP_150	12-Jan-04	16:20:47	0.02	Straight
LIR25_0P3_AR10_152	12-Jan-04	16:46:56	0.3	10
LIR24_0P02_AR10_153	12-Jan-04	17:07:13	0.02	10
LIR31_0P6_AR10_164	14-Jan-04	12:06:49	0.6	10
LIR31_0P6_AR10_165	14-Jan-04	12:36:36	0.5	10
LIR33_0P4_AR10_168	14-Jan-04	14:24:42	0.4	10
LIR34_0P3_AR10_169	14-Jan-04	14:57:49	0.3	10
LIR35_0P2_AR10_170	14-Jan-04	15:43:54	0.2	10
LIR36_0P1_AR10_171	14-Jan-04	16:13:08	0.1	10
LIR37_0P05_AR10_172	14-Jan-04	16:35:16	0.05	10

Experiments in Pre-sawn Ice:

Run Name	Test Date	Test Time	Model Velocity (m/s)	Run Pattern
PS_SQP_023	15-Dec-03	13:27:19	0.1	Straight
PS_SQP_023	15-Dec-03	13:27:19	0.6	Straight
PS_SQP_023	15-Dec-03	13:27:19	0.9	Straight
PS_SQP_023	15-Dec-03	13:27:19	0.02	Straight
PRESAWN_SQP_HB_112	7-JAN-2004	13:26:04	0.1	Straight
PRESAWN_SQP_HB_112	7-JAN-2004	13:26:04	0.3	Straight
PRESAWN_SQP_HB_112	7-JAN-2004	13:26:04	0.6	Straight
PRESAWN_SQP_HB_112	7-JAN-2004	13:26:04	0.02	Straight
PRESAWN_SQP_SC_113	7-JAN-2004	13:38:01	0.1	Straight
PRESAWN_SQP_SC_113	7-JAN-2004	13:38:01	0.3	Straight
PRESAWN_SQP_SC_113	7-JAN-2004	13:38:01	0.6	Straight
PRESAWN_SQP_SC_113	7-JAN-2004	13:38:01	0.02	Straight

Experiments in Open Water:

Open Water Test	Test Date	Test Time	Model Speed (m/s)	Arc Radius (m)	Rudder Angle (degrees)
OW1_OP1_RA0_AR999_053	22-Dec-03	15:48:41	0.1	Straight	0
OW1_OP6_RA0_AR999_054	22-Dec-03	16:00:08	0.6	Straight	0
OW2_0P9_RA0_AR999_057	23-Dec-03	8:45:41	0.9	Straight	0
OW4_0P1_RA0_AR50_058	23-Dec-03	9:05:41	0.1	50	0
OW5_0P6_RA0_AR50_059	23-Dec-03	9:40:34	0.6	50	0
OW6_0P9_RA0_AR50_060	23-Dec-03	9:49:42	0.9	50	0
OW7_0P1_RA0_AR10_061	23-Dec-03	9:57:38	0.1	10	0
OW8_0P6_RA0_AR10_062	23-Dec-03	10:08:16	0.6	10	0
OW9_0P9_RA0_AR10_063	23-Dec-03	10:18:20	0.9	10	0
OW9A_0P9_RA0_CR10_064	23-Dec-03	10:28:18	0.9	10	0
OW10_0P1_RA20_CR999_065	23-Dec-03	10:54:59	0.1	Straight	20
OW10_0P6_RA20_CR999_066	23-Dec-03	11:05:01	0.6	Straight	20
OW12_0P9_RA20_CR999_067	23-Dec-03	11:15:29	0.9	Straight	20
OW13_0P1_RA20_AR50_068	23-Dec-03	11:25:25	0.1	50	20
OW14_0P6_RA20_AR50_069	23-Dec-03	11:35:22	0.6	50	20
OW15_0P9_RA20_AR50_070	23-Dec-03	11:42:59	0.9	50	20
OW16_0P1_RA20_CR10_071	23-Dec-03	11:49:30	0.1	10	20
OW17_0P6_RA20_CR10_072	23-Dec-03	12:00:02	0.6	10	20
OW18_0P9_RA20_CR10_073	23-Dec-03	12:10:43	0.9	10	20
OW19_0P1_RA30_CR999_074	23-Dec-03	12:20:45	0.1	Straight	20
OW20_0P6_RA30_CR999_075	23-Dec-03	12:31:15	0.6	Straight	30
OW21_0P9_RA30_CR999_076	23-Dec-03	12:41:11	0.9	Straight	30
OW22_0P1_RA30_AR50_077	23-Dec-03	12:50:59	0.1	50	30
OW23_0P6_RA30_AR50_078	23-Dec-03	12:59:23	0.6	50	30
OW24_0P9_RA30_AR50_079	23-Dec-03	13:05:46	0.9	50	30
OW25_0P1_RA30_CR10_080	23-Dec-03	13:18:26	0.1	10	30
OW25A_0P1_RA30_CR10_083	23-Dec-03	13:44:18	0.1	10	30
OW26_0P6_RA30_CR10_081	23-Dec-03	13:28:54	0.6	10	30
OW27_0P9_RA30_CR10_082	23-Dec-03	13:38:36	0.9	10	30
OW28_0P1_OP6_0P9_RA00_CR999_084	23-Dec-03	13:55:08	0.1	Straight	0
OW28_0P1_OP6_0P9_RA00_CR999_084	23-Dec-03	13:55:08	0.6	Straight	0
OW28_0P1_OP6_0P9_RA00_CR999_084	23-Dec-03	13:55:08	0.9	Straight	0
OW29_0P6_RA0_AR999_096	5-JAN-04	13:31:25	0.6	Straight	0
OW30_0P3_RA0_AR999_097	5-JAN-04	13:41:20	0.3	Straight	0
OW31_0P1_RA0_AR50_101	5-JAN-04	15:11:15	0.1	50	0
OW32_0P6_RA0_AR50_102	5-JAN-04	15:20:38	0.6	50	0
OW33_0P3_RA0_AR50_098	5-JAN-04	14:17:29	0.3	50	0
OW34_0P1_RA0_AR10_103	5-JAN-04	15:28:34	0.1	10	0
OW35A_0P6_RA0_AR10_105	5-JAN-04	15:49:43	0.6	10	0
OW36_0P3_RA0_AR10_099	5-JAN-04	14:49:55	0.3	10	0

Appendix E

Channel Width Measurements in Ice Tests

The actual measured data for channel edge positions in the model tests are discontinuous and unavoidable with human errors. It is expected that the two edges of the channel width were parallel and concentric to the model path that was controlled by the PMM. Concentric circles of various radii were then fitted to the measurements to obtain the best match.

<u>Example</u>

For Run LIR31_0P6_AR10_165, the circling radius was 10m, and the model speed was 0.6m/s. The radii of the best fitted circular arcs for the inner and the outer edges were 9.45 and 10.65 m, respectively, with a channel width of 1.2 m, as shown in Figure E.1.

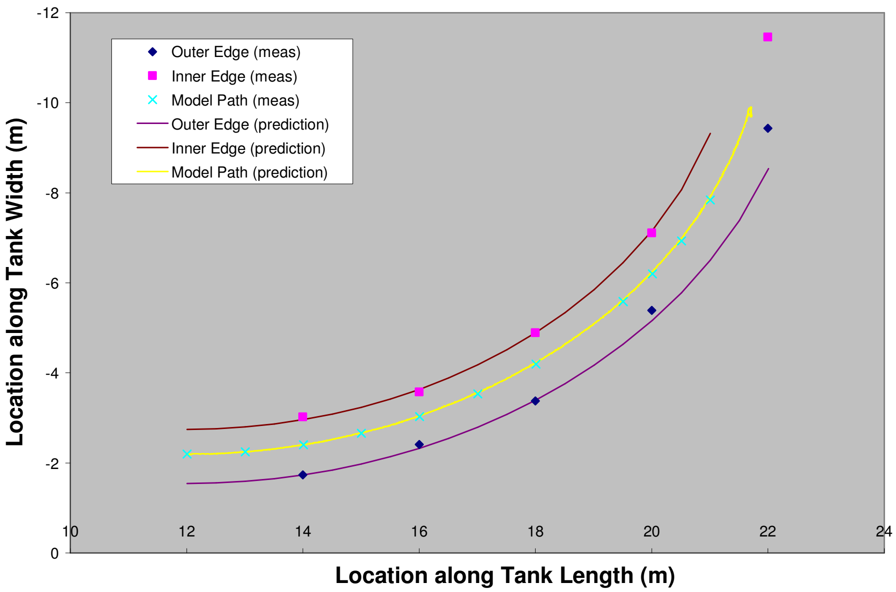

Figure E.1: The measured and predicted channel edge positions

Summary of Channel Width Measurements

Run Name: LIR11_0P1_AR50_128
Data: 9-Jan-04
Circle Radius (m): 50
Model Velocity (m/s): 0.1
Channel Width (m): 1.0

Position X (m)	North Edge Y_N (m)	South Edge Y_S (m)
2	1.83	2.73
4	1.91	2.90
6	2.22	3.16
8	2.56	3.52
10	2.91	3.97
12	3.25	4.36
14	3.77	4.88
16	4.44	5.65
18	5.09	6.23
20	5.81	7.28
22	6.85	8.15
24	8.39	8.84

Run Name: LIR12_0P3_AR50_130
Data: 9-Jan-04
Circle Radius (m): 50
Model Velocity (m/s): 0.3
Channel Width (m): 1.05

Position X (m)	North Edge Y_N (m)	South Edge Y_S (m)
24	1.93	2.85
26	1.81	3.01
28	2.32	3.36
30	2.55	3.62
32	3.03	3.98
34	3.60	4.61
36	4.18	5.29
38	4.64	5.91
40	5.44	6.67
42	6.56	7.55
44	7.44	8.57
46	8.33	9.69
48	9.81	10.75

Run Name: LIR13_0P3_AR10_132
Data: 9-Jan-04
Circle Radius (m): 10
Model Velocity (m/s): 0.3
Channel Width (m): 1.02

Position X (m)	North Edge Y_N (m)	South Edge Y_S (m)
48	2.16	3.52
50	3.02	4.33
52	4.59	6.14
54	6.88	10.30

Run Name: LIR14_0P1_AR10_133
Data: 9-Jan-04
Circle Radius (m): 10
Model Velocity (m/s): 0.1
Channel Width (m): 1.2

Position X (m)	North Edge Y_N (m)	South Edge Y_S (m)
54	1.97	3.20
56	2.83	4.08
58	3.86	5.79
60	6.49	8.89
62	11.35	11.35

Run Name: LIR21_OP6_AR50_144
Data: 12-Jan-04
Circle Radius (m): 50
Model Velocity (m/s): 0.6
Channel Width (m): 1.1

Position X (m)	North Edge Y_N (m)	South Edge Y_S (m)	Position X (m)	North Edge Y_N (m)	South Edge Y_S (m)
2	1.89	2.71	16	4.46	5.53
4	1.90	2.94	18	5.13	6.39
6	2.02	3.18	20	6.05	7.19
8	2.35	3.54	22	6.93	8.04
10	2.84	3.84	24	8.08	9.25
12	3.28	4.43	26	9.09	10.61
14	3.76	4.89	28	10.79	10.79

Run Name: LIR22_OP02_AR50_146
Data: 12-Jan-04
Circle Radius (m): 50
Model Velocity (m/s): 0.02
Channel Width (m): 1.0

Position X (m)	North Edge Y_N (m)	South Edge Y_S (m)
28	1.88	2.92
30	1.90	2.93
32	1.96	3.06
34	2.35	2.86

Run Name: LIR23A_OP6_AR10_148
Data: 12-Jan-04
Circle Radius (m): 10
Model Velocity (m/s): 0.6
Channel Width (m): 1.35

Position X (m)	North Edge Y_N (m)	South Edge Y_S (m)
40	1.60	3.14
42	2.16	3.57
44	3.14	4.69
46	4.76	6.47
48	7.34	8.86

Run Name: LIR25_0P3_AR10_152
Data: 12-Jan-04
Circle Radius (m): 10
Model Velocity (m/s): 0.3
Channel Width (m): 1.3

Position X (m)	North Edge Y_N (m)	South Edge Y_S (m)
48	1.94	3.23
50	2.71	4.36
52	4.16	6
54	5.65	9.44
56	11.53	11.53

Run Name: LIR24_0P02_AR10_153
Data: 12-Jan-04
Circle Radius (m): 10
Model Velocity (m/s): 0.02
Channel Width (m): 1.1

Position X (m)	North Edge Y_N (m)	South Edge Y_S (m)
52	1.89	3.08
54	1.89	3.08
56	2.62	3.89
58	4.16	4.16

Run Name: LIR31_0P6_AR10_164
Data: 14-Jan-04
Circle Radius (m): 10
Model Velocity (m/s): 0.6
Channel Width (m): 1.25

Position X (m)	North Edge Y_N (m)	South Edge Y_S (m)
8	1.63	3.07
10	2.39	3.81
12	3.67	5.22
14	5.27	7.44
15.5	7.7	8.93

Run Name: LIR31_0P6_AR10_165
Data: 14-Jan-04
Circle Radius (m): 10
Model Velocity (m/s): 0.5
Channel Width (m): 1.2

Position X (m)	North Edge Y_N (m)	South Edge Y_S (m)
14	1.74	3.02
16	2.41	3.58
18	3.38	4.89
20	5.39	7.11
22	9.43	11.46

Run Name: LIR33_0P4_AR10_168
Data: 14-Jan-04
Circle Radius (m): 10
Model Velocity (m/s): 0.4
Channel Width (m): 1.15

Position X (m)	North Edge Y_N (m)	South Edge Y_S (m)
22	1.77	2.99
24	1.99	3.49
26	3.39	4.77
28	5.47	7.46
30	8.43	10.99

Run Name: LIR34_0P3_AR10_169
Data: 14-Jan-04
Circle Radius (m): 10
Model Velocity (m/s): 0.3
Channel Width (m): 1.25

Position X (m)	North Edge Y_N (m)	South Edge Y_S (m)
28	1.83	2.94
30	2.26	3.45
32	2.89	4.42
34	4.73	6.49
36	6.41	10.09
36.5	10.92	10.92

Run Name: LIR35_0P2_AR10_170
Data: 14-Jan-04
Circle Radius (m): 10
Model Velocity (m/s): 0.2
Channel Width (m): 1.1

Position X (m)	North Edge Y_N (m)	South Edge Y_S (m)
40	1.84	3.02
42	2.42	3.92
44	3.57	5.18
46	6.02	7.85
47.5	8.36	10.85

Run Name: LIR36_0P1_AR10_171
Data: 14-Jan-04
Circle Radius (m): 10
Model Velocity (m/s): 0.1
Channel Width (m): 1.05

Position X (m)	North Edge Y_N (m)	South Edge Y_S (m)
46	1.9	3.06
48	2.25	3.43
50	3.41	4.71
52	4.87	6.66
54	8.37	10.75

Run Name: LIR37_0P5_AR10_172
Data: 14-Jan-04
Circle Radius (m): 10
Model Velocity (m/s): 0.05
Channel Width (m): 1.15

Position X (m)	North Edge Y_N (m)	South Edge Y_S (m)
54	2.05	3.4
56	2.91	4.37
58	4.7	6.35
60	8	9.95
60.5	10.15	10.15

Channel widths of straight model tests

The channel widths for the straight test runs were not obtained with the exception of LIR_022. The average channel width for this run is 0.99 m.

Run Name: LIR_022
Data: 15-Dec-03
Straight Test Run
Model Velocity (m/s): 0.1, 0.6, 0.9 and 0.02
Channel width (m): 0.99

Position (X) (m)	Channel Width (m)
2	1.04
4	1.02
6	1.02
8	1.015
10	0.96
12	0.97
14	1
16	1.05
18	1.03
20	0.92
22	0.99
24	0.93
26	0.965
28	1.05
30	0.95
32	1.05
34	1.01
36	0.98
38	0.95
40	0.95
42	0.943
44	0.945
46	0.91
48	1.09
50	0.99
52	1.065
54	0.94
56	1.06
58	1.06
60	0.99
62	0.98
64	1

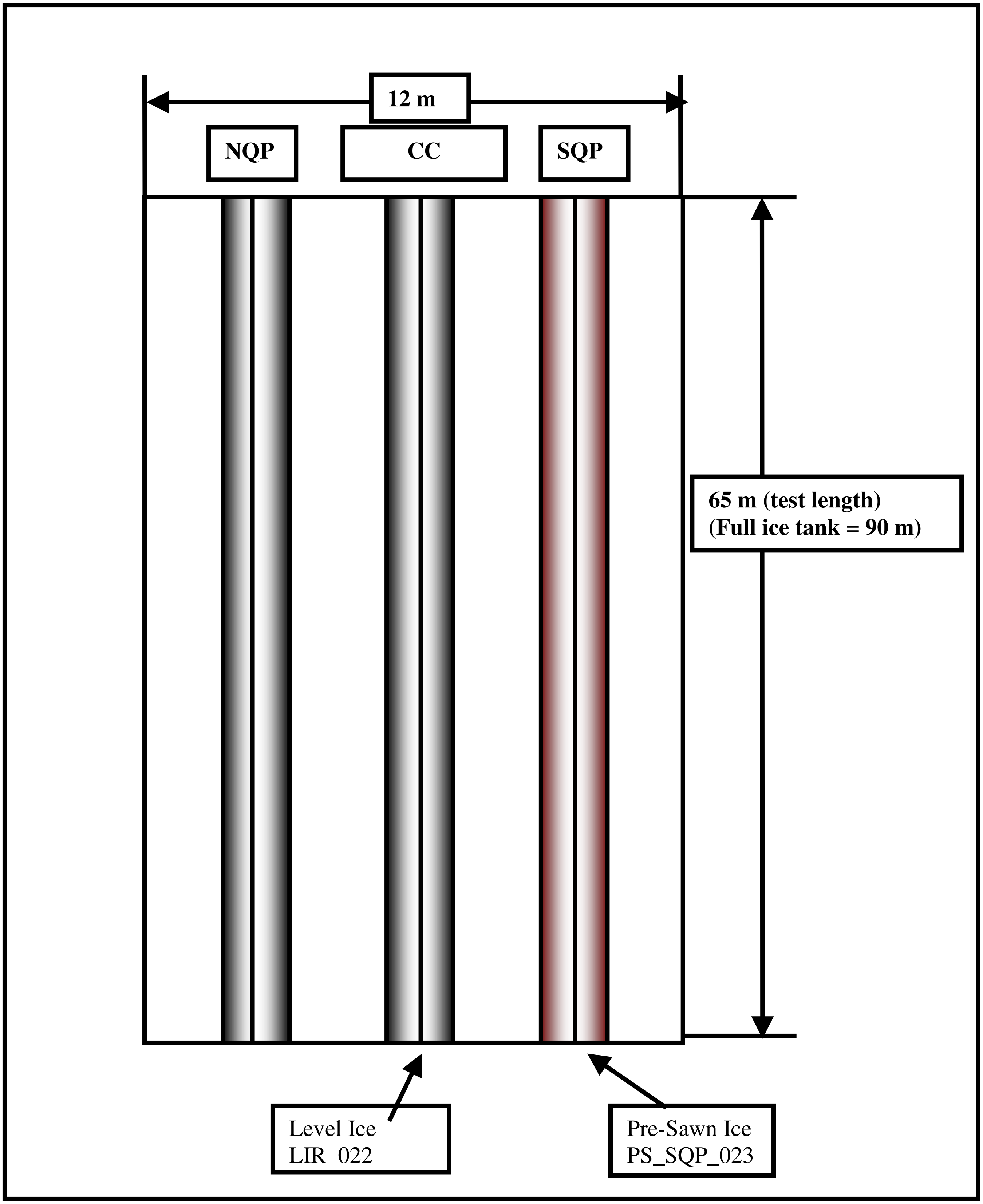

Figure E.2 : Run schematic for NMS1

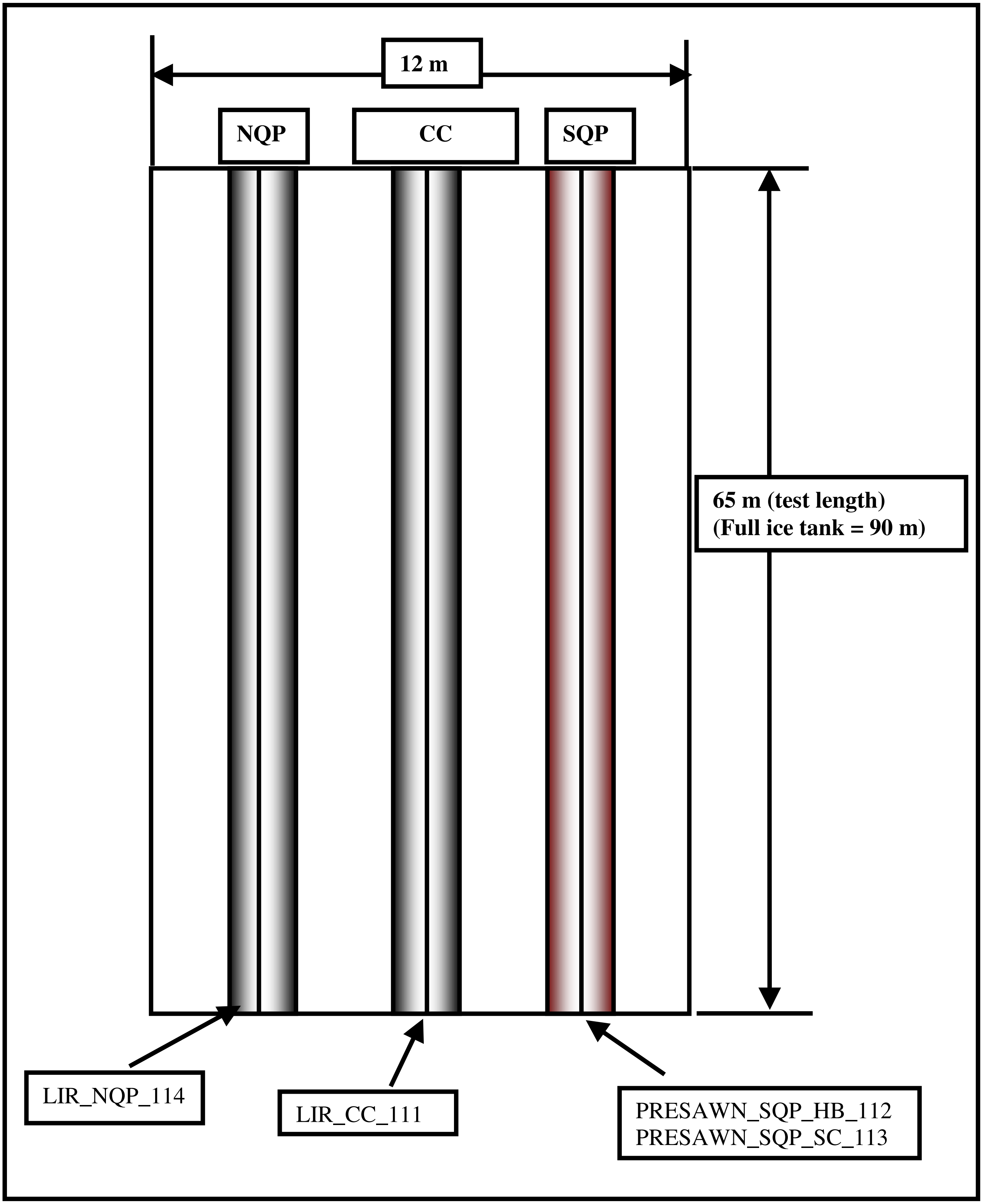

Figure E.3: Run schematic for NMS2

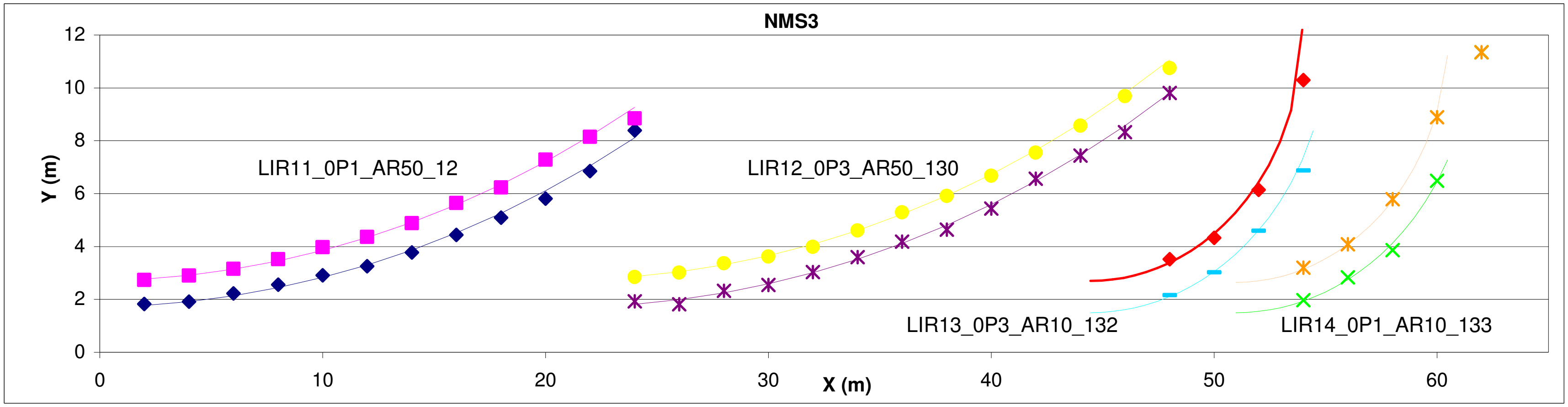

Figure E.4: Run schematic for NMS3

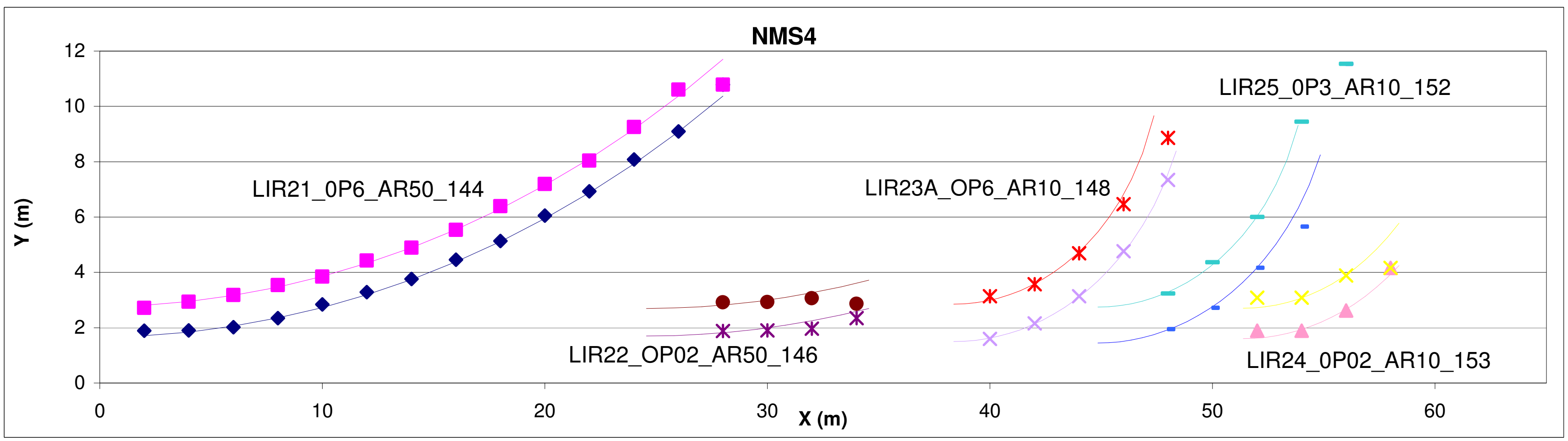

Figure E.5: Run schematic for NMS4

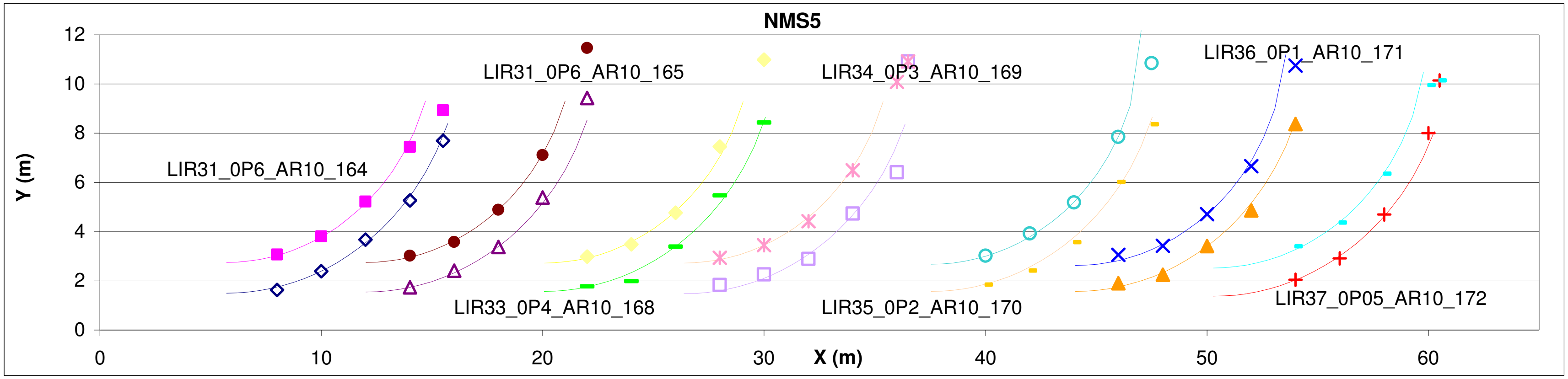

Figure E.6: Run schematic for NMS5

Appendix F

Typical Test Results

---- Tared Data ----

Analysis Date/Time = 4-NOV-2004 15:06:52
Acquired Date/Time = 9-JAN-2004 13:51:13
Input File = SHORT_S1
Output File = LIR12_0P3_AR50_130_STAT
Number of Samples = 3823
Segment Start Time = 46.060 seconds
Segment End Time = 122.50 seconds

Description	Unit	Min	Max	Mean	S.D.	Chan
Carriage Pos	m	32.728	54.380	43.823	6.2798	1
Surge Force	N	-321.74	42.141	-40.422	43.589	2
Fwd Sway Force	N	-280.78	401.37	-2.9793	69.398	3
Aft Sway Force	N	-123.36	58.446	-27.552	27.383	4
Sway Force	N	-318.65	372.47	-30.532	75.458	5
Yaw Moment	N-m	-277.74	427.40	25.955	71.160	6
Yaw	deg	-1.0460	0.028460	-0.44232	0.16563	7
Yaw Rate	deg/s	-0.91877	0.30031	-0.34316	0.14598	8
Sway Position	m	-7.2319	-0.18155	-2.8765	2.0751	9
Sway Velocity	m/s	-0.15904	-0.023292	-0.092805	0.037904	10
Fwd Heave	mm	-25.435	14.294	-3.5443	7.5967	11
Aft Heave	mm	1.7785	23.577	14.203	6.3322	12
Heave	mm	-38.884	-4.8861	-22.481	7.8800	13
Pitch	deg	-0.028460	1.0460	0.44232	0.16563	14
Surge Accel	m/s**2	-0.42561	0.098509	-0.057883	0.064508	15
Sway Accel	m/s**2	-0.11114	0.17385	0.028358	0.045376	16
Heave Accel	m/s**2	-0.20268	0.24203	-0.00077895	0.066082	17
Carriage Speed	m/s	0.25358	0.30048	0.28210	0.012611	18
Tangential Vel	m/s	0.29517	0.30406	0.29964	0.0012147	19
Cal_Yaw	deg	-31.807	-4.4612	-18.206	7.6650	20
Cal_Yaw - Yaw	deg	-1.2399	2.0189	0.66486	0.37142	21

Marine Structural Fragility and Software Validation
TERRY FOX - PMM/MANEUVER/ICE IOT

Analyzed: 04-NOV-2004 15:06:55
Acquired: 9-JAN-2004 13:51:13

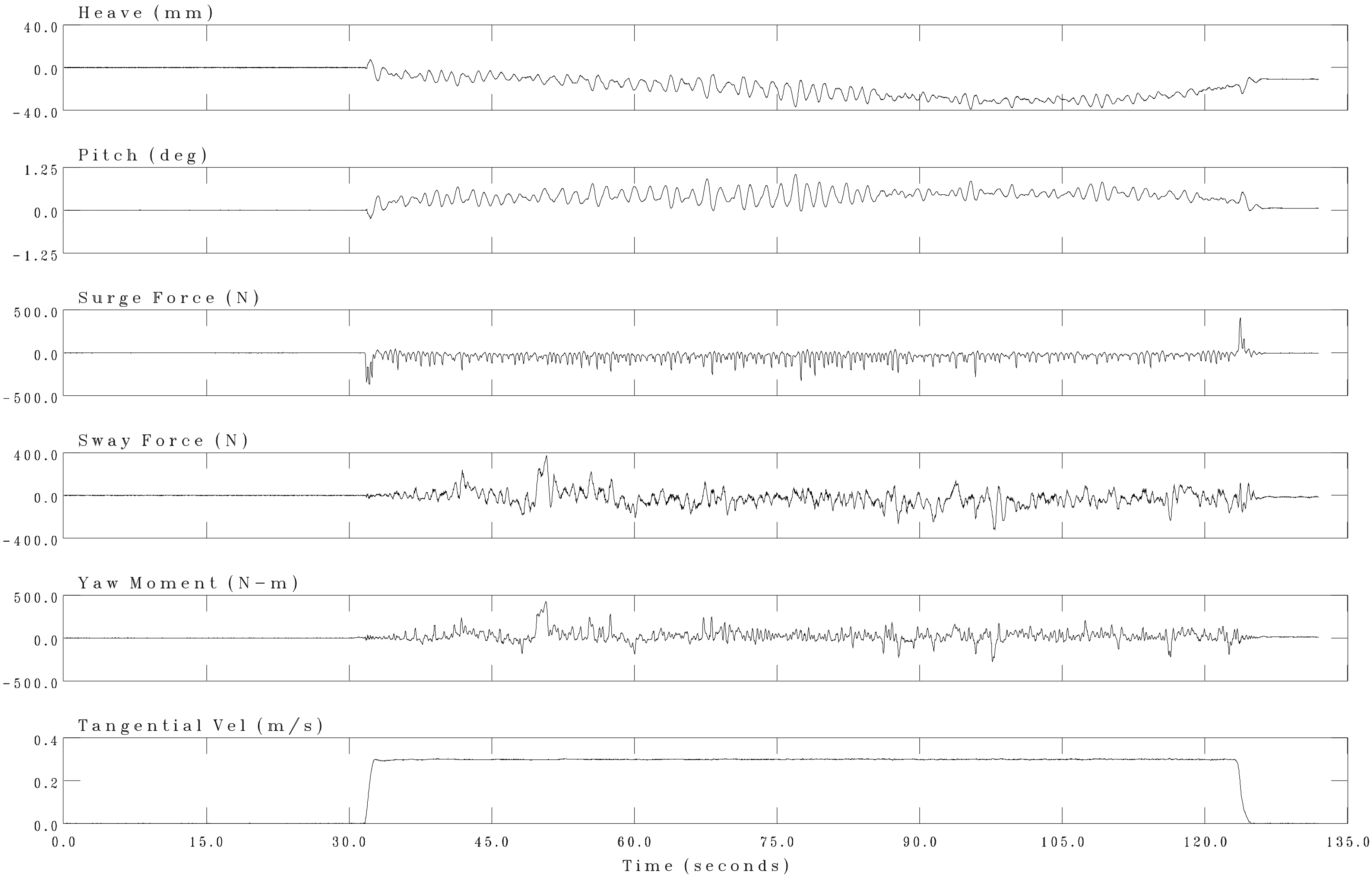

National Research Council Canada
Institute for Ocean Technology

GENERATED BY: LAUM	CHECKED BY:	APPROVED BY:

Figure 1 LIR12_OP3_AR50_130

Marine Structural Fragility and Software Validation
TERRY FOX - PMM/MANEUVER/ICE IOT

Analyzed: 04-NOV-2004 15:06:57
Acquired: 9-JAN-2004 13:51:13

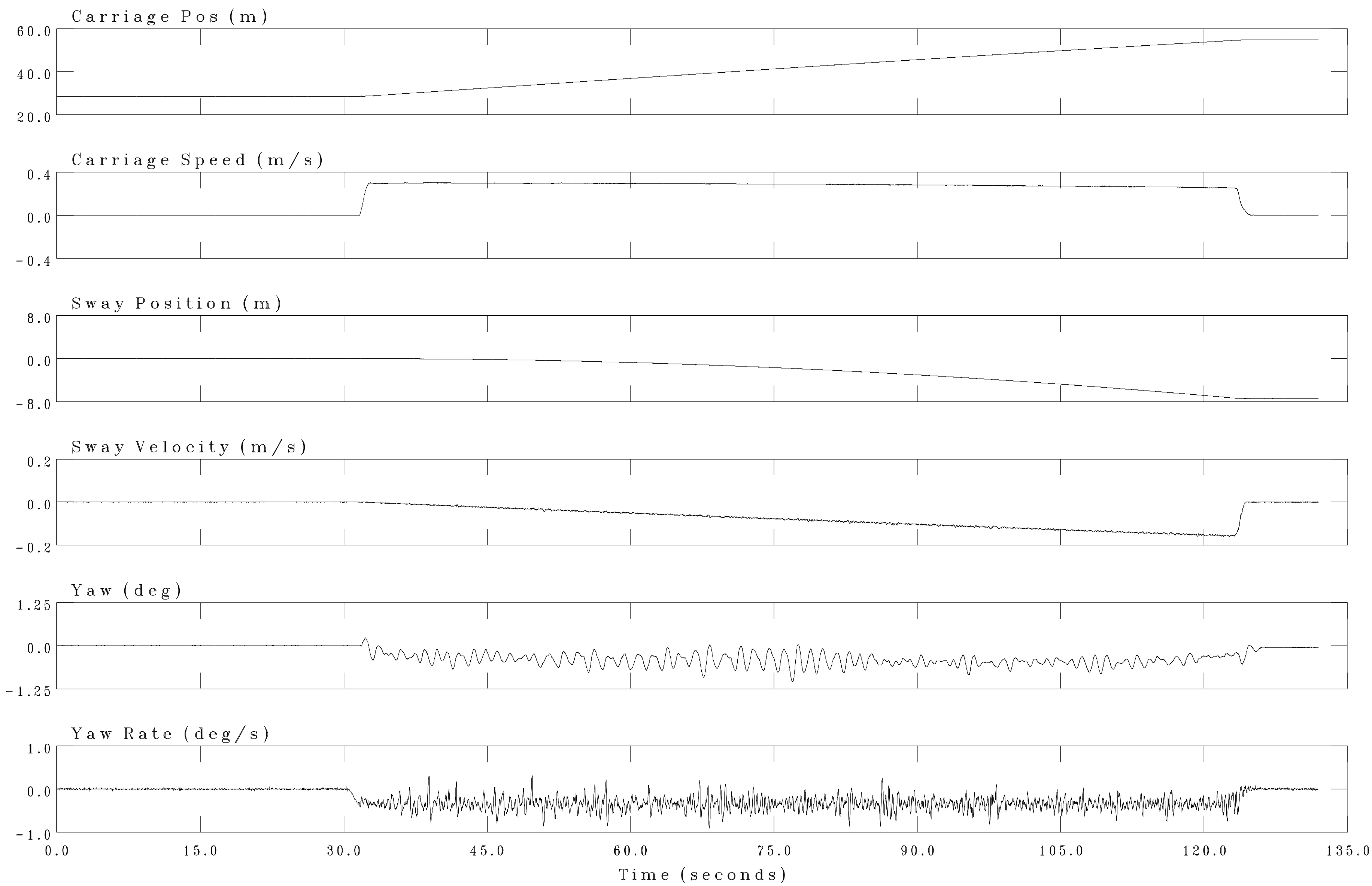

National Research Council Canada
Institute for Ocean Technology

GENERATED BY: LAUM	CHECKED BY:	APPROVED BY:

Figure 2 LIR12_OP3_AR50_130

Marine Structural Fragility and Software Validation
TERRY FOX - PMM/MANEUVER/ICE IOT

Analyzed: 04-NOV-2004 15:07:09
Acquired: 9-JAN-2004 13:51:13

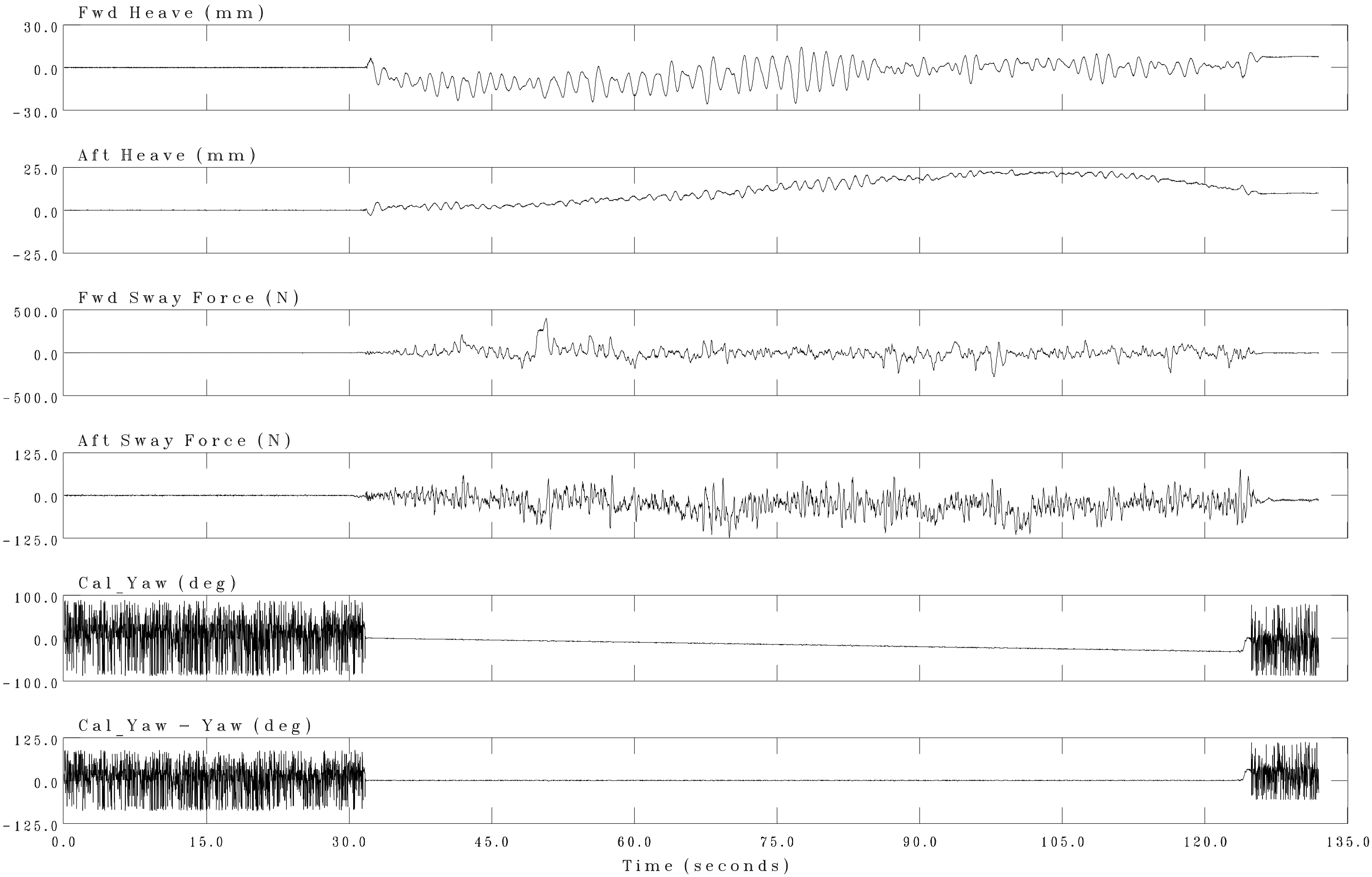

National Research Council Canada
Institute for Ocean Technology

GENERATED BY: LAUM | CHECKED BY: | APPROVED BY:

Figure 3 LIR12_0P3_AR50_130

Marine Structural Fragility and Software Validation
TERRY FOX - PMM/MANEUVER/ICE IOT

Analyzed: 04-NOV-2004 15:07:12
Acquired: 9-JAN-2004 13:51:13

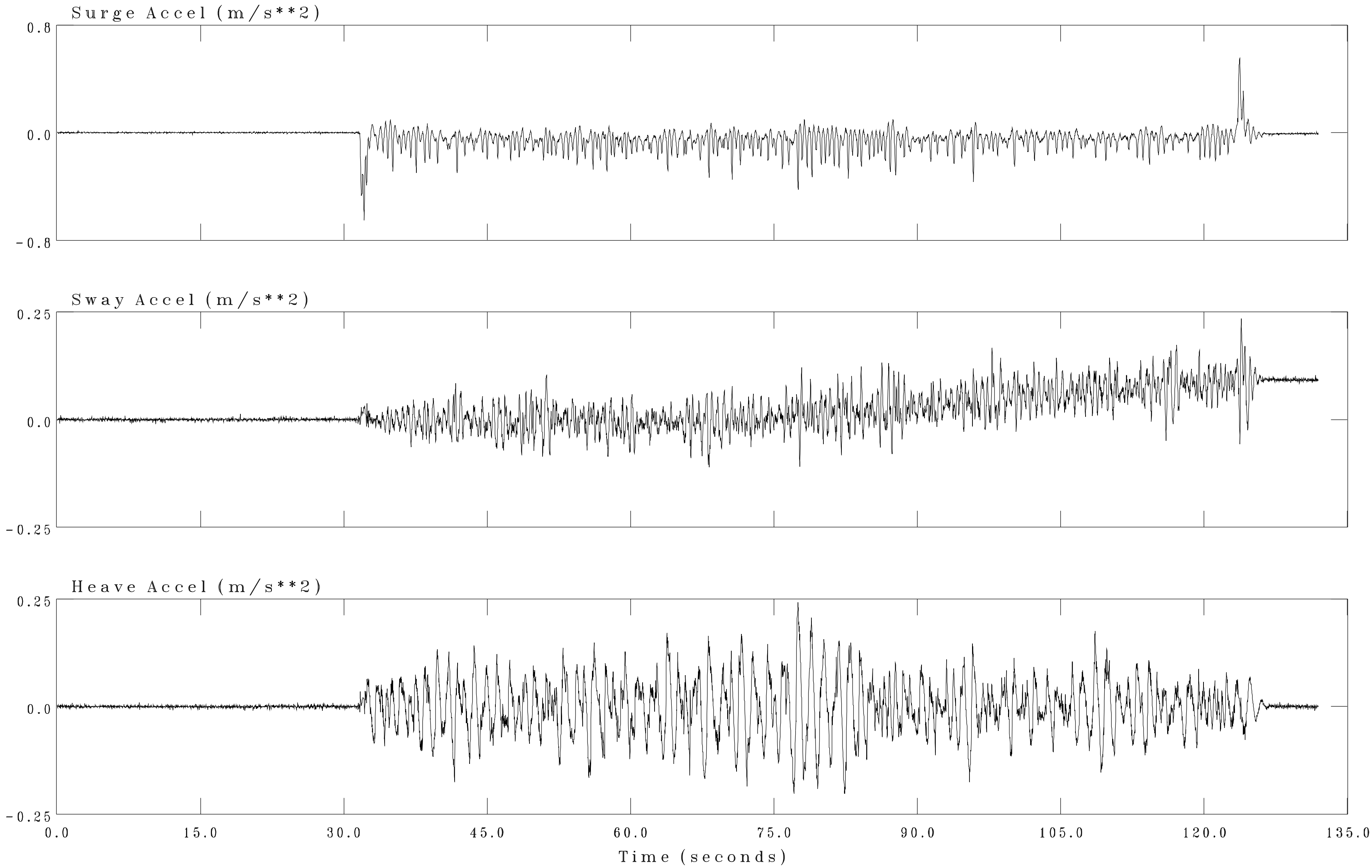

National Research Council Canada
Institute for Ocean Technology

GENERATED BY: LAUM	CHECKED BY:	APPROVED BY:

Figure 4 LIR12_OP3_AR50_130

Appendix G

Detailed Computations For Resistance Runs After IOT's Standard Analysis Procedure

Table G.1: Summary of Pre-Sawn Ice Resistance Analysis

	Summary of Pre-sawn Ice Resistance Analysis															
	Col.1	2	3	4	5	6	7	8	9	10	11	12	13	14	15	16
	Pre-sawn Res.	Open Water Res.	R_b+R_c	R_b+R_c	R_b	Model Speed	Ice Thickness	Ice Density	Ice Buoy.	C_b	R_b Recalc.	R_c (R_c+R_b)	C_c	F_n	ln. C_c	ln. F_n
	R_{ps}	R_{ow}	R_{ps}-R_{ow}	R_{ps}-R_{ow}	Fig. 3.3	V_M	h_i	ρ_i	Eqn. 3.9	Fig. 3.4	Eqn. 3.9	-R_b	Eqn. 3.4	Eqn. 3.7		
Run Name	N	N	N	N	N	$m.s^{-1}$	mm	$kg.m^{-3}$	N		N	N				
Present Test Series																
PRESAWN_SQP_HB_112	5.95	0.2034	5.75			0.0989	37.55	850.77	16.63	0.261	4.340368	1.41	5.7	0.16	1.74	-1.81
PRESAWN_SQP_HB_112	9.01	1.3464	7.66			0.2982	37.55	850.77	16.63	0.261	4.340368	3.32	1.5	0.49	0.39	-0.71
PRESAWN_SQP_HB_112	16.36	4.8242	11.53			0.5984	37.55	850.77	16.63	0.261	4.340368	7.19	0.8	0.99	-0.23	-0.01
PRESAWN_SQP_HB_112	4.50	0.0074	4.49		4.341	0.0195	37.55	850.77	16.63	0.261	4.340368	0.15		0.03		
Spencer et al (19988)																
K2-1	24	0.7195	23.28		9.6522	0.209	44.3	940	7.88	1.2242	9.652535	13.63	9.5	0.32	2.25	-1.15
K2-1	76	9.7479	66.25			0.868	44.7	940	7.96	1.2242	9.739691	56.51	2.3	1.31	0.82	0.27
K2-3	24	0.7195	23.28			0.209	44.3	940	7.88	1.2242	9.652535	13.63	9.5	0.32	2.25	-1.15
K2-3	76	9.7479	66.25			0.868	44.7	940	7.96	1.2242	9.739691	56.51	2.3	1.31	0.82	0.27

Note: Equation and figure reference to Section 3.1.

Table G.2: Summary of Breaking Resistance Analysis

	Summary of Breaking Resistance Analysis															
	Col. 1	2	3	4	5	6	7	8	9	10	11	12	13	14	15	16
	Model Speed	Ice Thickness	In. F_n	Ice Strength	Ice Density	S_n	In. S_n	Total Res.	In. C_c	C_c	R_c	R_b	R_{ow}	R_{br}	C_{br}	In. C_{br}
		h_i	Col 14	σ_f	ρ_I	Eqn. 3.6			Fig. 3.5		Eqn. 3.4	Eqn. 3.5		Eqn. 3.1	Eqn. 3.3	
Run Name	m/s	mm	Table 5.1	kPa	$kg.m^{-3}$			N			N	N	N	N		
Present Test Series																
LIR24A_SQP_149	0.10	39.7	-1.844	23.55	940	2.783	1.02	12.06	1.74	5.69	1.64	1.89	0.20	8.33	28.92	3.36
LIR24A_SQP_149	0.30	39.7	-0.739	23.55	940	8.409	2.13	17.91	0.51	1.67	4.40	1.89	1.35	10.27	3.91	1.36
LIR24A_SQP_149	0.60	39.7	-0.043	23.55	940	16.856	2.82	25.89	-0.26	0.77	8.18	1.89	4.82	11.00	1.04	0.04
LIR24B_SQP_150	0.10	39.1	-1.836	22.84	940	2.848	1.05	10.99	1.73	5.64	1.60	1.86	0.20	7.33	25.83	3.25
LIR24B_SQP_150	0.02	39.1	-3.470	22.84	940	0.556	-0.59	9.02	3.54	34.40	0.37	1.86	0.01	6.78	626.92	6.44
Spencer et al (19988)																
K2-1	0.209	44.4	-1.150	23	940	5.632	1.73	48.6	2.60	13.40	19.27	2.06	0.7195	26.55	18.46	2.92
K2-1	0.868	45.5	0.262	24	940	22.621	3.12	79.2	0.84	2.31	58.83	2.11	9.7479	8.51	0.33	-1.09
K2-3	0.209	45	-1.156	30	940	4.899	1.59	48	2.60	13.51	19.69	2.09	0.7195	25.50	17.49	2.86
K2-3	0.868	44.7	0.271	30	940	20.413	3.02	68.2	0.83	2.29	57.16	2.08	9.7479	-0.79	-0.03	#NUM!

Note: Equation and figure reference to Section 3.1.